Fundamental Investigations of Anhydrous Metal Dodecaborates for Energy Applications

何, 礼青

https://doi.org/10.15017/1543982

出版情報：九州大学, 2015, 博士（工学）, 課程博士
バージョン：
権利関係：全文ファイル公表済

Fundamental Investigations of Anhydrous Metal Dodecaborates for Energy Applications

A Dissertation Submitted

for the Degree of Doctor of Philosophy

Author: He Liqing

Supervisor: Akiba Etsuo

2015

Fukuoka, Japan

Fundamental Investigations of Anhydrous Metal Dodecaborates for Energy Applications

A Dissertation Submitted to Engineering of
KYUSHU UNIVERSITY
in Partial Satisfaction of the Requirements
for the Degree of Doctor of Philosophy

By

He Liqing

DEPARTMENT OF HYDROGEN ENERGY SYSTEMS
GRADUATE SCHOOL OF ENGINEERING
KYUSHU UNIVERSITY
Fukuoka, Japan

July, 2015

Abstract

Metal dodecaborates $M_{2/n}B_{12}H_{12}$ (n denotes the valence of the metal M), comprised of icosahedral polyatomic anion $[B_{12}H_{12}]^{2-}$, have been attracting increasing interest as potential energy materials, especially in the context of hydrogen storage and ionic conductivity. $M_{2/n}B_{12}H_{12}$ are generally formed as dehydrogenation intermediate compounds from metal borohydrides $M(BH_4)_n$ that are well known as high density hydrogen storage materials. The strong B—B bonding in the icosahedral $[B_{12}H_{12}]^{2-}$ is widely regarded as the key factor which prevent the rehydrogenation to form borohydrides. On the other hand, the high stability of icosahedral $[B_{12}H_{12}]^{2-}$ like $NaB_{12}H_{12}$ favors its potential application as solid electrolyte for all solid state batteries. Systematic investigation of $M_{2/n}B_{12}H_{12}$ compounds is, therefore, in great need from both strategies to improve hydrogen storage properties of metal borohydrides and to develop efficient superionic conductor used in commercial batteries.

$M_{2/n}B_{12}H_{12}$ is generally synthesized via wet chemistry processes followed by a careful dehydration process. However, this synthesis method is limited to some $M_{2/n}B_{12}H_{12}$ that does not react with water during dehydration process upon heating. In this study, I propose a new solvent free synthesis process via heat treatment of metal hydride/metal borohydride with decaborane. By using this new process, metal dodecaborates comprised of alkali metals and alkaline earth metals are successfully synthesized and their thermal decomposition behaviors are systematically investigated. Furthermore, several kinds of bimetallic dodecaborates are synthesized in order to figure out the strategy to tune thermal stabilities of metal dodecaborates. Among the synthesized bimetallic dodecaborates, $LiNaB_{12}H_{12}$ is found to exhibit outstanding superionic conductivity with long time of cyclability than its single counterparts. The main content of this dissertation is summarized in the following four parts:

(1) In the first part, I describe the new and facile solvent-free synthesis process of dodecaborates using $B_{10}H_{14}$ with a low melting point of 99.6 °C as a boron source. The successful synthesis of anhydrous $M_2B_{12}H_{12}$ (M = Li, Na and K) by heat treatment of two kinds of starting materials (a) $2MH + 1.2B_{10}H_{14}$ and (b) $2MBH_4 + B_{10}H_{14}$ at 200-450 °C conditions was confirmed by XRD, Raman and NMR analysis. Comparison on the yields of $M_2B_{12}H_{12}$ synthesized from the abovementioned two routes indicates that route (b) $2MBH_4 + B_{10}H_{14}$ is feasible for syntheses of $M_2B_{12}H_{12}$.

The synthesized anhydrous $M_2B_{12}H_{12}$ (M = Li, Na and K) exhibit multistep decomposition accompanied with the formation of H-deficiency $M_2B_{12}H_{12-x}$ followed by the polymerization of $M_2B_{12}H_{12-x}$ to form $(M_2B_yH_z)_n$.

(2) In the second part, I successfully synthesize anhydrous alkaline earth metal dodecaborates $MB_{12}H_{12}$ (M = Mg, Ca) for the first time using the developed solvent free process, i.e. heat treatment of starting materials $M(BH_4)_2 + B_{10}H_{14}$ (M = Mg, Ca). Like those of anhydrous $M_2B_{12}H_{12}$ (M = Li, Na and K), both $MgB_{12}H_{12}$ and $CaB_{12}H_{12}$ exhibit multistep decomposition accompanied with the formation of H-deficiency $MB_{12}H_{12-x}$ with the icosahedral B_{12} skeletons followed by a polymerization process to produce $(MB_yH_z)_n$. Though the decomposition temperature range varies largely with the kinds of metal M, all the decomposition behaviors of metal dodecaborates comprised of alkali metal or alkaline earth metal are fairly different from the dehydrogenation of corresponding borohydrides.

(3) In the third part, I attempt to tune the thermal stabilities of dodecaborates through syntheses of bimetallic dodecaborates such as $LiNaB_{12}H_{12}$, $Li_6K_4(B_{12}H_{12})_5$ and $Na_8K_2(B_{12}H_{12})_5$. The synthesized bimetallic dodecaborates exhibit distinct stabilities from those of corresponding single counterparts, suggesting the feasibility of designing bimetallic dodecaborates to stabilize/destabilize the single counterparts.

(4) In the fourth part, I investigate the reversible phase transition and outstanding superionic conductivity of $LiNaB_{12}H_{12}$. $LiNaB_{12}H_{12}$ has a cubic structure with space group *Pa*-3 at room temperature, and transforms to a high temperature phase with *Fm*-3*m* symmetry at approximately 215 °C, which is lower than that of $Li_2B_{12}H_{12}$ and $Na_2B_{12}H_{12}$. The ionic conductivity at around 280 °C reaches 0.79 S/cm, which is approximately 8 times higher as that for $Na_2B_{12}H_{12}$ at the same temperature. The Li/Na compositional and thus an induced positional disorder in $LiNaB_{12}H_{12}$ are suggested to be responsible for the reduced phase transition temperature and the improved superionic conductivity compared to its monometallic counterparts.

Acknowledgments

This dissertation would not be smoothly completed if without great help, trust and support from many persons to whom I would like to sincerely appreciate.

At first, I would like to thank Prof. Etsuo Akiba who gave me the chance to be a doctoral student in Kyushu University and patiently supervised me for three years. Prof. Etsuo Akiba is a very kind, knowledgeable and famous scientist, and I am grateful to him for his selfless guidance and help from all aspects. One of the unforgettable things is that he spent time to seriously correct my Japanese mistakes even though he was in his very busy situation, which made rapid progress in my Japanese study. His help on my research was too much to express here, my research achievements were reached only under his careful supervision, his counsels and suggestions will be helpful all over my life.

I would like to thank Assoc. Prof. Hai-Wen Li for his great concerns and help to my living and research in Japan. Assoc. Prof. Hai-Wen Li is a serious, humorous and kindhearted person whom you can well get along with. From picking me up at Saga airport three years ago, his help never stopped. In lives, he helped me in a wide range from the enrollment procedures to knowledge of daily life in Japan, his economic support to me is also unforgettable forever in my mind; In research, he taught me a series of experimental skills and research methods, all of my research achievements were impossible to be completed and published on journals if without his great help.

I would like to thank the members of defense committee including Prof. Etsuo Akiba, Prof. Kohei Ito and Prof. Yoshihiro Yamazaki. Their kind advices are very much helpful to complete this dissertation.

I would like to specially thank Prof. Yaroslav Filinchuk, Assoc. Prof. Hans Hagemann, Asst. Prof. Hironori Nakajima, Dr. Son-Jong Hwang, Dr. Nikolay Tumanov and Mr. Manish Sharma for their friendly collaboration resulting in the published and submitted papers.

I am grateful to Assoc. Prof. Miho Yamauchi and Asst. Prof. Motonori Watanabe in I2CNER for their great help on nuclear magnetic resonance (NMR) measurement.

I would like to thank Asst. Prof. Huaiyu Shao, Dr. Jianhui Wang, Dr. Huaijun Lin and Mr. Guoliang Wang for their great concern and support in all time especially when I was lost in hesitation and sorrow.

I would also like to thank all the members in my laboratory including Dr. Biswajit Paik, Dr. Hoda Emami, Ms. Yuka Nagashima, Ms. Hidemi Yoshimura, Mr. Kazuji Tanioka, Mr. Yoshinobu Horita, Mr. Hiromasa Hirano, Ms. Yui Azuma, Mr. Yuki Sonoda, Mr. Ryuichi Koga, Mr. Hiroshi Ogihara, Mr. Atsushi Shimokawa, Mr. Sascha Dietzel, Mr. Syota Itano, Mr. Hiroki Murakami, Mr. Masataka Katagami, Mr. Soichiro Kitamura and Mr. Kentaro Harano.

I am grateful to my family, relatives, classmates and friends for their continuous support and help. Especially, I strongly appreciate to my mother who gave birth to me and bred me to an adult, but unfortunately she passed away in the spring of 2014. My mother was a very thin but diligent and easygoing female who kept all family things orderly and got along well with others. My mother was the first person who taught me justice, kindness and tolerance which I always keep in mind. I am very depressed that I was not able to watch her face for the last time at the end of her life when I went back home from Japan. I was ever lost in great sorrow for a long time but I will bravely and confidently go ahead following her earnest expectance.

Last but not least I am also grateful to the financial support from International Research Center for Hydrogen Energy, JSPS Invitation Fellowship for Research (Short-Term) and the International Institute for Carbon Neutral Energy Research (WPI-I2CNER) in Japan.

Table of Contents

List of Figures

List of Tables

List of Publications

Master's Publications

1) **He L**, Luo C, Hou Y, Li C, Zhou Q, Sun Y, Wang W, Zhang B, Wang X, The effects of micellar media on the photocatalytic H_2 production from water, *International Journal of Hydrogen Energy*, 36, pp10593-10599, 2011.

2) **He L**, Luo C, Zhou Q, Hou Y, Zhang B, Wang X, Use Electrostatic Attraction to Improve the Photocatalytic Hydrogen Evolution Efficiency，*Imaging Science and Photochemistry*, 29, pp270-277, 2011.

3) Luo C, Zhou Q, Jiang G, **He L**, Zhang B, Wang X, The synthesis and $^1O_2$ photosensitization of halogenated asymmetric aniline-based squaraines, *New Journal of Chemistry*, 35, pp1128-1132, 2011.

Doctoral Publications (For Dissertation)

1) **He L**, Li H-W, Huang S, Akiba E, Facile Solvent-free Synthesis of Anhydrous Alkali Metal Dodecaborate $M_2B_{12}H_{12}$ (M = Li, Na, K), *J. Phys. Chem. C*, 118, pp6084-6089, 2014.

2) **He L**, Li H-W, Akiba E, Thermal Decomposition of Anhydrous Alkali Metal Dodecaborate $M_2B_{12}H_{12}$ (M = Li, Na, K). To be submitted to *Energies*.

3) **He L**, Li H-W, Tumanov N, Filinchuk Y, Akiba E, Facile Synthesis of Anhydrous Alkaline Earth Metal Dodecaborate $MB_{12}H_{12}$ (M = Mg, Ca) from $M(BH_4)_2$. Submitted to *Dalton Transactions*.

4) **He L**, Li H-W, Filinchuk Y, Nakajima H, Tumanov N, Filinchuk Y, Huang S, Sharma M, Hagemann H, Akiba E, Synthesis of a Bimetallic Dodecaborate $LiNaB_{12}H_{12}$ with Out-standing Super Ionic Conductivity. Submitted to *Chemistry of Materials*.

Chapter 1

Introduction

In this chapter, the state-of-art of hydrogen mediated society has been introduced with the emphasis on one of the promising hydrogen storage materials, i.e. metal borohydrides $M(BH_4)_n$ and their dehydrogenation intermediate metal dodecaborates $M_{2/n}B_{12}H_{12}$. Furthermore, the motivation and the objective of this research are described in the latter part.

1.1 Hydrogen

Though the great progress in industries based on fossil fuels, human beings are confronting with unprecedented resource and environmental issues which seriously threaten the survivals and prevent the sustainable development of human beings. New non-polluting and sustainable fuels are in great necessity and urgency to be developed for replacement of conventional fossil fuels in order to protect the earth and also our human beings. Hydrogen which can be obtained from various resources using many kinds of methods and combust into only zero pollution of water becomes the key to solve the abovementioned issues.

1.1.1 About Hydrogen

Hydrogen firstly discovered by the British scientist Henry Cavendish, is the first and lightest element in Mendeleev Periodic Table.[1] Hydrogen composes 75 mass% of our universe and widely exists in inorganic and organic substances on earth.[2] The most common existence of hydrogen in our lives is water, water includes two hydrogen atoms in every its molecule.

The simple substance of hydrogen element is H_2, which is a kind of flammable (4 volume% to 75 volume% of hydrogen in air) gas without any color or smell at room temperature and under standard atmospheric pressure.[3] The reaction equation of

combustion of H_2 is exhibited as:

$$H_2\ (g) + 1/2O_2\ (g) \rightarrow H_2O \qquad (1.l)$$

with enthalpy change as −286 kJ/(mol H_2).[4] The unique product of H_2 combustion is water without greenhouse gases or other pollutants. The calorific value of H_2 is shown in Figure 1.1 and compared with some common fuels.[5-6] H_2 has much higher per unit weight of combustion heat than that of all the conventional fuels which means it is a more efficient energy carrier.

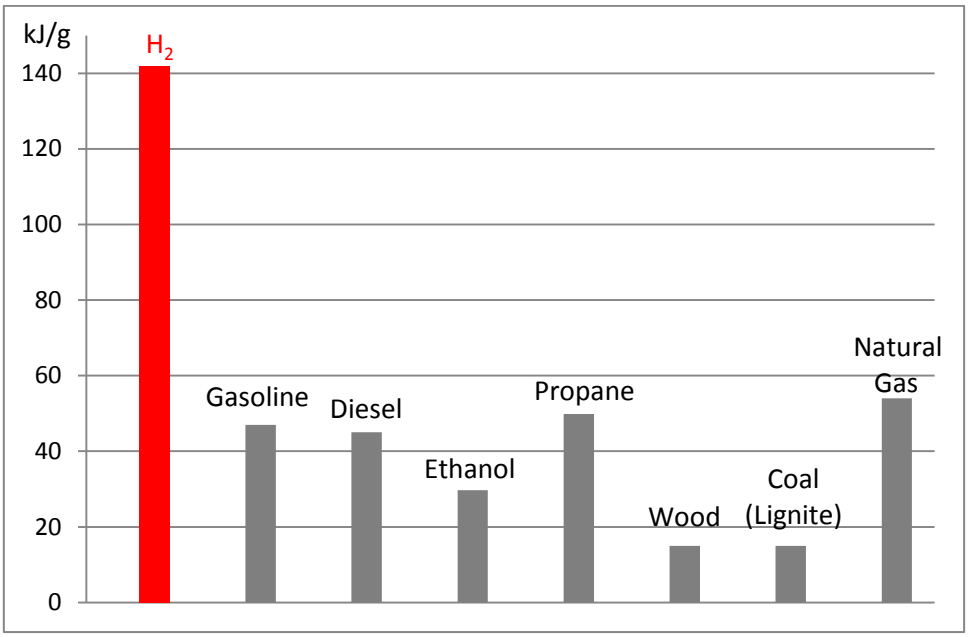

Figure 1.1 The calorific value of hydrogen and some common fuels.[5-6]

As we know, H_2 can be reversibly produced by splitting of water. Therefore, "hydrogen society" has been conceived as an economical and environmental-friendly society in which the secondary energy H_2 is used as recyclable energy carrier and renewable energy such as solar and wind energies are used as primary energy.[7] Figure 1.2 briefly explains the composition of hydrogen society, the sustainable hydrogen society is normally comprised of three parts: hydrogen production, hydrogen storage and hydrogen utilization.[8-10]

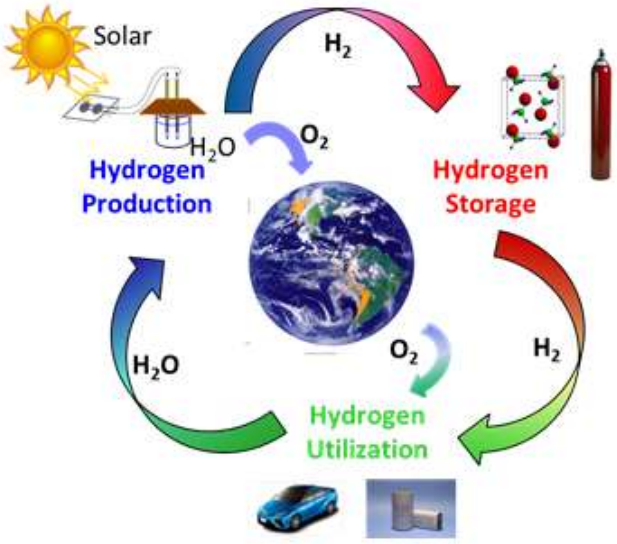

Figure 1.2 The brief illustration of hydrogen society.[8-10]

1.1.2 Hydrogen Production

Though hydrogen is widely existed in various substances on earth, the simple substance of molecular H_2 is hardly obtained via physical purification for the volume percentage of H_2 in air is only 0.5 ppm.[11]

To obtain H_2 for human requirement, wide variety of chemical methods have been developed for H_2 production.

In industry, the production of H_2 is mainly based on extraction of hydrogen from fossil fuels such as coal, oil and natural gas. At present, about 96% of H_2 production all over the world is from fossil fuels, only 4% is from electrolysis of water (Figure 1.3).[12]

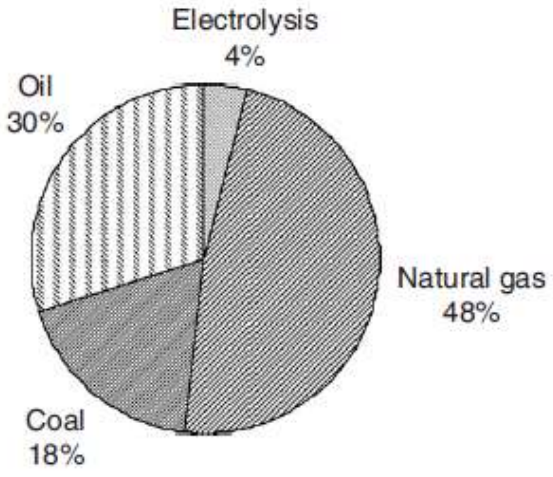

Figure 1.3 Feedstock of the global H_2 production.[12]

In laboratory, H_2 can be obtained from the reaction of active metals with strong acid, for example:

$$Zn + H_2SO_4 \rightarrow ZnSO_4 + H_2 \quad (1.2)$$

The amount of produced H_2 is only competent for laboratory research by taking into account the production costs.

With the exhaustion of fossil fuels and deterioration of global environment, renewable energy sources are attracting more and more attention for hydrogen production.

Solar is an ideal renewable energy source. The conversion of solar energy into hydrogen is one of the feasible ways to smooth the power fluctuation depending on weather, season, and location. In 1972, Fujishima and Honda firstly achieved photocatalytic H_2O splitting into H_2 using TiO_2 electrodes.[13] At the beginning, only ultraviolet light is absorbed by photocatalyst. With about 40 years of research, many kinds of more efficient photocatalysts have been developed and the absorption wavelengths have been extended to 660 nm of red light via using $BaTaO_2N$.[14-15] Photocatalytic water splitting for large amount of H_2 production is still at the stage of fundamental research.

Wind power and hydropower are also considered to be converted into H_2 energy through electrolysis of H_2O molecules to H_2 and O_2.[12, 16] Besides of them, biomass is also potentially available for renewable H_2 production.[16]

1.1.3 Hydrogen Storage

As the lightest gas known to human up to now, H_2 has very low boiling point of -253 °C, the density of H_2 at 0 °C and 1 atm is only 0.09 g/L.[17] How to store H_2 safely, efficiently, economically and conveniently for transportation and utilization, remains a very important issue to be resolved.

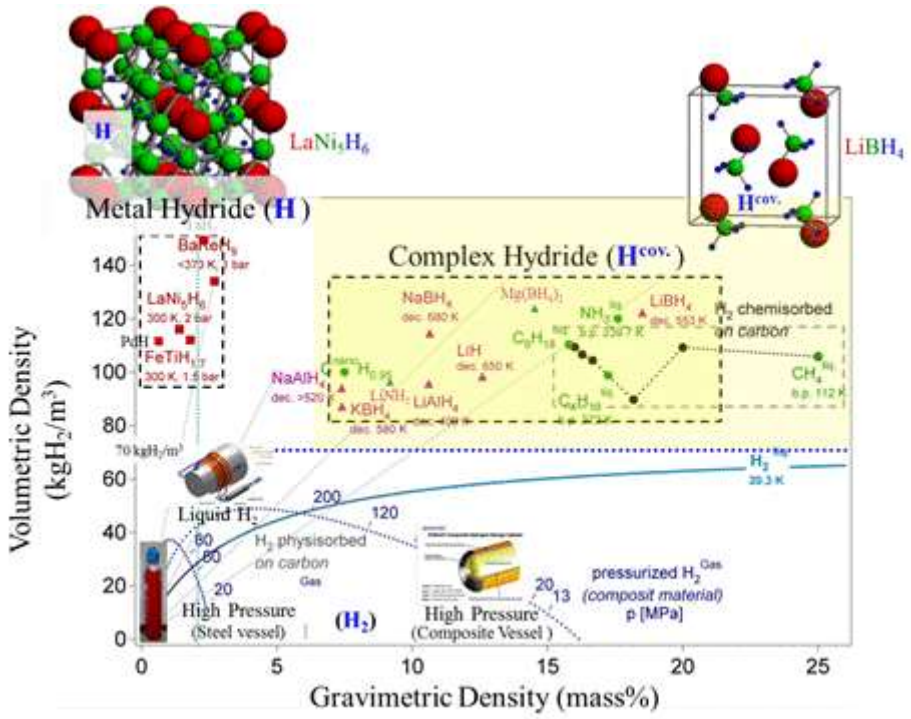

Figure 1.4 Hydrogen densities in different storage systems.[18]

At present, H_2 is mainly stored by means of three strategies: compression, liquefaction and hydrogen storage materials. Figure 1.4 exhibits the different hydrogen densities in various hydrogen storage systems.[18]

It is very common to compress H_2 into cylinders up to 15 MPa for laboratory use, however, the systematic H_2 density is less than 2 wt%. For widespread application, cylinder has to be designed to withstand 70 MPa of H_2 pressure with 110 kg of weight for storing 7 kg of H_2, in order to reach 6% of gravimetric and 30 kg/m^3 of volumetric densities.[19] External energy is needed for H_2 compression which increases the cost to use cylinders for hydrogen storage.

Liquefaction is a kind of hydrogen storage method with high gravimetric and volumetric H_2 density. In this method, very low temperature (< -252 °C) and open systems of cryogenic containers are essential for liquid hydrogen storage. Hydrogen has critical temperature at -243 °C, and around 1/3 of heat energy that hydrogen possesses will be consumed for the liquefaction process. Furthermore, liquid hydrogen easily emits into atmosphere in open systems. How to improve the efficiency of liquefaction process and prevent H_2 boil-off, are considered to be two critical issues to hamper the progress of liquid hydrogen utilization. At present, liquefaction of H_2 is used in few special fields such as being fuel of rocket used in

aerospace.[19-20]

Material hydrogen storage is usually divided into physically bound hydrogen and chemically bound hydrogen.[21] H_2 can be stored in porous materials via physisorption and stored in metals or compounds via chemical reaction. The advantage of this method is the high hydrogen storage density (e.g. 7.6 wt% of H in MgH_2; 18.5 wt% of H in $LiBH_4$) and high safety without using high pressure of 70 MPa or low temperature of below -252 °C. Hydrogen storage materials with high H_2 density, therefore, are expected to be developed for practical storage and transportation.

1.1.4 Hydrogen Utilization

H_2 has been widely used in many fields of our society such as industry, agriculture, commercial, transportation, community, electricity generation and so forth.[17] The direct and simple utilization of H_2 is combustion in air or oxygen to release large amount of heat, this energy is used for metal cutting or melting. H_2 is widely used in industry for cracking and refining of oil, synthesizing ammonia and ethanol, ammonia can be subsequently process into fertilizer for agricultural usage. In hydrogen society, most of H_2 will be consumed in fuel cells and electricity generation in order to supply power to various aspects in our lives.[7]

1.2 Hydrogen Storage Materials

Though hydrogen is the ideal substitution to fossil fuels, the safe and effective storage and transportation of hydrogen remains an issue because of the wide explosive range (4 volume% to 75 volume% of hydrogen in air) and low density (0.09 g/L at 0 °C and 1 atm) of molecular hydrogen.[3, 19] For wide applications of hydrogen, hydrogen storage technology by which hydrogen can be safely stored in high density (>70 kg H_2/m^3)[18] are in great importance to be developed. Hydrogen storage materials which well fulfill the demands are worthy of careful study.

1.2.1 Target for Onboard Hydrogen Storage

Development of hydrogen storage materials for onboard application of fuel cell vehicle (FCV) is one of the most challenging targets. A large number of progresses on hydrogen storage materials have been achieved, nevertheless, no material can fulfill all the criteria for onboard storage has been developed.[22] The ideal hydrogen storage

materials should work at 0 – 100 °C under pressures from 1 to 10 atm to meet wide application of human.[23] Besides that, the high hydrogen density (volumetric and gravimetric), fast reaction kinetics, good reversibility and safety and acceptable cost, should be considered for ultimately commercial application.[24] The ideal onboard hydrogen storage systems are anticipated to meet more demands, e.g. cycle life, charging/discharging rates and loss of usable H_2. The detailed target roadmap of onboard hydrogen storage has been drawn up by U.S. DRIVE Partnership (a voluntary partnership among the U.S. Department of Energy and other organizations or companies on energies or cars), which is shown in Table 1.1.[25]

Table 1.1 Technical system targets of onboard hydrogen storage[25]

Storage Parameter	**Units**	**2017**	**Ultimate**
System Gravimetric Capacity:	kWh/kg	1.8	2.5
Usable, specific-energy from H_2	(kg H_2/kg system)	(0.055)	(0.075)
System Volumetric Capacity:	kWh/L	1.3	2.3
Usable energy density from H_2	(kg H_2/L system)	(0.040)	(0.070)
Storage System Cost:	$/kWh net	12	8
Fuel cost	$/gge at pump	2-4	2-4
Operating ambient temperature	ºC	-40/60	-40/60
Min/max delivery temperature	ºC	-40/85	-40/85
Operational cycle life	Cycles	1,500	1,500
Min delivery pressure	bar (abs)	5	3
Max delivery pressure	bar (abs)	12	12
Onboard efficiency	%	90	90
“Well” to powerplant efficiency	%	60	60
Charging/Discharging Rates: (5 kg)	min	3.3	2.5
Minimum full flow rate	(g/s)/kW	0.02	0.02
Start time to full flow (20°C)	s	5	5
Start time to full flow (-20°C)	s	15	15
Loss of Useable H_2:	(g/h)/kg H_2 stored	0.05	0.05

Note: Useful constants: 0.2778 kWh/MJ; lower heating value for H_2 is 33.3 kWh/kg H_2; 1 kg H_2 ≈ 1 gal gasoline equivalent (gge).

1.2.2 Physical Adsorption

Physical adsorption happens in materials surface where molecular hydrogen is bounded by van der Waals forces. Materials with large specific surface areas are typical physical adsorption materials such as carbon nanomaterials, activated carbon, zeolite and metal-organic frameworks (MOFs). Such materials display H_2 storage abilities for the microporous structure in them, and the H_2 storage density can be improved by increasing the surface area.[26] The Figure 1.5 exhibits the structures of some representative adsorbents.[27-28]

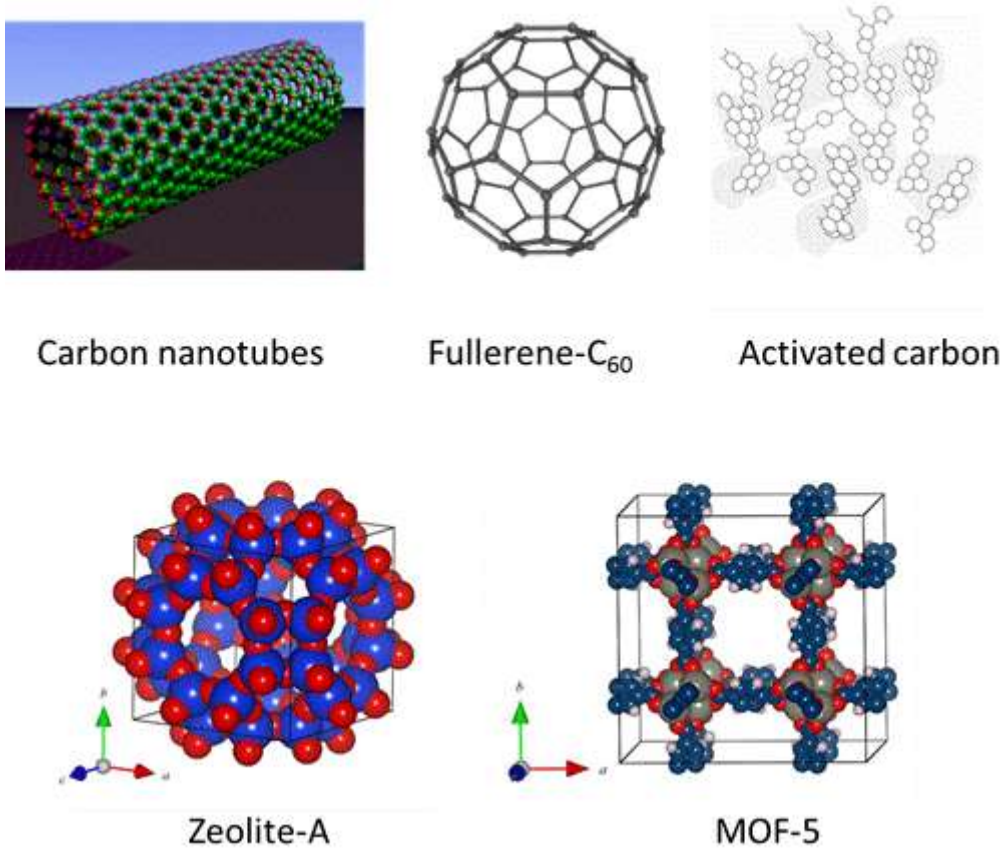

Figure 1.5 Structures of some representative adsorbents.[27-28]

The advantages of carbon hydrogen storage materials are their light weight and good cycle stabilities. H_2 storage properties of a series of carbon materials had been investigated. Hydrogen storage via activated carbon was reviewed by Noh et al in 1987, the paper indicates that the efficiency of activated carbon can be improved by two methods: acidity modification and metal impregnation on the activated carbon surface.[29] In 1991, carbon nanotubes were described by Iijima for the first time.[30] In

1997, Jones et al indicated narrow, single-walled nanotubes can store high density of H_2.[31] Carbon nanotubes were subsequently comprehensively studied for developing them to be promising hydrogen storage materials, however, the high H_2 densities in carbon nanotubes are still to be confirmed. The research on carbon nanotubes as H_2 storage materials has reduced because it is difficult for carbon nanotubes to store enough hydrogen for practical application at moderate pressures and temperatures.[32]

Zeolite is easily to adsorb/desorb gas, however, its H_2 adsorption capacity is less than 10 cm^3 H_2/g at 0 °C and 1 bar (150 to 700 cm^3 H_2/g in metal hydride systems at the same conditions) because of its heavy weight which hampers its utilization as H_2 storage.[33] Metal-organic framework materials have been also synthesized for H_2 storage. Rosi et al reported MOF-5 with composition $Zn_4O(BDC)_3$ to adsorb H_2 up to 4.5 mass% at 78 K and 1.0 mass% at room temperature under 2 MPa pressure.[34] In this method, partial solvent molecules in MOF are hard to be removed which affects the H_2 capacity. Ice exhibits irregular melting behavior at hydrogen pressures of 100 – 360 MPa to form clathrate phase of hydrate of H_2.[35-36] Though clathrates for H_2 storage has attracted many interest from different groups,[37-39] the severe synthesis conditions and low H_2 capacity means it is not appropriate to store hydrogen for practical use.

1.2.3 Chemical Storage

1.2.3.1 Metal Hydrides

Metal hydrides are also known as interstitial hydrides in which hydrogen atoms occupy the interstitial sites in the crystal lattices. The research on metal hydrides as hydrogen storage materials started from 1960s. Mg_2Ni as the first case was reported by Reilly et al from Brookhaven National Laboratory to reversibly store H_2 with 3.6 mass% in 1968.[40] Followed by it, Kuijpers et al from Philips Research Laboratory reported the reversible hydrogenation and dehydrogenation properties of $LaNi_5$ alloys at room temperature.[41] In 1970s, the Ni/MH battery was discovered and it was quickly commercialized in 1990s, metal hydrides as H_2 storage materials gradually received wide attentions.[42-43] As a result, the Ni/Cd battery was quickly replaced by Ni/MH battery for the excellent functions of the latter on portable application.[44-46]

The alloys for H_2 storage are usually comprised of two parts, A and B. A represents metal which is easy to form metal hydride, such as La, Mg, Ti, Zr, V and so forth;

while B represents metal which is hard to absorb H_2, such as Fe, Ni, Al and so forth.[23, 47]

Hydrogen storage alloys are usually divided into AB_5, AB_2, AB, A_2B intermetallic compounds and solid solution alloys.[23] AB_5 intermetallic compounds are usually with hexagonal structures, the typical representative in $LaNi_5$;[48] AB_2 alloys are generally in Laves phase with C14 or C15 structure, the typical examples are ZrV_2, TiV_2 and $ZrMn_2$;[49] Typical AB type of alloys are TiFe, TiFe alloys are economical but with severe activation conditions which are commonly used for high pressure hydrogen storage;[50] A_2B type of alloys include Zr_2Ni and Mg_2Ni as representatives, A_2Bs are too stable to considerably absorb H_2 in the 0-100 °C and 1-10 atm range;[23] Solid solution alloys based on the solvents of Pd, Ti, Zr, Nb and V reversibly absorb H_2, $Ti_{25}Cr_{35}V_{40}$ with 2.2 mass% of H_2 capacity at room temperature has attracted wide research interest for application.[23, 49] However, the high cost of noble metals and heavy weight may restrict the development of solid solution as H_2 storage materials.

1.2.3.2 Complex Hydrides

Complex hydride is generally expressed as $M(M'H_x)_n$, where n is the valence of metal M, M' is Al, N or B. Distinct from that of metal hydride, hydrogen makes a covalent bond with the atom M' to form a polyatomic anion such as $[AlH_4]^-$, $[NH_2]^-$ and $[BH_4]^-$. Sodium alanate $NaAlH_4$, lithium amide $LiNH_2$ and lithium borohydride $LiBH_4$ are known as typical complex hydrides. The study of complex hydrides as high density hydrogen storage materials was triggered by the pioneering achievement by Bogdanović et al. in 1997,[51] in which the reversible hydrogen storage of sodium alanate $NaAlH_4$ was realized by the addition of Ti-based catalyst.

1.2.3.2.1 Alanates

Alanates with higher H_2 density than that of alloys are also considered to be hydrogen storage materials. Lithium and sodium alanates are commercially available, other metals of alanates are obtained by metathesis reaction, ball milling or reaction between metal hydrides with aluminum.[52] Crystal structures of some alanates are shown in Figure 1.6.[52-58]

The decomposition of metal alanates usually experiences two processes, taking the decomposition of $NaAlH_4$ as an example, they are:

$3NaAlH_4 \rightarrow Na_3AlH_6 + 2Al + 3H_2$ (1.3)

$Na_3AlH_6 \rightarrow 3NaH + Al + 3/2H_2$ (1.4)

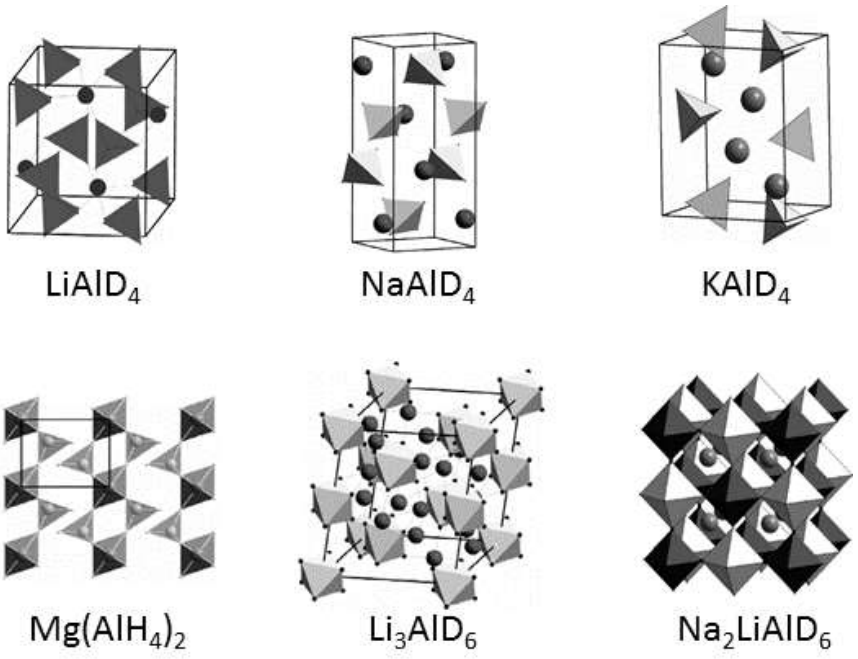

Figure 1.6 Crystal structures of some metal alanates.[52-58]

The first step happens at 210 – 220 °C with 3.7 mass% H_2 loss to form Na_3AlH_6 and the second step is the subsequent decomposition of Na_3AlH_6 to NaH and Al at 250 °C with loss of 3 H.[59-60] $NaAlH_4$ was firstly reversibly obtained from its dehydrogenation products by Clasen in tetrahydrofuran solutions at 150 °C and 13.6 MPa of H_2 pressure catalyzed by triethylaluminum.[61] Followed by it, Ti-doped alkali metal aluminum hydrides were carefully studied by Bogdanović et al as new reversible H_2 storage systems, the work attracted wide interest to the research on complex hydrides.[51] Though a series of alanates have been studied, only sodium alanate can be charged directly in H_2. Besides of that, only 3-4 mass% of cycling H_2 capacity of alanates means they are still immature candidates for practical application.[52]

1.2.3.2.2 Amides

Alkali metal amides were successfully synthesized since more than 100 years ago and they were traditionally used as reagents for organic synthesis.[62] The gas phase of decomposition products of amides are ordinarily ammonia rather than H_2. Amides

were firstly reported by Chen et al as reversible hydrogen storage materials in $LiNH_2$-2LiH system with overall 10.5 mass% of H_2 capacity.[63] The dehydrogenation/rehydrogenation processes are as follows:

$$LiNH_2 + 2LiH \rightleftharpoons Li_2NH + LiH + H_2 \rightleftharpoons Li_3N + 2H_2 \quad (1.5)$$

Figure 1.7 shows the enthalpy changes and decomposition temperatures of $LiNH_2$, LiH and combined system of $LiNH_2$-LiH. $LiNH_2$ decomposes at a temperature higher than 300 °C with the release of ammonia. LiH dehydrogenates at temperatures above 600 °C. However, the combined $LiNH_2$-LiH system starts to release H_2 only above 150 °C (<180 °C).[63-64] The results proved the feasibility to tune the thermodynamic stability by making a composite system, which opens the gate for studying amides as advanced hydrogen storage materials.

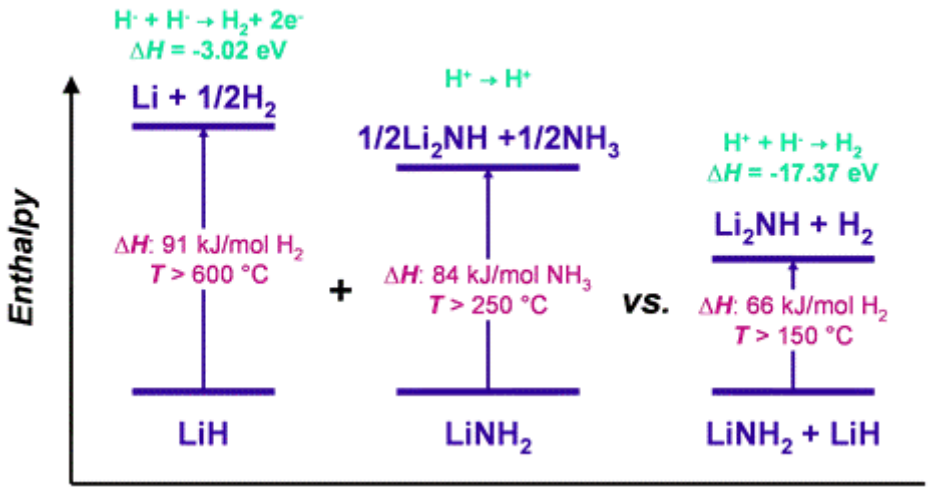

Figure 1.7 The enthalpy diagram of $LiNH_2$-LiH system.[63]

The dehydrogenation and rehydrogenation of amide-hydride system usually encounter with kinetic barriers, which may be originated from hydrogen dissociation, interface reactions between two solid phases, nucleation and nuclei growth, and /or diffusion.[64] Catalytic additive is considered to be a good route to improve reaction kinetics of amide systems. For example, 3.0 mol% KH was introduced to $Mg(NH_2)_2$-2LiH system and an achievement of notable enhancement of kinetics was observed.[65] In amide systems, sometimes H_2 releases with formation of ammonia and reversible H_2 capacity decreases with cycles,[66-67] it is still important issue to be resolved that how to improve the reaction kinetics, control the releasing of ammonia and keep the cycling stability.

1.2.3.2.3 Borohydrides

Borohydrides $M(BH_4)_n$ with higher volumetric and gravimetric hydrogen densities than the target values shown in Table 1.2, such as $LiBH_4$ (H capacity: 18.5 mass% and 122 kg H_2/m^3), $Mg(BH_4)_2$ (14.9 mass% and 147 kg H_2/m^3) and $Ca(BH_4)_2$ (11.6 mass % and 124 kg H_2/m^3), have been regarded as potential candidates for onboard hydrogen storage materials.[68] Among the known hydrogen storage materials, borohydrides have been classified as the group with the highest hydrogen capacity that can be reversibly stored. Borohydrides, therefore, have been extensively investigated for onboard storage, including the development of synthesis process, fundamental dehydrogenation and rehydrogenation, as well as performance improvement from both aspects of thermodynamics and kinetics. The typical achievements and key issues of borohydrides are described in detail in Section 1.3.

1.3 Metal Borohydrides $M(BH_4)_n$

As the abovementioned description, metal borohydrides with highest hydrogen capacity (higher than the target values for onboard hydrogen storage) among the known hydrogen storage materials can reversibly store hydrogen and hopefully be developed for practical applications such as onboard hydrogen storage for FCVs.

1.3.1 Hydrogen Density in $M(BH_4)_n$

To develop feasible hydrogen storage materials for commercial application, many factors have to be considered, such as high hydrogen density, moderate temperature and rate of dehydrogenation/rehydrogenation, durable cycling stability and economic efficiency.[69] Metal borohydrides $M(BH_4)_n$ with high hydrogen density are attracting extensive interest for utilization as practical hydrogen storage materials. To meet the ultimate technical system targets of onboard hydrogen storage, the gravimetric and volumetric hydrogen densities should be higher than 7.5 mass% and 70 kg/m^3, respectively.[25, 70] Here, I list some of the metal borohydrides with hydrogen density that meet the ultimate target, as shown in Table 1.2.[71-72] At least 9 kinds of metal borohydrides are included in the candidate range to be developed, the highest hydrogen density of $Be(BH_4)_2$ up to 20.8 mass% is far higher than that of demanded value of 7.5 mass%. Though $Be(BH_4)_2$ is not suitable for hydrogen storage because of

its high volatility, reactivity and extreme toxicity,[24] other borohydrides also with high H_2 density such as $LiBH_4$ (18.5 mass%, 122.1 kg/m^3), $NaBH_4$ (10.7 mass%, 114.5 kg/m^3), $Mg(BH_4)_2$ (14.9 mass%, 147.4 kg/m^3), $Ca(BH_4)_2$ (11.6 mass%, 124.1 kg/m^3) and $Zr(BH_4)_4$ (10.7 mass%, 126.2 kg/m^3) are promising to be developed as advanced high density hydrogen storage materials.

Table 1.2 Density and H_2 density of partial $M(BH_4)_n$ which meet ultimate target for hydrogen storage.[71-72]

$M(BH_4)_n$	Gravimetric Density (g/mol)	Volumetric Density (kg/L)	Gravimetric H_2 Density (mass%)	Volumetric H_2 density (kg/m^3)
$LiBH_4$	21.8	0.66	18.5	122.1
$NaBH_4$	37.8	1.07	10.7	114.5
KBH_4	53.9	1.17	7.5	87.8
$Be(BH_4)_2$	38.7	0.702	20.8	146.0
$Mg(BH_4)_2$	54.0	0.989	14.9	147.4
$Ca(BH_4)_2$	69.8	(1.07)	11.6	(124.1)
$Mn(BH_4)_2$	84.6	(1.24)	9.5	(117.8)
$Al(BH_4)_3$	71.5	0.79	16.9	133.5
$Zr(BH_4)_4$	150.6	1.179	10.7	126.2

Densities in brackets shows the value calculated from the crystal structure.

1.3.2 Synthesis of $M(BH_4)_n$

In 1940, Schlesinger and Burg et al firstly reported the synthesis of metal borohydrides using reaction between methyl derivatives and B_2H_6. $Al(BH_4)_3$, $Be(BH_4)_2$ and $LiBH_4$ are successfully synthesized according to the following equations [73-76]:

$$Al(CH_3)_3 + 2B_2H_6 \rightarrow B(CH_3)_3 + Al(BH_4)_3 \quad (1.6)$$

$$3Be(CH_3)_2 + 4B_2H_6 \rightarrow 2B(CH_3)_3 + 3Be(BH_4)_2 \quad (1.7)$$

$$3LiC_2H_5 + 2B_2H_6 \rightarrow B(C_2H_5)_3 + 3LiBH_4 \quad (1.8)$$

This method is difficult to synthesize large amount of borohydrides for the complicated preparation processes of metal alkyls especially the less volatile alkali metal alkyls. Besides that, this reaction kinetics is too slow and excess of B_2H_6 is

needed to remove alkyl groups.

Schlesinger et al discovered the reactions between B_2H_6 and metal hydrides in ethereal solvents produced borohydrides with high yields, the reaction equation is as follows:[77]

$MH_n + n/2B_2H_6 \rightarrow M(BH_4)_n$ (n = valence of M) (1.9)

Synthesis of borohydrides from simple substances of metal, boron and H_2 has also reported in German Patent in 1958 by Goerrig.[78] In this method, all the simple substances are treated at temperature more than 500 °C and with H_2 pressure more than 3 MPa, the reaction equation is like this:

$M + nB + 2nH_2 \rightarrow M(BH_4)_n$ (n = valence of M) (1.10)

This method is useful for synthesis of alkali and alkaline earth metal borohydrides.

For more types of metal borohydride synthesis, such as transition metal borohydrides, metathetical reactions using alkali metal borohydrides as starting materials would be useful routes.[79] The reaction equations are as follows:

$M'Cl_n + nMBH_4 \rightarrow M'(BH_4)_n + nMCl$ (n = valence of M', M = alkali metals) (1.11)

Aluminum borohydride and beryllium borohydride are available by metathesis of $LiBH_4$ or $NaBH_4$ with chlorides or bromides.[80] Other metal borohydrides such as $Mg(BH_4)_2$, $Zn(BH_4)_2$ and $Zr(BH_4)_4$ were also reported to be produced via this method.[81-84]

1.3.3 Hydrogen Storage Properties of $M(BH_4)_n$

$LiBH_4$ is the first example among metal borohydrides $M(BH_4)_n$ with 18.5 mass% H capacity, which was considered for hydrogen storage materials in 2003.[85] The decomposition processes of $LiBH_4$ experience three different steps which indicates the possible formation of intermediate compounds during its decomposition.[86] Theoretical calculation and experimental research confirmed the formation of $Li_2B_{12}H_{12}$ as intermediate.[87-89] Because of the high decomposition temperature of LiH (900 °C), the available H capacity of $LiBH_4$ is 13.9 mass%.[90] When $LiBH_4$ decomposes into $LiH + B + 3/2H_2$ with releasing 13.9 mass% H_2, the enthalpy and entropy changes are decided as 74 kJ mol^{-1} H_2 and 115 J K^{-1} mol^{-1} H_2, and the decomposition temperature at 1 bar of H_2 is 370 °C. The dehydrogenated $LiBH_4$ is rehydrogenated at 155 bar at 600 °C in 200 min with 8.3 mass% of hydrogen rehydrogenation.[91]

$Mg(BH_4)_2$ with 14.9 mass% H capacity is widely studied as potential hydrogen storage materials.[64, 72] $Mg(BH_4)_2$ loses all H when heated up to 600 °C, the decomposition processes also experience formation of complicated intermediates, as shown in Figure 1.8.[72, 92-95] $MgB_{12}H_{12}$ has been theoretically predicted and laboratory confirmed as one existent intermediate which is similar to that in $LiBH_4$.[89, 94, 96-98] The enthalpy and entropy changes of decomposition of $Mg(BH_4)_2$ to MgH_2 had ever been estimated by Matsunaga et al using PCT measurement as 39 kJ mol^{-1} H_2 and 91 J K^{-1} mol^{-1} H_2 , respectively.[99] However, the different values reported by Li et al were: ΔH = 57 kJ mol^{-1} H_2 and ΔS = 128 J K^{-1} mol^{-1} H_2, the different values may derive from different measurement conditions they used.[94] About 6.1 mass% of hydrogen can be rehydrogenated at 270 °C under 40 MPa of H_2 pressure for 48 h, the rehydrogenation product is $MgB_{12}H_{12}$.[94, 100] The rehydrogenation of decomposition products to $Mg(BH_4)_2$ is much more difficult than to $MgB_{12}H_{12}$ intermediate and it happens at about 400 °C under 90 MPa H_2 pressure for several days of keeping.[101-102]

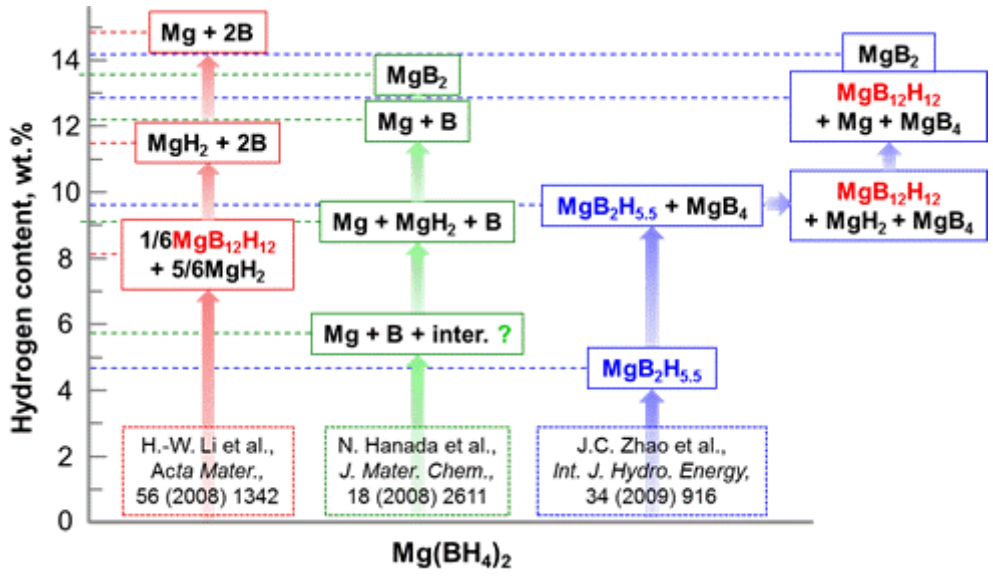

Figure 1.8 The observed decomposition processes of $Mg(BH_4)_2$ based on different reports.[72]

$NaBH_4$, $Ca(BH_4)_2$, $Y(BH_4)_3$ and $Ce(BH_4)_3$ are also reported to experience multistep dehydrogenation processes with formation of intermediates.[103-106] Other transition metal borohydrides (e.g. M = Zn, Zr, Ti) usually decompose at relatively low temperatures, but most of them are found to be not practical for hydrogen storage due

to their low melting temperatures and release of B_2H_6.[81, 107-109] Figure 1.9 shows the gaseous dehydrogenation products of some representative borohydrides, their decomposition temperatures and H-content are set as vertical and horizontal axes, respectively.[110] From the abovementioned fact, to carefully investigate the intermediate compounds in order to prevent their production or prompt their decomposition is essential for development of borohydride hydrogen storage systems for practical application.

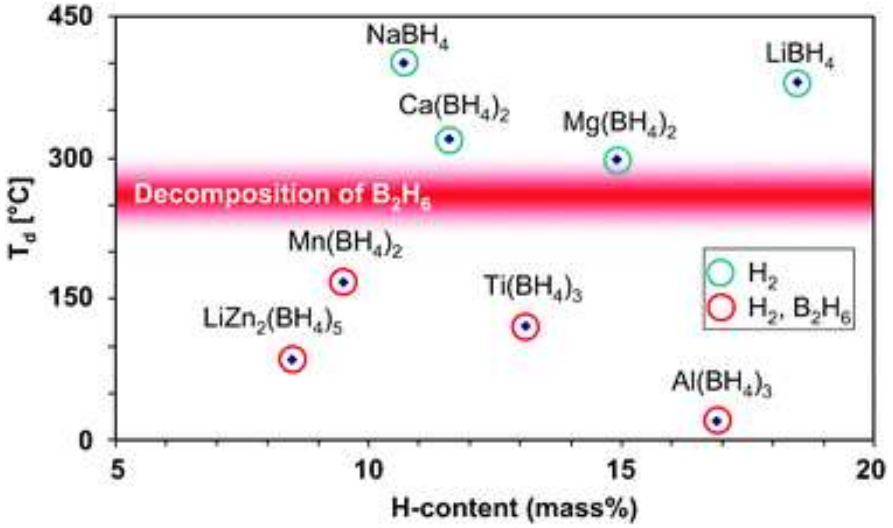

Figure 1.9 The gaseous dehydrogenation products of some representative borohydrides vs their decomposition temperatures and H-contents (**O:** borohydrides emit B_2H_6 and H_2; **O:** borohydrides mainly emit hydrogen).[110]

1.3.4 Improvement of Hydrogen Storage Properties in $M(BH_4)_n$

1.3.4.1 Thermodynamic Adjustment

1.3.4.1.1 Pauling Electronegativities

The formation enthalpy ΔH_f of $M(BH_4)_n$ may be estimated by the Pauling electronegativity χ_p of the corresponding M. Nakamori et al found the good linear relationship between ΔH_f of $M(BH_4)_n$ and χ_p of M, and also the negative correlation between the decomposition temperature T_d of $M(BH_4)_n$ and χ_p of M (Figure 1.10).[111] This finding indicates that to decrease the decomposition temperature of borohydrides can be achieved by improving electronegativities of the corresponding cations. Based on this finding, the thermodynamic stability is suggested to be tuned by producing bimetallic borohydrides $MM'(BH_4)_n$ in which M and M' with different electronegativities are mixed together.[112] Many bimetallic borohydrides such as

$LiZr(BH_4)_5$, $LiK(BH_4)_2$, $LiZn_2(BH_4)_5$, $Na_2Mn(BH_4)_4$ and $KSc(BH_4)_4$ have been successfully synthesized.[112-116] Most of $MM'(BH_4)_n$ present compromised thermodynamic stabilities between $M(BH_4)_n$ and $M'(BH_4)_n$ except few examples to produce huge $[M'(BH_4)_n]^{m-}$ clusters, e.g. $[Sc(BH_4)_4]^-$.[117]

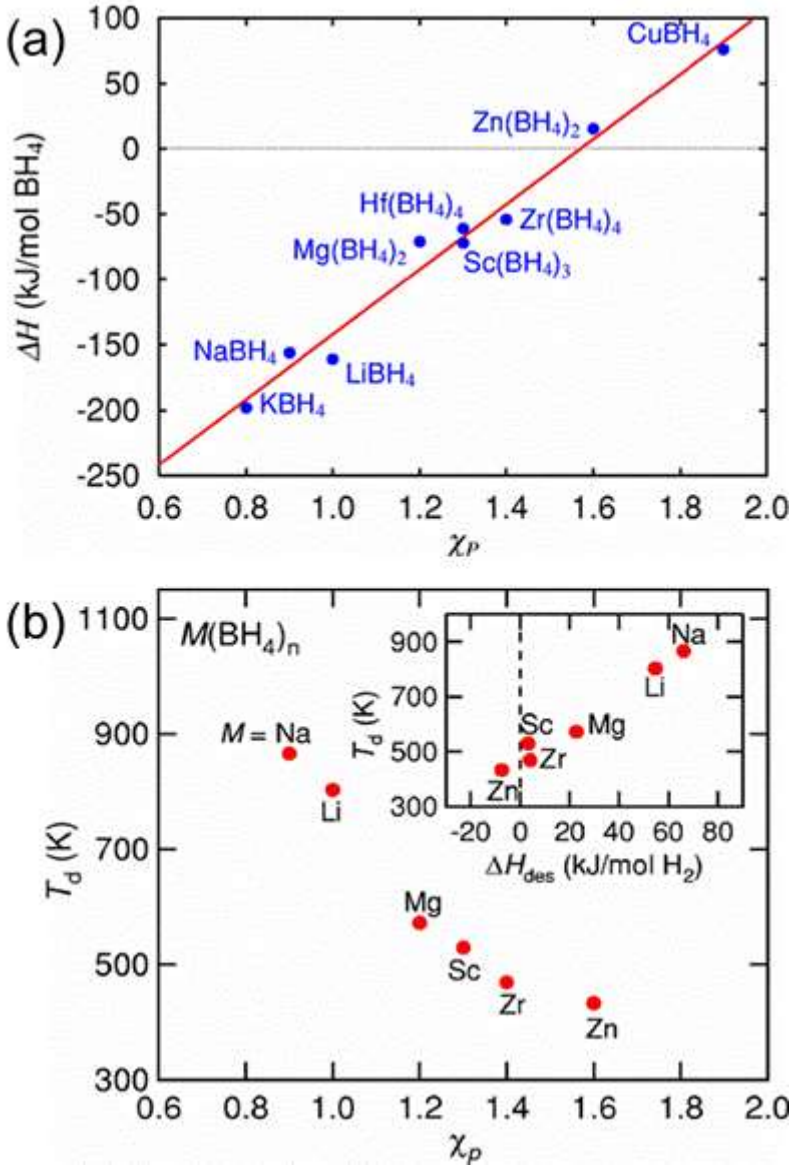

Figure 1.10 (a) the relationship between ΔH_f of $M(BH_4)_n$ and χ_p of M, and (b) the negative correlation between the decomposition temperature T_d of $M(BH_4)_n$ and χ_p of M.[111]

1.3.4.1.2 Combination

Enthalpy change of decomposition of $M(BH_4)_n$ can be reduced by making bimetallic borohydrides, the aim of this method is to destabilize the borohydrides. To

form more stable dehydrogenation products by combining $M(BH_4)_n$ with other materials such as metal hydrides, is another efficient method to reduce enthalpy change of dehydrogenation. Pure $LiBH_4$ decomposes into LiH with 13.8 mass% H release based on the following equation:

$$LiBH_4 \rightleftharpoons LiH + B + 3/2H_2 \quad (1.12)$$

The enthalpy change of this reaction is 67 kJ/mol H_2 and the equilibrium pressure of 1 bar will only be achieved above 400 °C. However, the enthalpy change can be reduced to 46 kJ/mol H_2 and the equilibrium pressure of 1 bar is achieved at about 225 °C if MgH_2 is combined to $LiBH_4$ according to the following equation:[118]

$$LiBH_4 + 1/2MgH_2 \rightleftharpoons LiH + 1/2MgB_2 + 2H_2 \quad (1.13)$$

Formation of more stable dehydrogenation product of MgB_2 not only decreases the decomposition temperature of $LiBH_4$, but also improved the reversibility. The $LiBH_4$ + $1/2MgH_2$ shows reversible hydrogen capacity 8-10 mass%.

More combination systems such as $LiBH_4$ + $1/6CaH_2$,[119] $LiBH_4$ + $1/4YH_3$,[120] $LiBH_4$ + $2LiNH_2$[121] and $Mg(BH_4)_2$ + $LiNH_2$[122] are subsequently developed to release H at lower temperatures than that of pure borohydrides. Among them, the $LiBH_4$ + $1/6CaH_2$ system with reaction enthalpy of 59 kJ/mol H_2 can reversibly store 9.1 mass% of hydrogen.[119]

1.3.4.2 Kinetic Improvement

1.3.4.2.1 Additives

Most borohydrides confront with the formation of complicated intermediates and sluggish kinetics. Many kinds of additives such as halides, metals, oxides and carbon materials have been investigated in order to enhance reaction kinetics.[123-126] Among them, halides present outstanding catalytic ability. For example, $LiBH_4$ + $0.2MgCl_2$ + $0.1TiCl_3$ system begins to dehydrogenate from 60 °C and can reversibly rehydrogenate 4.5 mass% H_2 at 600 °C at 70 bar of pressure;[127] The incubation period of the first dehydrogenation in $2LiBH_4$-MgH_2 system is substantially reduced by addition of 10 mol% $ZrCl_4$;[128] $TiCl_3$ is also an efficient additive to $Mg(BH_4)_2$ as the initial decomposition temperature which was reported to be reduced from 262 °C to 88 °C by introducing $TiCl_3$.[93]

1.3.4.2.2 Nanoconfinement

Incorporating borohydrides into nanoporous materials in order to fabricate and maintain the nanosized structure of metal borohydride structure, is efficient to shorten diffusion distance and enhance reaction kinetics and finally improve hydrogen storage properties. This method is firstly used to decrease H_2 release temperature and prevent borazine gas production in NH_3BH_3.[129] The hydrogen release rate in $LiBH_4$ was reported to be 50 times faster than that in neat $LiBH_4$, if it is incorporated into 13 nm pore size of carbon scaffolds.[130] Besides of that, the cycle stability in improved to be only 40 % capacity loss after three de/rehydrogenation cycles. The synergetic effects of nanoconfinement and metal Ni as additive can significantly improve the rehydrogenation rate and the rehydrogenation amount of $LiBH_4$.[131] The pore-size effects on nanoconfinement of $LiBH_4$ have been investigated by Liu et al, their finding shows both of dehydrogenation temperature and partial pressure of B_2H_6 monotonically decrease with shortening pore size.[132]

1.3.5 Challenges Caused by $M_{2/n}B_{12}H_{12}$ as Dehydrogenation Intermediate of $M(BH_4)_n$

Though the abovementioned progresses have been achieved, continuous efforts are expected to put on the further development of borohydrides for practical hydrogen storage materials. Formation of stable $[B_{12}H_{12}]^{2-}$ intermediate compounds resulting in high decomposition temperature and degraded reversibility of borohydrides, have been considered as critical obstacle to utilize borohydrides as practical hydrogen storage materials.

In 2006, $Li_2B_{12}H_{12}$ was predicted to be the most stable dehydrogenation intermediate (Figure 1.11) by Ohba et al using first-principles calculation. The proposed dehydrogenation/rehydrogenation processes via the formation of $Li_2B_{12}H_{12}$ are shown below:[88]

$$LiBH_4 \rightleftharpoons 1/12\ Li_2B_{12}H_{12} + 5/6LiH + 13/12H_2 \rightleftharpoons LiH + B + 3/2H_2 \quad (1.14)$$

The first confirmation of formation $Li_2B_{12}H_{12}$ during $LiBH_4$ decomposition in experiments was done by Orimo et al in 2006 using Raman spectra.[87] Followed by this achievement, formation of dehydrogenation intermediates comprised of $[B_{12}H_{12}]^{2-}$ have been also confirmed in decomposition of various borohydride systems, such as $LiSc(BH_4)_4$, $Mg(BH_4)_2$, $2NaBH_4 + MgH_2$, $Ca(BH_4)_2 + MgH_2$, $2LiBH_4 + MgH_2$, and

$Y(BH_4)_3$.[96, 100, 103, 133-135]

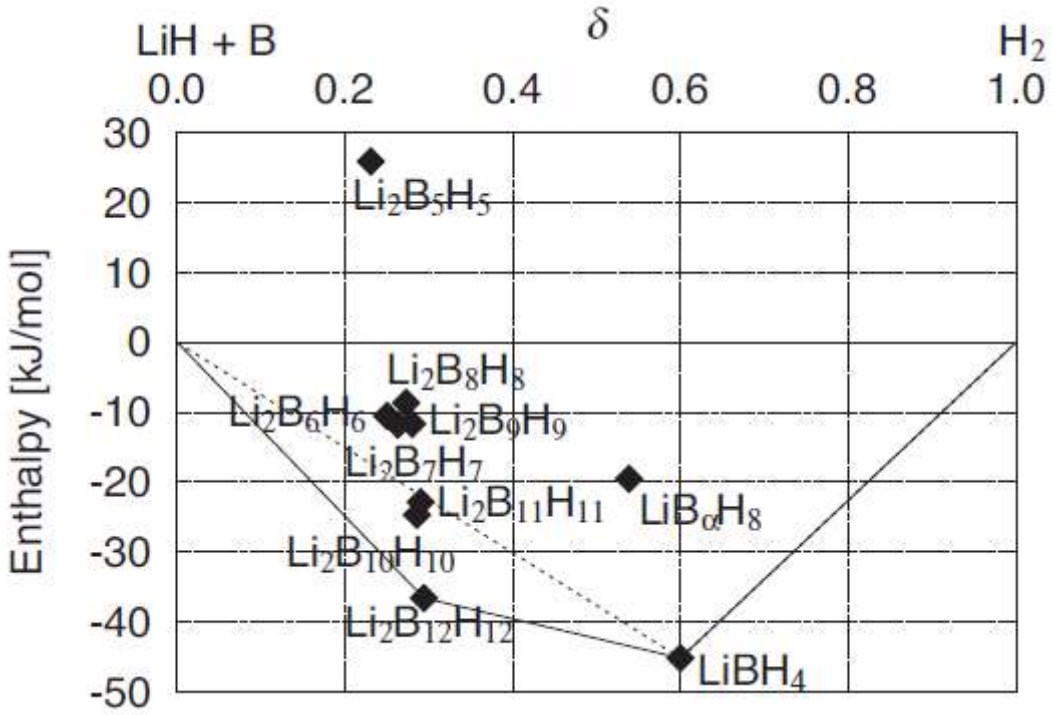

Figure 1.11 Formation enthalpy of LiB_xH_y where reactants are $(1-\delta)\times$[LiH+B] and δ mole H_2 (The solid line indicates the most stable products).[88]

The dependence of dehydrogenation products on hydrogen back pressure in borohydride systems was first observed by Bösenberg et al.[136] For the system of $2LiBH_4 + MgH_2$, the formation of MgB_2 rather than $Li_2B_{12}H_{12}$ above certain hydrogen back pressure (e.g. 0.3 MPa) was found to be critical for keeping the reversibility. Furthermore, upon heating ramp, $Li_2B_{12}H_{12}$ was formed at hydrogen pressures lower than 1.0 MPa. The formation of $Li_2B_{12}H_{12}$ was found to hamper the formation of MgB_2, as shown in Figure 1.12,[134] and thus degrade the reversibility of the $2LiBH_4 + MgH_2$ composite system. Similar phenomena that the formation of metal boride depending on the hydrogen back pressure are found in a series of $LiBH_4$-based reactive hydride composites including $4LiBH_4 + YH_3$, $6LiBH_4 + CeH_2$ and $6LiBH_4 + CaH_2$.[120] Therefore, systematic investigations and effective control of $[B_{12}H_{12}]^{2-}$ intermediates are indispensable for the improvement of rehydrogenation properties of borohydrides for practical applications.

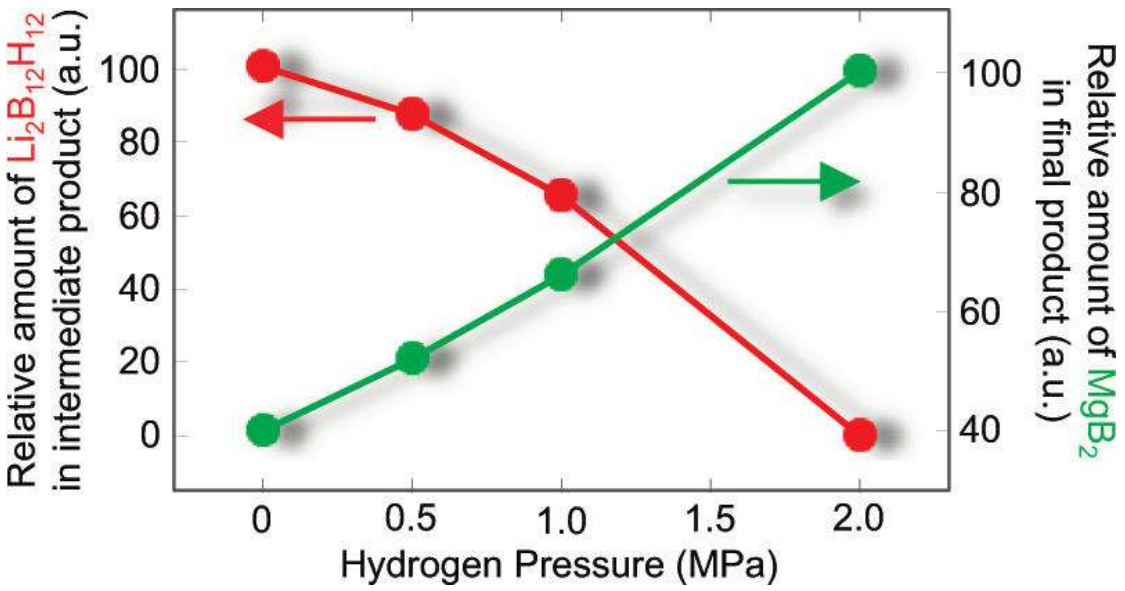

Figure 1.12 $Li_2B_{12}H_{12}$ and MgB_2 formation as a function to hydrogen back pressure in $2LiBH_4 + MgH_2$ system.[134]

1.4 Metal Dodecaborates $M_{2/n}B_{12}H_{12}$

Metal borohydrides with largest possibly reversible hydrogen capacity among the known hydrogen storage materials have been widely regarded as potential candidates for onboard hydrogen storage. Most of the meal borohydrides tend to experience stepwise decomposition accompanying with the formation of intermediates such as metal dodecaborates comprised of stable icosahedral boron cage of $[B_{12}H_{12}]^{2-}$. The $[B_{12}H_{12}]^{2-}$ intermediate with strong B-B bond in the icosahedral boron cage has been widely regarded as an obstacle for the rehydrogenation to $M(BH_4)_n$.[94, 133, 137-139] In this thesis I have been conducted to clarify the role of the $[B_{12}H_{12}]^{2-}$ intermediate. For that purpose, the nature of $[B_{12}H_{12}]^{2-}$ intermediate should be understood for the first step and then I carried out literature survey of this compounds and made the clear plan to investigation described in this thesis.

1.4.1 Structure and Properties of $M_{2/n}B_{12}H_{12}$

The structure of $[B_{12}H_{12}]^{2-}$ anion is schematically illustrated in Figure 1.13, the 12 B atoms configurate regular icosahedral skeleton and 12 H atoms link to 12 B atoms.[140] The length of adjacent B-H bond is 1.208 Å and that of adjacent B-B is 1.787 Å; the distance of B1-B12 is reported to be 3.360 Å and the cluster diameter measured by H1-H12 is calculated to be about 5.776 Å.[141] $[B_{12}H_{12}]^{2-}$ anion is very stable which had been predicted as early as in 1955 by Longuet-Higgins et al.[142] The

stability is derived from the spatial aromatic character of B-B bond in B_{12} cage. $[B_{12}H_{12}]^{2-}$ anion is easy to form a number of salts $M_{2/n}B_{12}H_{12}$ with various metal cations.[143] $M_{2/n}B_{12}H_{12}$ salts are soluble in water and easy to produce $M_{2/n}B_{12}H_{12}\bullet xH_2O$. $M_{2/n}B_{12}H_{12}$ with thermally stable cations such as Na^+ and Cs^+ display high stability, e.g. $Cs_2B_{12}H_{12}$ does decompose even heated up to 810 °C.[144] Because of its aromatic character, $[B_{12}H_{12}]^{2-}$ is used to produce various derivatives which are widely used in medicine and potentially applied for advanced rechargeable batteries.[143]

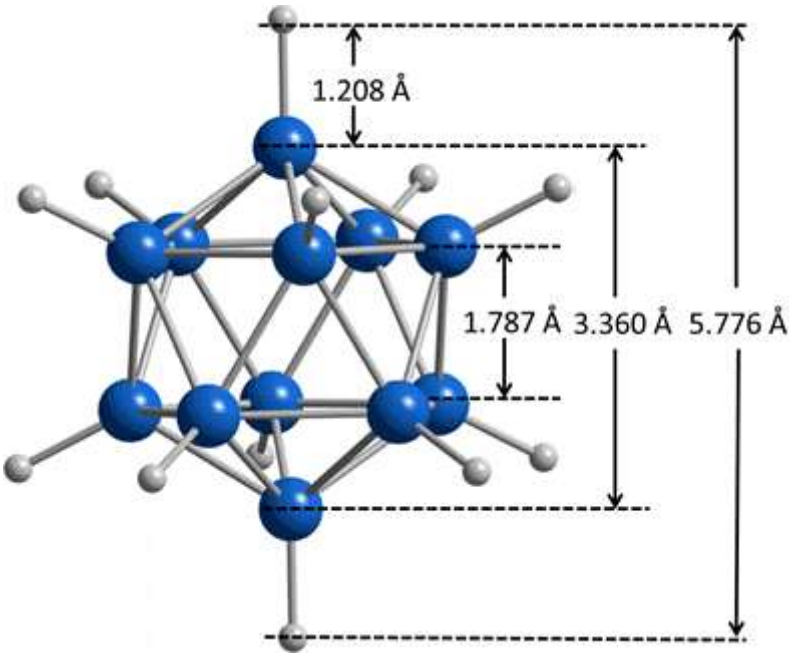

Figure 1.13 Schematic structure of icosahedral $[B_{12}H_{12}]^{2-}$ anion. Blue: B atoms; gray: H atoms.[140]

1.4.2 Conventional Synthesis Methods of $M_{2/n}B_{12}H_{12}$

The dodecaborate was firstly obtained in 1960 by Pitochelli and Hawthorne from the reaction between 2-iododecaborane and trimethylamine but with very low yield.[145] In 1963, Miller et al reported the route for $[B_{12}H_{12}]^{2-}$ synthesis, as shown in the following equation:

$$2Et_3NBH_3 + 5B_2H_6 \rightarrow (Et_3NH)_2B_{12}H_{12} + 11H_2 \quad (1.15)$$

and he found the obtained triethylammonium salt through this method is directly in analytical purity.[146] In 1967, Miller et al further found $B_{10}H_{14}$ can be used to replace B_2H_6, the reaction for $[B_{12}H_{12}]^{2-}$ production happens in ultrasene as follows:[147]

$$2Et_3NBH_3 + B_{10}H_{14} \rightarrow (Et_3NH)_2B_{12}H_{12} + 3H_2 \quad (1.16)$$

The produced $(Et_3NH)_2B_{12}H_{12}$ is subsequently reacted with aqueous solution of base to form crystalline hydrate of $M_{2/n}B_{12}H_{12}$, further dehydration will achieve anhydrous $M_{2/n}B_{12}H_{12}$, the steps are as follows:[147]

$$(Et_3NH)_2B_{12}H_{12} + 2/nM(OH)_n \xrightarrow{H2O} M_{2/n}B_{12}H_{12}\bullet xH_2O + 2Et_3N \quad (1.17)$$

$$M_{2/n}B_{12}H_{12}\bullet xH_2O \xrightarrow{Heat} M_{2/n}B_{12}H_{12} + xH_2O \quad (1.18)$$

This liquid phase method has been used for anhydrous dodecaborate $M_{2/n}B_{12}H_{12}$ synthesis for a long period as traditional procedure.[143, 148] The preliminary product synthesized via these liquid phase processes is $M_{2/n}B_{12}H_{12}\bullet xH_2O$, which subsequently needs careful dehydration processes to remove crystal water.[149-150]

Such careful dehydration process, however, causes the decomposition of $M_{2/n}B_{12}H_{12}$ and fails in the synthesis of anhydrous $M_{2/n}B_{12}H_{12}$. For example, the crystal water will react with $MgB_{12}H_{12}$ during the dehydration process according to the following equation:[151]

$$Mg(H_2O)_6B_{12}H_{12} \xrightarrow{200°C} Mg(H_2O)_3B_{12}H_{12} \xrightarrow{250°C} Mg(\mu\text{-}OH)_xB_{12}H_{12-x} \quad (1.19)$$

As a result, the liquid phase process is limited to synthesize the metal dodecaborate $M_2B_{12}H_{12}$ with relatively weak bonding with crystal water. Therefore, solvent-free synthesis process is in great need for the systematic investigation of anhydrous dodecaborates.

1.4.3 $M_{2/n}B_{12}H_{12}$ as a Potential Superionic Conductor

Polymorphism has been observed in metal dodecaborates especially the alkali metal dodecaborates $M_2B_{12}H_{12}$. In 2011, Verdal et al reported the second-order transition to reorientational disorder in cubic $K_2B_{12}H_{12}$, $Rb_2B_{12}H_{12}$ and $Cs_2B_{12}H_{12}$ were 578 °C, 469 °C and 256 °C, respectively.[152] Subsequently, the high temperature of phase transition in $Li_2B_{12}H_{12}$ and $Na_2B_{12}H_{12}$ were also reported by different research groups.[153-154] $Li_2B_{12}H_{12}$ exhibits first-order phase transition to β-$Li_2B_{12}H_{12}$ polymorph at 355 °C with ca. 8.7% expansion of unit cell volume, Figure 1.14 shows the discontinuous expansion of lattice parameter from α-phase to β-phase.[153] Verdal et al claimed that phase transition in $Li_2B_{12}H_{12}$ and $Na_2B_{12}H_{12}$ happen at about 342 and 256 °C, they also verified the largely enhanced anion mobility in high-temperature phases of the two cases and suggested their potential application as superionic conductors.[154]

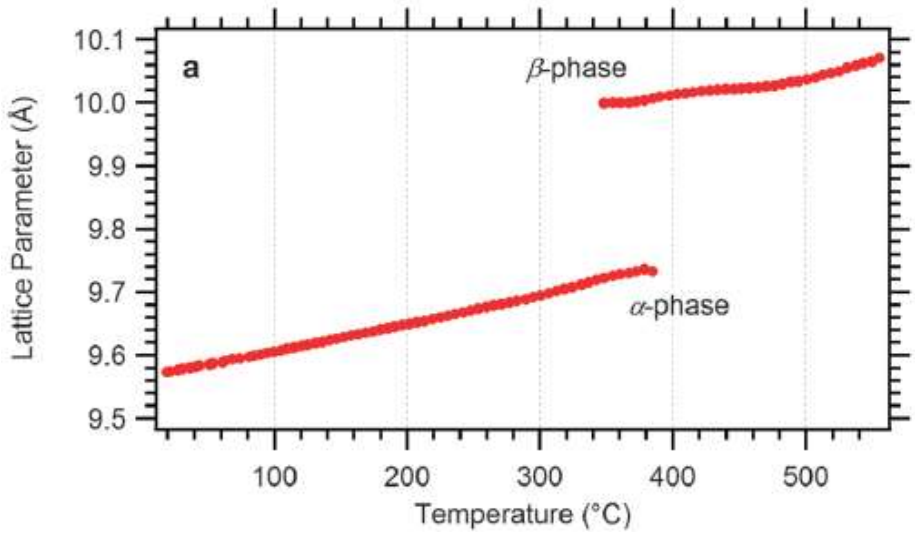

Figure 1.14 Temperature dependence of the lattice parameter in $Li_2B_{12}H_{12}$.[153]

In 2014, Udovic et al reported the superionic conductivity in $Na_2B_{12}H_{12}$. Their measurements show dramatically high superionic conductivity of 0.1 S cm^{-1} in high-temperature phase of disordered $Na_2B_{12}H_{12}$ between 267 and 300 °C, as shown in Figure 1.15.[155] This work open the gate to study dodecaborates as potential superionic conductor used for next-generation batteries, more analogous systems such as $Li_2B_{12}H_{12}$, $MgB_{12}H_{12}$ and multi-cation dodecaborates with potentially outstanding superionic conductivities are highly worthy to be investigated.

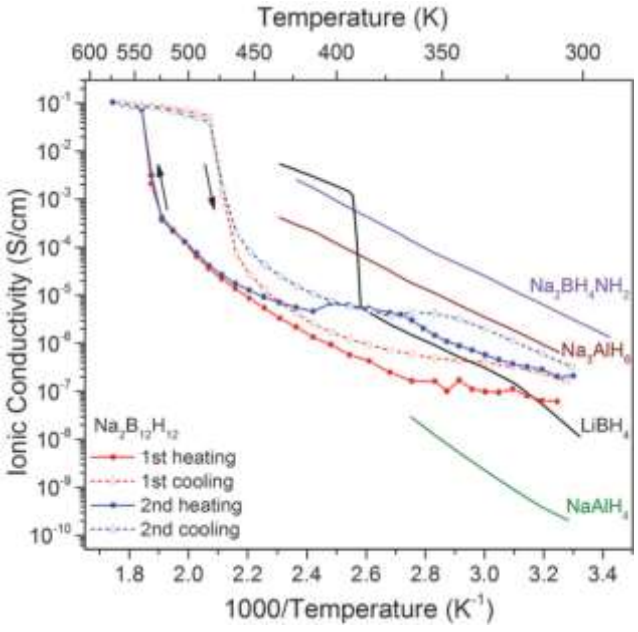

Figure 1.15 Temperature dependence of conductivity in $Na_2B_{12}H_{12}$ (other complex hydrides are shown for comparison).[155]

1.4.4 Current Issues

Systematic investigations of metal dodecaborate $M_{2/n}B_{12}H_{12}$ compounds are in great need from both strategies to improve hydrogen storage properties of metal borohydrides and to develop efficient superionic conductors used in commercial batteries.[72, 156] However, the current wet chemistry synthesis process is limited only to the $M_{2/n}B_{12}H_{12}$ which has weak bonding with water because the dehydration via heating under vacuum may result in the decomposition of $M_{2/n}B_{12}H_{12}$. Development of a solvent-free synthesis process is therefore the most important issue for the systematic investigations.[151] Comprehensive understanding of thermal stability, thermal decomposition mechanism and ionic conductivity are not possible because only few anhydrous $M_{2/n}B_{12}H_{12}$ can be synthesized via the conventional wet chemistry process. Furthermore, extensive efforts are expected to put on the destabilization of $M_{2/n}B_{12}H_{12}$ in order to improve the rehydrogenation for the reproduction of borohydrides aiming at onboard application, as well as the stabilization of $M_{2/n}B_{12}H_{12}$ for robust ionic conductors practically used in solid state rechargeable batteries.

1.5 Objectives of This Study

Metal dodecaborates $M_{2/n}B_{12}H_{12}$ as typical dehydrogenation intermediates of metal borohydrides $M(BH_4)_n$ have been attracting increasing interest as potential energy materials, especially in the context of high density hydrogen storage and super ionic conductivity.

In order to solve the abovementioned issues of metal dodecaborates, in this study, the first objective is developing solvent free synthesis process. Hinted by the reported synthesis processes of metal alanates $M(AlH_4)_n$ and metal amides $M(NH_2)_n$ that can be synthesized from the corresponding metal hydrides MH_n with AlH_3 or NH_3,[52] metal dodecaborates may be synthesized from the corresponding metal hydrides/metal borohydrides with boron hydrides such as diborane gas B_2H_6 or decaborane $B_{10}H_{14}$. B_2H_6, however, is difficult to handle because of its very high toxicity. Furthermore, the Gibbs free energies are estimated to be significantly negative, suggesting the exothermic reactions between metal hydrides/metal borohydrides with $B_{10}H_{14}$ producing the anhydrous metal dodecaborates.[157] In order to improve the synthesis

reactions, starting materials of metal hydrides/metal borohydrides with $B_{10}H_{14}$ are homogeneously mixed using ball milling and then heat treated at temperatures higher than the melting point (99.6 °C) of decaborane.

Systematic investigation of thermal decomposition behavior of metal dodecaborate is of great importance, not only for the improvement of rehydrogenation to produce metal borohydride, but also for figuring out the operation temperature range for ionic conductor application. The second objective of this study, therefore, is to elucidate the decomposition mechanism of metal dodecaborates comprised of alkali metals and alkaline earth metals to be synthesized by the developed solvent free process. The decomposition behaviors of metal dodecaborates are carefully compared with those of the corresponding metal borohydrides in order to understand the role of dodecaborate in the dehydrogenation of borohydrides and to figure out the clues to improve the rehydrogenation of borohydrides. Based on the understanding of the thermal decomposition mechanism, the thermal stabilities of metal dodecaborates are expected to be tuned for hydrogen storage or ionic conductor applications. The third objective is to figure out a strategy for tuning thermal stability of metal dodecaborates through designing bimetallic dodecaborates, because the thermal stabilities of metal borohydride systems are reported to be tuned by making bimetallic borohydrides.[72]

Inspired by the recently reported superionic conductivity in $Na_2B_{12}H_{12}$,[155] comparison on the ionic conductivities between bimetallic dodecaborates and its single counterparts is conducted, in order to achieve the fourth objective, i.e. to find clues for further improvement of ionic conductivity.

Through implementation of this study, the above objectives are expected to be achieved, which will provide profound impact on the understanding the decomposition mechanisms of both metal dodecaborates and also metal borohydrides. These important knowledges can not only provide important guiding principles for the significant improvement of rehydrogenation of metal borohydrides for the next generation high density hydrogen storage materials, but also contribute directly to the development of advanced hydrogen storage materials for FCV onboard applications that can drastically accelerate the spread of hydrogen mediated society. Furthermore, new guidance for designing superionic conductors is expected to be proposed and the development of dodecaborate based electrolyte with long-term cycle stability and

outstanding conductivity will significantly improve the energy storage performance of all solid state batteries.

Chapter 2

Experimental

In this chapter, sample synthesis and characterizations on crystal structure, chemical bonding, thermal analysis and ionic conductivity are described in detail.

2.1 Materials

Taking into account the high hydrogen density of alkali and alkaline earth metal borohydrides, I focus on the synthesis of their corresponding dodecaborate intermediates using the following chemical reagents. As listed in Table 2.1, commercial LiH (98%) was purchased from Alfa Aesar; $B_{10}H_{14}$ (99%) was purchased from Wako; NaH (95%), $LiBH_4$ (95%), $NaBH_4$ (99.99%), KBH_4 (98%), $Mg(BH_4)_2$ (95%) and $Ca(BH_4)_2$ (95%) were purchased from Aldrich. Among them, $Mg(BH_4)_2$ exhibits γ-phase and $Ca(BH_4)_2$ is comprised of α and β phases.[138, 158-159] All the chemical reagents are stored in a glove box (Figure 2.1) under Ar gas protection with O_2 (H_2O) density less than 1 ppm and used without further purification.

Table 2.1 Chemicals used in experiments.

Chemicals		Purity	Maker	CAS Number
$B_{10}H_{14}$	Decaborane	99.00%	Wako	048-22823
LiH	Lithium hydride	98%	Alfa Aesar	7580-67-8
NaH	Sodium hydride	95%	Aldrich	7646-69-7
$LiBH_4$	Lithium borohydride	95%	Wako	16949-15-8
$NaBH_4$	Sodium borohydride	99.99%	Aldrich	16940-66-2
KBH_4	Potassium borohydride	≥98%	Aldrich	13762-51-1
$Mg(BH_4)_2$	Magnesium borohydride	95%	Aldrich	16903-37-0
$Ca(BH_4)_2$	Calcium borohydride	95%	Aldrich	17008-95-0

Figure 2.1 The glove box with gas purification system.

2.2 Methods

Here are the synthesis and characterization methods I used in our experiments, their mechanisms and the measurement conditions are introduced.

2.2.1 Ball Milling

As shown in Figure 2.2, different proportions (mole rate) of starting materials such as $2LiH + 1.2B_{10}H_{14}$, $2NaH + 1.2B_{10}H_{14}$, $2LiBH_4 + B_{10}H_{14}$, $2NaBH_4 + B_{10}H_{14}$, $2KBH_4 + B_{10}H_{14}$, $Mg(BH_4)_2 + B_{10}H_{14}$, $Ca(BH_4)_2 + B_{10}H_{14}$ and $LiBH_4 + NaBH_4 + B_{10}H_{14}$ were firstly hand milled in Ar gas glove box for 10 min to make a homogeneous mixture. Then the powders were transferred into jars and seals with covers for mechanical milling. Fritsch P-7 ball milling machine was used for mechanical milling in our experiments. The powder state of starting materials were mechanically milled at room temperature using planetary ball mill with 10 steel balls (7 mm in diameter, 1.5 g in weight) in a hardened steel vial (30 cm^3 in volume) under 0.1 MPa Ar for 5 h (15 min milling, 5 min pausing). Every time about 0.3 g sample was ball milled to meet the powder to ball weight ratio as 1 : 50. The rotational speed was set as 400 rpm. After ball milling, samples were retrieved and stored in Ar gas glove box for the next step of heat treatment.

Figure 2.2 Preparations for ball milling.

2.2.2 Heat Treatment

The ball milled samples were sealed into stainless steel crucibles (~0.7 cm^3 in volume, 38.3 g in weight for every set), the sample weight was controlled to be about 0.12 - 0.13 g in order to keep a crucible to sample weight ratio around 300 : 1 for every heat treatment. Then the sealed crucibles were further sealed in stainless steel tube, all the operation procedures were finished in Ar gas glove box. Subsequently the tube was put in Muffle furnace for heat treatment with 1 to 20 h at temperature range of 200 to 450 °C, the temperature was controlled by temperature controller made by SHINKO TECHNOS CO., LTD. Figure 2.3 schematically illustrates the heat treatment apparatus.

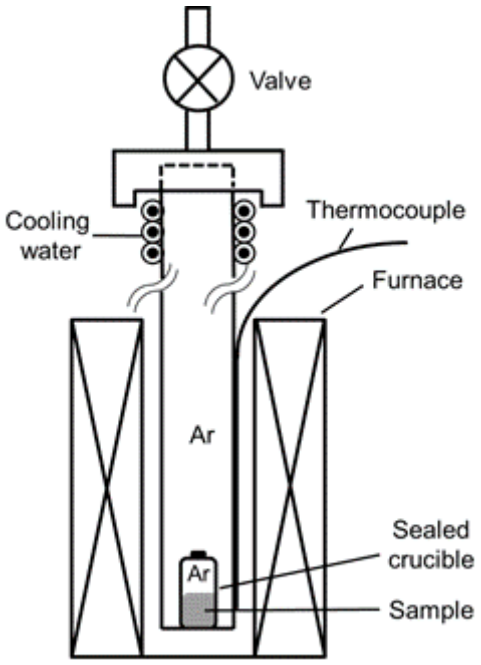

Figure 2.3 Schematic illustrations of the heat treatment apparatus.[157]

2.2.3 X-ray Diffraction (XRD)

Powder X-ray diffraction (XRD) is a kind of effective method to analyze the crystalline structures of samples. X-ray is a kind of radiation wave and crystal can be treated as gratings of X-ray. If X-ray passes through crystal structures, the coherent scatter will result in wave interference which increases or decreases the intensity of X-ray. The intensity addition in a few angles is determined by Bragg's law (Figure 2.4): [160]

$$2d\sin\theta = n\lambda \qquad (2.1)$$

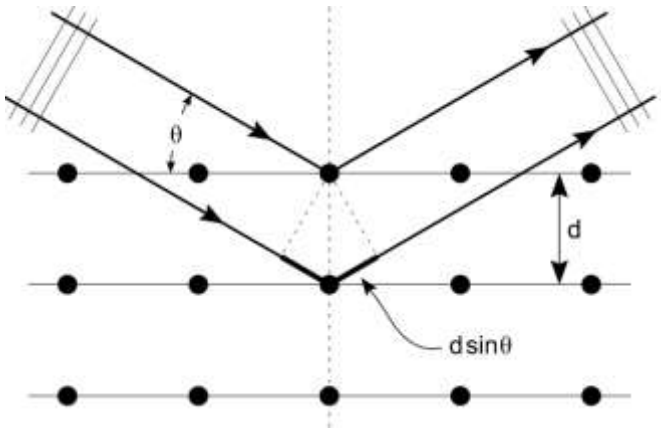

Figure 2.4 Schematic illustrations of Bragg's law.[160]

Here d is the distance between crystalline planes, θ is the random angle, n is integer, and λ is the wavelength of the X-ray. The different peaks appeared in the diffraction pattern reflect the regular array of scatters and as well as the arrangement of atoms in different crystals.[160] Now more than tens of thousands of crystalline structure data have been collected in The International Centre for Diffraction Data (ICDD), I can simply analyze the crystalline structures of my unidentified samples by comparing the XRD results with ICDD.[161]

Powder X-ray diffraction (XRD) patterns were obtained from Rigaku Ultima IV X-ray diffractometer with Cu-Kα radiation (λ = 1.54 Å) with accelerating voltage and tube current as 40 kV and 40 mA. The powder state of samples was paved in a glass plate/ single crystal silicon plate sealed by Scotch tape to prohibit contamination by air during the measurement (Figure 2.5).

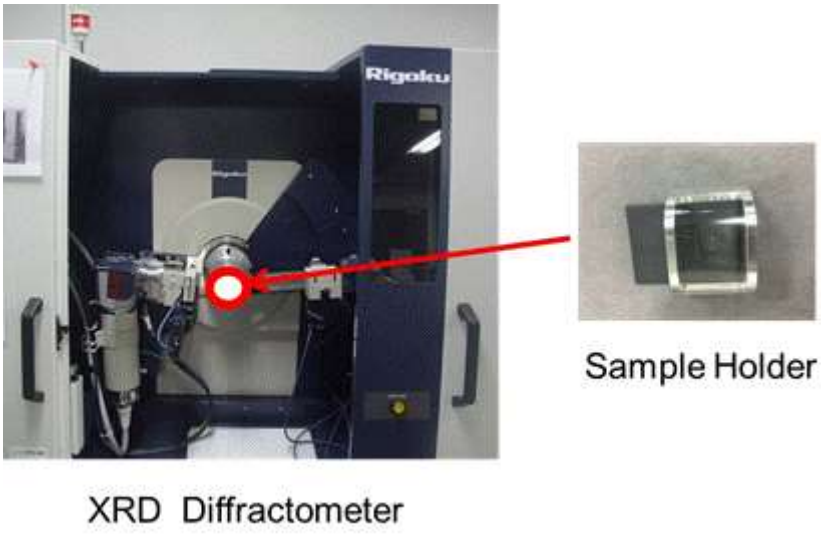

Figure 2.5 X-ray diffraction measurements.

2.2.4 Raman Spectra

Raman scattering indicates the frequency change of the incident light after being scattered by substances. The scattered light with different frequency from that of incident light, reflects the information of molecular vibration and rotation and then molecular structures. Raman spectra are scattering spectra which can be applied for structure analysis. In our experiments, Raman and In-situ Raman spectra were observed on RAMAN-11 VIS-SS (Nanophoton) machine via a laser with 532 nm wavelength (green).

As shown in Figure 2.6, for room temperature Raman measurement, samples were smoothly paved on the bottom of Al crucible (5 mm in diameter) and then sealed into squared stainless steel chamber (80 mm × 68 mm) with transparent glass cover in Ar gas glove box to avoid oxidation and deliquescence during measurement; For in-situ Raman measurement, samples were also smoothly paved on the bottom of Al crucible (5 mm diameter) but then sealed into circular stainless steel chamber (20 mm in inner diameter, 49 mm in outer diameter) with transparent glass cover in Ar gas glove box. The chamber was then linked to high pressure He or H_2 pipes to change measurement atmosphere using auto connector, linked to THERMO CONTROLLER TC-100 WA to tune temperature of sample and linked to cooling water to cool down the chamber. 50 magnification of lens was used for signals collection and the center wavenumber was set as 2000 cm^{-1}.

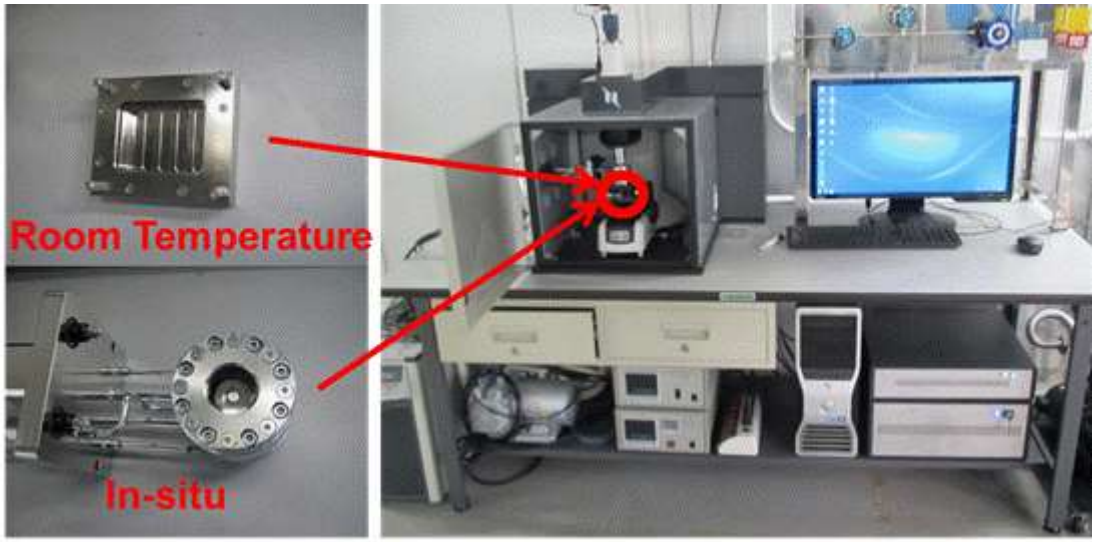

Figure 2.6 Room temperature and in-situ Raman spectra measurements.

2.2.5 Nuclear Magnetic Resonance (NMR)

The spin levels of nuclei with non-zero magnetic moment experience Zeeman splitting into more energy levels under an external magnetic field, this physical process resonantly absorbs a certain radio frequency radiation and is so called NMR. NMR is affected by many kinds of interactions such as anisotropy of chemical shift and dipole - dipole interaction. In solution-state NMR measurement, the fast motion of molecules cancels out these interactions and the inherent NMR spectra of molecules can be obtained; For the solid-state NMR measurement, the fast motion of molecules is restricted and the NMR signal is interfered by various interactions which result in low resolution of solid-state NMR spectra. Because of the necessity of solid-state NMR for analysis of solvent-undissolved samples, to improve the resolution of solid-state NMR is important. Magic angle spinning (MAS) technology using high speed of spinning of rotors in the special angle (54.73°) to the static magnetic field, can effectively cancel out various interactions in solid samples and achieve similar high resolution to that in solution-state NMR. Figure 2.7 shows the schematic illustrations of solid-state MAS-NMR.[162]

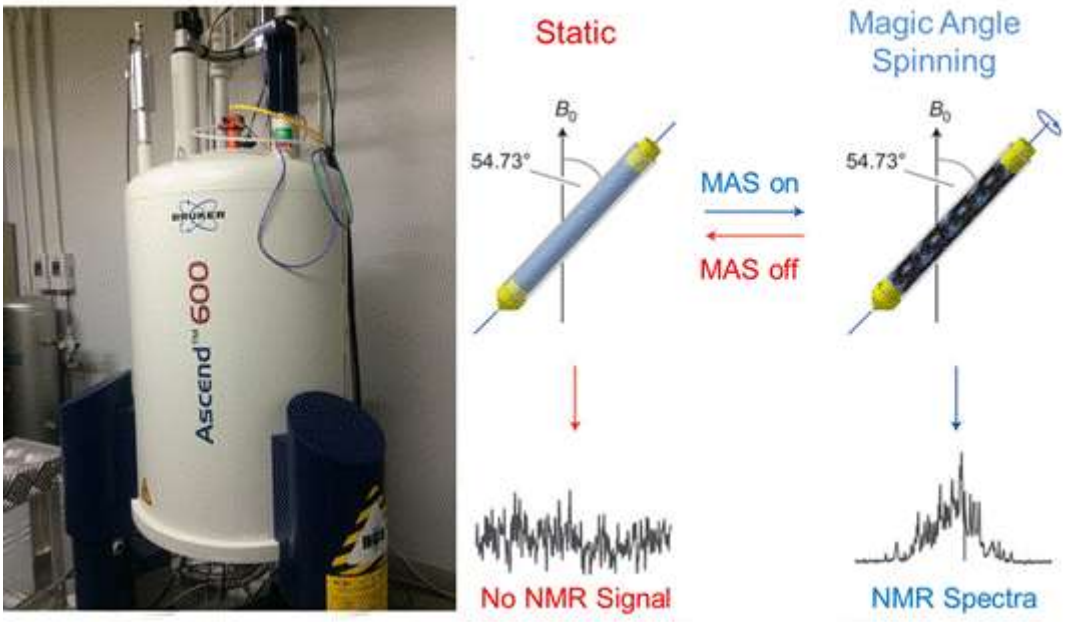

Figure 2.7 Schematic illustrations of solid-state MAS-NMR.[162]

Solution-state ^{11}B NMR spectra were carried out by Bruker Ascend-600 using 5 mm × 178 mm NMR sample tubes, dimethyl sulfoxide (DMSO-d_6) was used as solvent and saturated $B(OH)_3$ aqueous solution at 19.4 ppm was used as external standard sample.

Solid-state magic angle spinning (MAS) nuclear magnetic resonance (NMR) spectra were recorded using a Bruker DSX-500 or Bruker Ascend-600 spectrometer and boron background free 4 mm Bruker MAS probe at room temperature. NMR samples were pressed and sealed in 2.5 mm rotors for spinning, the preparations of samples were always finished in glove box protected by pure Ar gas and sample spinning was achieved using dry N_2 gas. ^{11}B MAS NMR spectra were obtained after a short pulse (0.5 μs – π/12 pulse used in DSX-500, 6.5 μs – π/2 pulse used in Ascend-600) and with strong ^{1}H decoupling pulses, spinning speeds were set as 14 kHz in DSX-500 and 16 kHz in Ascend-600. BF_3OEt_2 (δ = 0.00 ppm) was used as external standard for confirmation of ^{11}B NMR chemical shifts.

2.2.6 Thermogravimetry (TG)

The TG instrument is usually used for thermal analysis, it continuously records the weight change of a sample when it is heated to certain temperatures. With the temperature increasing, different components of the sample decompose and the

weight change percentage can be continuously observed. The weight change curve can be made as a function of temperature or time for practical needs. In our TG measurement recorded by Rigaku Thermo Plus Evo II TG-DTA 8120/S AEMK, samples were put into 5 mm Al or Pt pots and 200 ml/ min He flow was used to protect the sample and take out gas-state decomposition products. Figure 2.8 shows the TG and DSC instruments I used.

TG DSC

Figure 2.8 TG and DSC instruments.

2.2.7 Differential Scanning Calorimetry (DSC)

Differential Scanning Calorimetry (DSC) is another kind of thermoanalytical technique. In DSC measurement, the temperature program is designed to keep the linear correlation between sample holder temperature increasing and time, both the sample and reference are kept at the same temperature though the temperature changes. Different heat requirements for heating the sample and the reference are recorded as a function of time or temperature. In our experiments, samples were placed in 5 mm Al pots, DSC profiles were examined by Thermo plus2 DSC8230HP AEMK under different pressures of H_2 or He with a gas flow rate of 200 ml/min.

2.2.8 Mass Spectrometry (MS)

Mass spectrometry (MS) is a kind of structural analysis method through measurement of the mass-to-charge ratio and ion abundance. Motive ions in electric and magnetic fields meet the following equation:[163]

$$(m/q)\mathbf{a} = \mathbf{E} + \mathbf{Bv} \quad (2.2)$$

where m is ion mass, q is ion charge, **a** is acceleration, **v** is ion velocity and **E** and **B**

are electric and magnetic fields, respectively. Ions with different mass-to-charge ratios (*m/q*) are separated and detected by mass analyzers. The common mass spectrometer is comprised of ion source, magnetic field and detector, the vacuum system is also needed to protect electron gun and the charged particle beams. Figure 2.9 indicates the configuration of a simple mass spectrometer.[163] In our experiments, MS was linked to TG using 5 - 10 °C/min of heating ramp under 1 bar of He with 200 ml/min flow, it was recorded by quadrupole mass spectrometer.

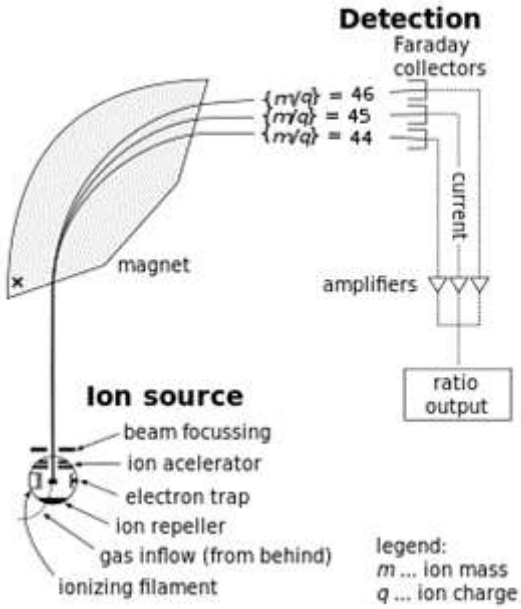

Figure 2.9 Schematic illustrations of a simple mass spectrometer.[163]

2.2.9 Deliquescence

For deliquescence experiments, samples were firstly put into the 5 mm Al pots in glove box and then transferred into air in laboratory with relatively humidity of 35% at 20 °C. The deliquescence time was calculated from taking samples out of glove box.

2.2.10 Synchrotron XRD Measurement

High-resolution X-ray powder diffraction patterns were measured at variable temperature using a synchrotron radiation source at BM1A station at the Swiss-Norwegian Beam Lines at the ESRF (λ = 0.68857 and 0.698509 Å, Pilatus 2M hybrid pixel detector). Nominal sample-to-detector distances (344 mm), coordinates of beam center and detector tilts were calibrated using LaB_6 (NIST standard 660b). The powdered sample was filled in the sapphire single crystal capillary for the

experiment with H_2 pressure and in the quartz capillary for the experiment without pressure load. All manipulations were done in the argon-filled glove box ($p(O_2, H_2O)$ < 1 ppm). First capillary was placed in a specially developed *in situ* sample cell for investigation of solid-gas reactions.[164] The samples were heated with a rate of 5 °C/min in P(Ar) ≈ 1 bar and $P(H_2)$ ≈ 160 bar. Raw powder diffraction data were processed (calibration, integration) using the Fit2D program.[165] Uncertainties of the integrated intensities were calculated at each 2θ-point by applying Poisson statistics to the intensity data, considering the geometry of the 2D detector.[166-167] The structures were refined by the Rietveld method using a Fullprof Suite software.[168]

2.2.11 Ionic Conductivity

Ionic conductivities were measured with electrochemical impedance spectroscopy for the sample pressed into a pellet with a diameter of 8 mm and a thickness of approximately 2 mm.[169] Cu foils with a thickness of 20 μm were used as electrodes, which were mechanically fixed on both sides of the pellet sample in an air-tight cell (Hohsen, HS-cell, Figure 2.10). Impedance plots were measured at the open circuit potential between 27 and 277 °C using a frequency response analyzer (Ono Sokki, DS-2100/DS-266/DS-273) combined with a potentio/galvanostat (Hokuto Denko, HA-301) in a frequency range from 0.1 MHz to 1 Hz. Ionic conductivities of the sample were derived from the high frequency resistances obtained by the complex nonlinear least-squares fitting (Scribner, Z-View) for the impedance spectra.[169] The spectra did not exhibit clear separation of overlapping contributions of the bulk and grain boundary. All the sample preparations and the air-tight cell assembly were always handled in a glove box protected by purified Ar gas. Transport number of Lithium ion was measured by potentiostatic polarization measurement.[170-171] Time variations of the current were recorded by a data logger (GRAPHTEC, midi LOGGER GL820) for the sample sandwiched by Li foil electrodes with a thickness of 100 μm in the air-tight cell under constant potential differences with time applied between the electrodes by the potentio/galvanostat.

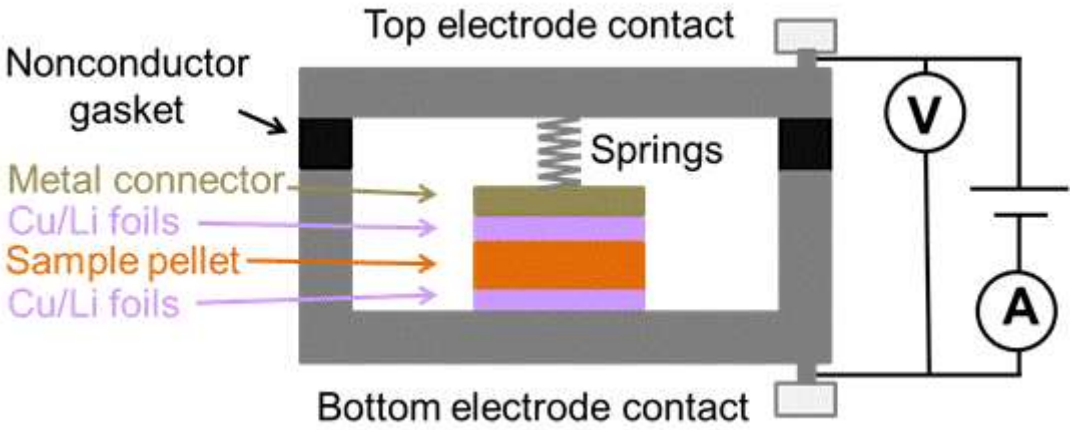

Figure 2.10 Schematics of air-tight cell for ionic impedance measurement using 4-point probes method.

Chapter 3

Synthesis and Decomposition of Anhydrous Alkali Metal Dodecaborates $M_2B_{12}H_{12}$ (M = Li, Na, K)

The chapter is based on the published and to be submitted papers:

He L, Li H-W, Hwang S.-J, Akiba E, Facile Solvent-Free Synthesis of Anhydrous Alkali Metal Dodecaborate $M_2B_{12}H_{12}$ (M= Li, Na, K). *The Journal of Physical Chemistry C* **2014**, *118*, 6084-6089.

He L, Li H-W, Akiba E, Thermal Decomposition of Anhydrous Alkali Metal Dodecaborate $M_2B_{12}H_{12}$ (M = Li, Na, K). To be submitted to *Energies*.

In this chapter, a facile solvent-free synthesis process of anhydrous dodecaborates is developed via heat treatment of metal hydrides (MH) or metal borohydrides (MBH_4) with $B_{10}H_{14}$. By such method, anhydrous alkali metal dodecaborates $M_2B_{12}H_{12}$ (M= Li, Na, K) has been successfully synthesized as case studies. Furthermore, systematic investigations on the thermal decomposition behaviors of the synthesized $M_2B_{12}H_{12}$ indicate a multistep decomposition accompanied with the formation of H-deficiency $M_2B_{12}H_{12-x}$ in the icosahedral B_{12} skeletons followed by the polymerization processes to produce $(M_2B_yH_z)_n$ polymers.

3.1 Introduction

Metal borohydride $M(BH_4)_n$ with high volumetric and gravimetric H_2 storage densities, has been researched for more than ten years as potential candidates for efficient hydrogen storage.[64, 72] Multistep reaction in decomposition processes of $M(BH_4)_n$ is found to accompany with the formation of complicated intermediate compounds, such as $[B_3H_8]^-$, $[B_5H_9]^{2-}$, $[B_{12}H_{12}]^{2-}$.[172-173] Among them, metal dodecaborates $M_{2/n}B_{12}H_{12}$ with strong B-B framework in the icosahedral cage has

been widely considered as a barrier of the rehydrogenation and results in the incomplete reversibility of $M(BH_4)_n$ along with cycled utilization.[87-88, 92, 94-96, 103, 133, 149, 172-175] As a result, it is important for us to systematically investigate the basic thermodynamic and kinetic properties of $M_{2/n}B_{12}H_{12}$ in order to finally improve the H_2 storage performance of $M(BH_4)_n$ for practical application.

$M_{2/n}B_{12}H_{12}$ is conventionally synthesized via wet chemistry processes, liquid organic reagent triethylamineborane (Et_3NBH_3) and aqueous solution of $M(OH)_n$ should be both used. The general multi-step processes are:[143, 146-148]

$$2Et_3NBH_3 + 5B_2H_6 \rightarrow (Et_3NH)_2B_{12}H_{12} + 11H_2 \quad (3.1)$$

or $$2Et_3NBH_3 + B_{10}H_{14} \rightarrow (Et_3NH)_2B_{12}H_{12} + 3H_2 \quad (3.2)$$

and $$(Et_3NH)_2B_{12}H_{12} + 2/nM(OH)_n \rightarrow M_{2/n}B_{12}H_{12} + 2Et_3N + 2H_2O \quad (3.3)$$

The preliminarily synthesized product is $M_{2/n}B_{12}H_{12}\bullet xH_2O$, anhydrous $M_{2/n}B_{12}H_{12}$ can be finally obtained after careful dehydrating process. [150, 176] Though partial anhydrous such as $Li_2B_{12}H_{12}$ and $Na_2B_{12}H_{12}$ have been successfully synthesized by this method, anhydrous $MgB_{12}H_{12}$ still can't be obtained from simple dehydration process of $Mg(H_2O)_6B_{12}H_{12}\bullet 6H_2O$ because of the reaction between crystal water and $[B_{12}H_{12}]^{2-}$ cluster, the solvent method may be only available for the synthesis of alkali metal dodecaborate $M_2B_{12}H_{12}$.[151] As a result, solvent-free methods are in great importance to be developed for synthesis of various anhydrous $M_{2/n}B_{12}H_{12}$.

In this chapter, I propose a facile solvent-free synthesis method of anhydrous $M_{2/n}B_{12}H_{12}$ via heat treatment (HT) of metal hydrides MH or metal borohydrides $M(BH_4)_n$ with low melting point (99.6 °C) of $B_{10}H_{14}$, as shown in the following equations:

$$2MH + 1.2B_{10}H_{14} \rightarrow M_2B_{12}H_{12} + 3.4H_2 \text{ (M = Li, Na)} \quad (3.4)$$

$$2MBH_4 + B_{10}H_{14} \rightarrow M_2B_{12}H_{12} + 5H_2 \text{ (M = Li, Na, K)} \quad (3.5)$$

I have also compared the reactivity via $2MH + 1.2B_{10}H_{14}$ and $2MBH_4 + B_{10}H_{14}$ routes for the purpose to improve the solvent-free synthesis method. HT of $2MBH_4 + B_{10}H_{14}$ as shown in equation (3.5) with fast kinetics is found to be a more feasible process for dodecaborate synthesis. Based on anhydrous alkali metal dodecaborates synthesized from equation (3.5), their thermal decomposition behaviors are further carefully investigated using thermogravimetry (TG), mass spectrometry (MS), X-ray diffraction (XRD), Raman spectra and nuclear magnetic resonance (NMR) spectra. Besides of that, the decomposition mechanisms of $M_2B_{12}H_{12}$ (M = Li, Na, K) are

discussed in comparison with those in-situ produced during the decomposition of corresponding borohydrides MBH_4, in order to search feasible routes for substantially improving the reversibility of borohydrides.

3.2 Experimental Section

$LiBH_4$ (95%, Aldrich), $NaBH_4$ (99.99%, Aldrich), KBH_4 (98%, Aldrich), LiH (98%, Alfa Aesar), NaH (95%, Aldrich) and $B_{10}H_{14}$ (99%, Wako) were all purchased from chemical companies and stored in glove box protected by pure Ar and used without purification. Different mole ratios of $2LiH + 1.2B_{10}H_{14}$, $2NaH + 1.2B_{10}H_{14}$, $2LiBH_4 + B_{10}H_{14}$, $2NaBH_4 + B_{10}H_{14}$ and $2KBH_4 + B_{10}H_{14}$ as starting materials were firstly mechanically milled by Fritsch P-7 ball milling machine at room temperature with 10 steel balls (7 mm in diameter) in a hardened steel vial (30 cm^3 in volume) under 0.1 MPa Ar for 5 h (15 min milling, 5 min pausing). Subsequently, the products after ball milling (BM) were sealed into stainless steel crucibles (~ 0.7 cm^3 in volume, 38.3 g in weight for every set) for HT at 200-450 °C with 10 to 20 h, respectively.

Powder X-ray diffraction (XRD) patterns were obtained from Rigaku Ultima IV X-ray diffractometer with Cu-Kα radiation (λ = 1.54 Å) with accelerating voltage and tube current as 40 kV and 40 mA. The powder state of samples was placed in a glass plate/ single crystal silicon plate sealed by Scotch tape to prohibit contamination by air during the measurement. Raman spectra were observed on RAMAN-11 VIS-SS (Nanophoton) machine via a laser with 532 nm wavelength (green). Gas release was analyzed by TG linked to MS, using 5 °C/min of heating ramp under 1 bar of He with 200 ml/min flow. TG and MS were recorded by Rigaku Thermo Plus Evo II TG-DTA 8120/S AEMK and quadrupole mass spectrometer, respectively.

In sample synthesis section, solid-state magic angle spinning (MAS) nuclear magnetic resonance (NMR) spectra were measured by a Bruker DSX-500 spectrometer and 4mm Bruker MAS probe without boron background at room temperature. ^{11}B MAS NMR spectra were obtained at excitation pulses of 0.5 μs（π/12 pulse) and with strong ^{1}H decoupling pulses. ^{11}B NMR peak simulation was carried out using Gaussian functions by Peakfit v4.12 software. In decomposition behavior investigation section, solid-state MAS NMR spectra were recorded by Bruker Ascend-600 spectrometer at room temperature. ^{11}B MAS NMR spectra were obtained at excitation pulses of 6.5 μs（π/2 pulse) and with strong ^{1}H decoupling pulses. NMR

sample preparations were always operated in glove box protected with pure Ar and sample spinning was achieved using dry N_2 gas. BF_3OEt_2 (δ = 0.00 ppm) was used as external standard for confirmation of ^{11}B NMR chemical shifts.

Solution-state ^{11}B NMR experiments were carried out using the same apparatus of Bruker Ascend-600, dimethyl sulfoxide (DMSO-d_6) was used as solvent and saturated $B(OH)_3$ aqueous solution at 19.4 ppm[177] was used as external standard sample.

3.3 Results and Discussion

3.3.1 Synthesis from 2MH + 1.2$B_{10}H_{14}$ (M = Li, Na)

XRD patterns and Raman spectra of samples synthesized from 2MH + 1.2$B_{10}H_{14}$ before and after HT are shown in Figure 3.1. After ball milling (BM), both 2LiH + 1.2$B_{10}H_{14}$ and 2NaH + 1.2$B_{10}H_{14}$ systems show XRD patterns of physical mixture of starting materials but without any new compounds. In Raman spectra only $B_{10}H_{14}$ was observed, which consistently indicates that chemical reaction between MH and $B_{10}H_{14}$

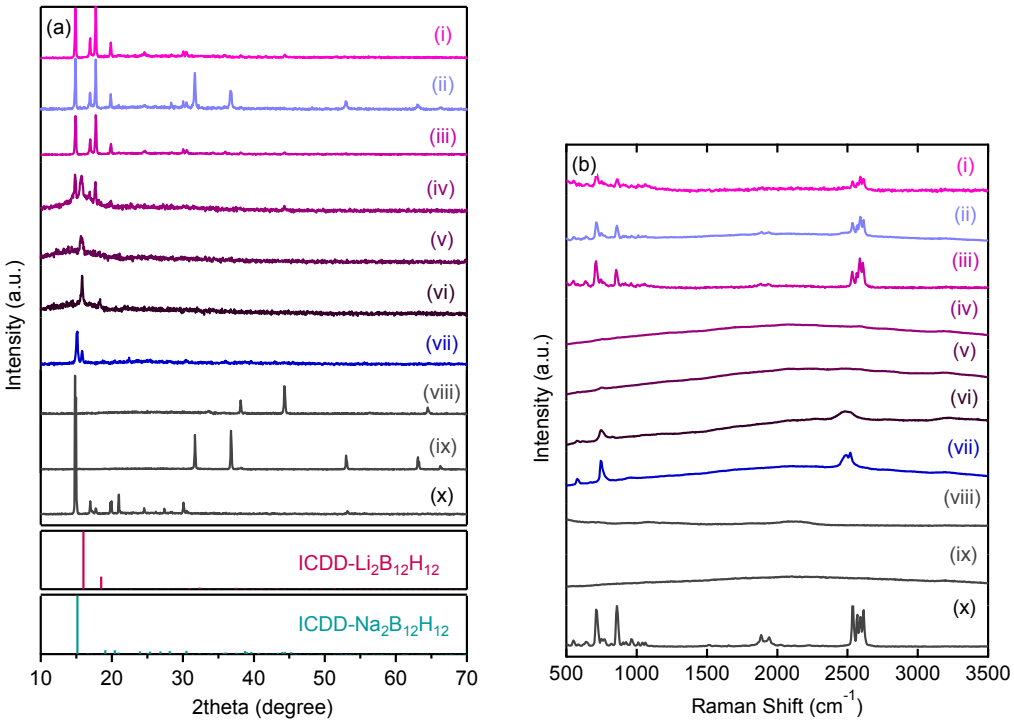

Figure 3.1 (a) XRD patterns and (b) Raman spectra of samples 2MH + 1.2$B_{10}H_{14}$ heat treated at different conditions. (i) 5 h BM of 2LiH + 1.2$B_{10}H_{14}$; (ii) 5 h BM of 2NaH + 1.2$B_{10}H_{14}$; (iii), (iv), (v) and (vi) are 5 h BM of 2LiH + 1.2$B_{10}H_{14}$ followed by HT at 200 °C for 10 h, 200 °C for 15 h, 250 °C for 15 h and 300 °C for 15 h, respectively; (vii) 5 h BM of 2NaH + 1.2$B_{10}H_{14}$ followed by HT at 450 °C for 20 h; (viii), (ix) and (x) are LiH, NaH and $B_{10}H_{14}$, respectively.

does not happen after BM.

In order to enhance the reaction between MH and $B_{10}H_{14}$, HT at optimized temperature was carried out in Ar atmosphere. HT of $2LiH + 1.2B_{10}H_{14}$ at 200 °C with 10 h does not show any new diffraction or Raman peaks except those from the residual starting materials of $B_{10}H_{14}$ and LiH. When the HT time was extended to 15 h, a new diffraction peak at 2θ = 15.80° ascribed to $Li_2B_{12}H_{12}$ comes out in XRD patterns, nevertheless, no obvious Raman bands from $Li_2B_{12}H_{12}$, $B_{10}H_{14}$ or LiH are found as a result of the strong fluorescence effect.[178]

Subsequently, the HT temperature was further increased to 250 °C and 300 °C. The diffraction peaks from $B_{10}H_{14}$ and LiH disappear and those from $Li_2B_{12}H_{12}$ are obviously observed under these two conditions. When HT of $2LiH + 1.2B_{10}H_{14}$ was carried out at 300 °C with 15 h, the other characteristic diffraction peak from $Li_2B_{12}H_{12}$ at 2θ = 18.35° becomes easily observed.[178] Raman spectra also indicate the production of $Li_2B_{12}H_{12}$. For HT of $2LiH + 1.2B_{10}H_{14}$ at 300 °C for 15 h, the B-H bending at 745 cm^{-1} and B-H stretching at 2500 cm^{-1} from $Li_2B_{12}H_{12}$ in Raman spectra are distinctly observed.[87, 134] Besides of those above mentioned, no signals of water are identified in Raman spectra of $2LiH + 1.2B_{10}H_{14}$ after HT, which means anhydrous $Li_2B_{12}H_{12}$ has been successfully synthesized. The experimental results show that HT of starting materials at appropriate conditions is in favor of synthesis of anhydrous $Li_2B_{12}H_{12}$ via interaction between $B_{10}H_{14}$ and LiH.

Based on the synthesis experience of $Li_2B_{12}H_{12}$, $Na_2B_{12}H_{12}$ was also synthesized by HT of starting materials $2NaH + 1.2B_{10}H_{14}$ after BM. For HT of $2NaH + 1.2B_{10}H_{14}$ at 450 °C with 20 h, Figure 3.1 indicates disappearance of diffraction peaks from NaH and $B_{10}H_{14}$ (starting materials), but appearance of $Na_2B_{12}H_{12}$ diffraction peaks at 2θ = 15.15°.[150] I also observe one low diffraction peak at 2θ = 15.80° and identify it as $Na_2B_{12}H_{12}\bullet xH_2O$ (Figure 3.2), which implies $Na_2B_{12}H_{12}$ is apt to deliquesce with absorbing water during the diffraction experiments. The B-H bending vibration modes at 500 to 1000 cm^{-1} and B-H stretching vibration modes at 2500 cm^{-1} from $Na_2B_{12}H_{12}$ are clearly observed in Raman spectra as shown as Figure 3.1(b). The successful synthesis of $Na_2B_{12}H_{12}$ via HT of $2NaH + 1.2B_{10}H_{14}$ is also consistently confirmed by both XRD patterns and Raman spectra.

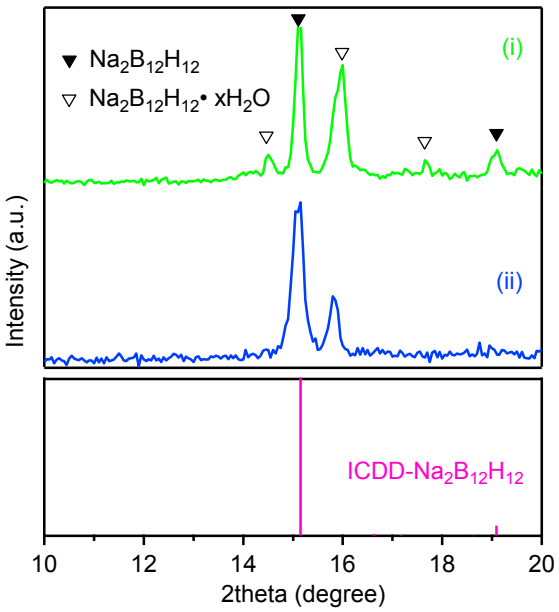

Figure 3.2 XRD patterns of $Na_2B_{12}H_{12}$ as synthesized. (i) 5h BM of $2NaBH_4$ + $B_{10}H_{14}$ followed by HT at 450 °C for 20 h (1 min exposure in air before measurement); (ii) 5h BM of 2NaH + $1.2B_{10}H_{14}$ followed by HT at 450 °C for 20 h.

3.3.2 Synthesis from $2MBH_4 + B_{10}H_{14}$ (M = Li, Na, K)

Figure 3.3 shows XRD patterns and Raman spectra of $2MBH_4 + B_{10}H_{14}$ (M = Li, Na, K) sample after BM and after BM with HT. Similar to that of $2MH + 1.2B_{10}H_{14}$, after BM, only signals of MBH_4 and $B_{10}H_{14}$ in diffraction patterns and Raman spectra can be observed, which means that the interaction between MBH_4 and $B_{10}H_{14}$ did not happen during BM. The starting materials of $2MBH_4 + B_{10}H_{14}$ after BM are still physical mixture, similar to that of $2MH + 1.2B_{10}H_{14}$ after BM.

A series of reaction conditions from both thermodynamics (reaction temperature) and kinetics (reaction time) for the interaction between MBH_4 and $B_{10}H_{14}$ to $M_2B_{12}H_{12}$ production have been explored and I found HT of $2MBH_4 + B_{10}H_{14}$ at the following optimized conditions largely improved yields of $M_2B_{12}H_{12}$: for M = Li, at 200 °C with 15 h, for M = Na, at 450 °C with 20 h and for M = K, at 450 °C with 20 h. After HT at the abovementioned conditions, diffraction patterns of MBH_4 and $B_{10}H_{14}$ disappear and new diffraction patterns identified as $M_2B_{12}H_{12}$ appear with cubic $Pa\bar{3}$

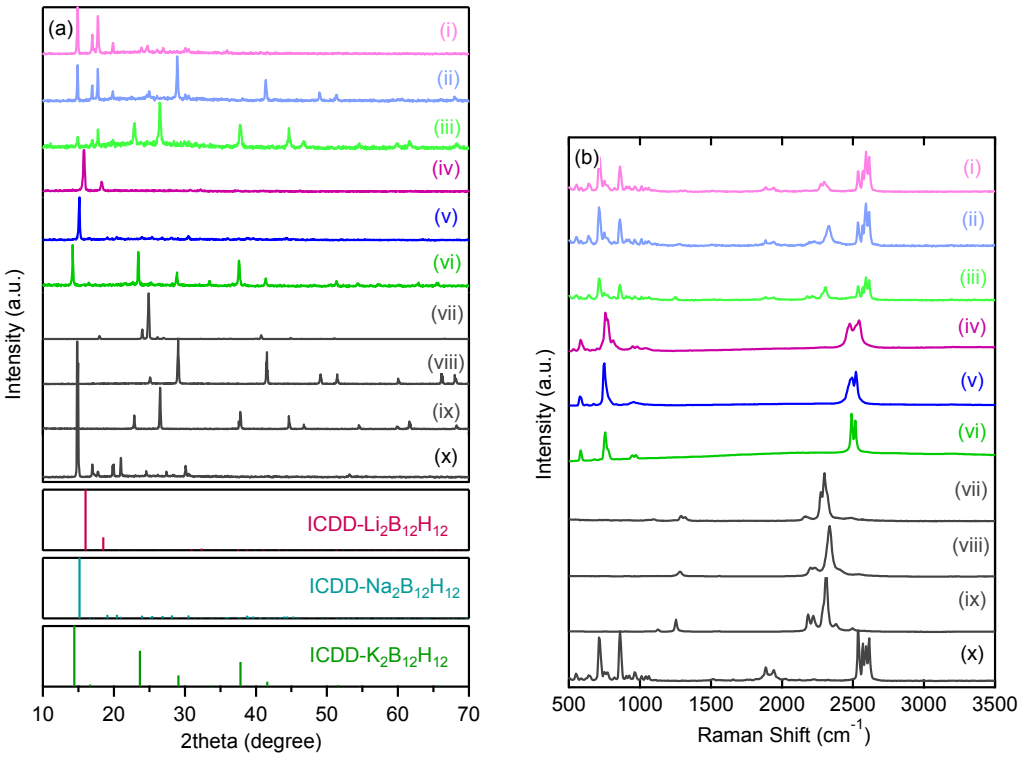

Figure 3.3 (a) XRD patterns and (b) Raman spectra of samples $2MBH_4 + B_{10}H_{14}$ heat treated at different conditions. (i) 5 h BM of $2LiBH_4 + B_{10}H_{14}$; (ii) 5 h BM of $2NaBH_4 + B_{10}H_{14}$; (iii) 5 h BM of $2KBH_4 + B_{10}H_{14}$; (iv) 5 h BM of $2LiBH_4 + B_{10}H_{14}$ followed by HT at 200 °C for 15 h; (v) 5 h BM of $2NaBH_4 + B_{10}H_{14}$ followed by HT at 450 °C for 20 h; (vi) 5 h BM of $2KBH_4 + B_{10}H_{14}$ followed by HT at 450 °C for 20 h; (vii), (viii), (ix) and (x) are $LiBH_4$, $NaBH_4$, KBH_4 and $B_{10}H_{14}$, respectively.

($Li_2B_{12}H_{12}$), monoclinic $P2_1/n$ ($Na_2B_{12}H_{12}$) and cubic $Fm\bar{3}$ ($K_2B_{12}H_{12}$) structures, respectively.[150, 179-180] The successful synthesis of alkali metal dodecaborates $M_2B_{12}H_{12}$ (M = Li, Na, K) from $2MBH_4 + B_{10}H_{14}$ are also proved by Raman spectra, i.e. the B-H vibration including bending and stretching modes from $[B_{12}H_{12}]^{2-}$ cluster are clearly observed from 500 to 1000 cm^{-1} and around 2500 cm^{-1}.[87] In $Li_2B_{12}H_{12}$ as synthesized, the Raman peaks at 584, 756, 772, 947, 2476 and 2543 cm^{-1} are ascribed to H_g, A_g, H_g, H_g, H_g and A_g modes, respectively.[181-182] No O-H signals of water are detected in Raman analysis, which indicates anhydrous $M_2B_{12}H_{12}$ (M = Li, Na, K) have been successfully synthesized via HT of $2MBH_4 + B_{10}H_{14}$.

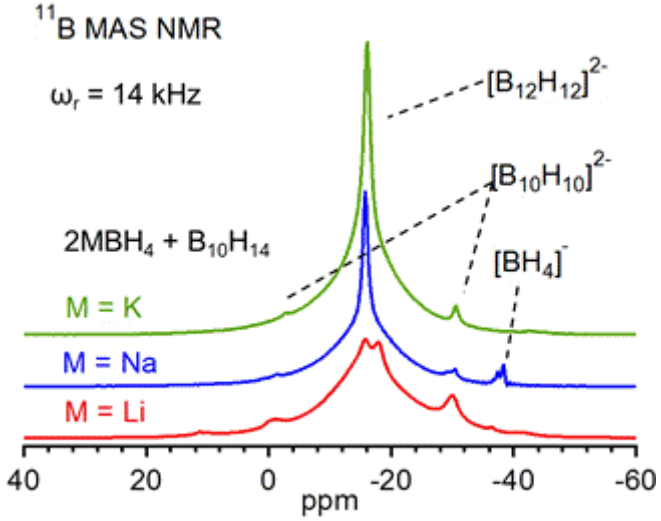

Figure 3.4 ^{11}B MAS NMR spectra of samples $2MBH_4 + B_{10}H_{14}$ heat treated at different conditions. (M = Li: 5h BM, HT at 200 °C for 15 h; M = Na: 5h BM, HT at 450 °C for 20 h; M = K: 5h BM, HT at 450 °C for 20 h)

^{11}B MAS NMR measurements in Figure 3.4 further proved the successful synthesis of $M_2B_{12}H_{12}$ via HT of $2MBH_4 + B_{10}H_{14}$. Resonance peak at chemical shift of about -16 ppm is ascribed to $[B_{12}H_{12}]^{2-}$ cluster.[96, 103, 183] Both $Na_2B_{12}H_{12}$ and $K_2B_{12}H_{12}$ show sharper resonance profile overlapped onto the broad resonance in comparison with that of $Li_2B_{12}H_{12}$, which implies that both $Na_2B_{12}H_{12}$ and $K_2B_{12}H_{12}$ exhibit two different mobility phases of the $[B_{12}H_{12}]^{2-}$ cluster. Considering molecular motion of metal dodecaborates $[B_{12}H_{12}]^{2-}$ can be well probed by ^{11}B spectral line and alkali-metal $[B_{12}H_{12}]^{2-}$ in ^{11}B MAS NMR spectra using similar MAS spinning rate exhibit a characteristic line width of ~ 2000 Hz for the center band if the crystallites are anhydrous.[176, 184] The ^{11}B MAS spectra of both synthesized $Na_2B_{12}H_{12}$ and $K_2B_{12}H_{12}$ are similar to that of $MgB_{12}H_{12}(H_2O)_6$ as reported.[176] ^{1}H MAS spectra of our synthesized $Na_2B_{12}H_{12}$ and $K_2B_{12}H_{12}$ (Figure 3.5) did not present peaks of crystal water, indicating no possibility that the observed mobile phases of $[B_{12}H_{12}]^{2-}$ clusters are related to possible contamination of H_2O.

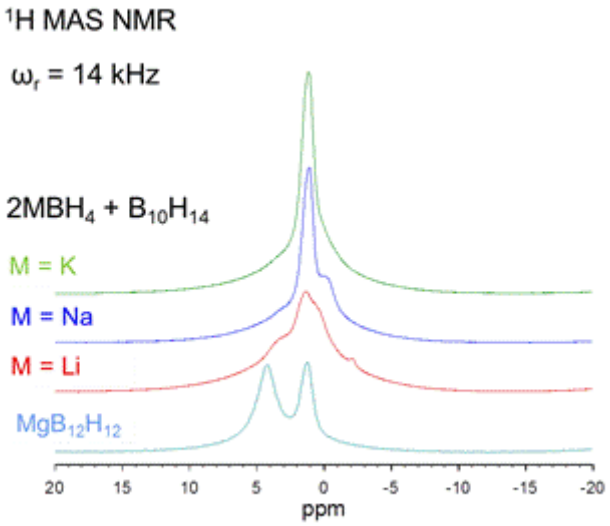

Figure 3.5 ^{1}H MAS NMR spectra of samples $2MBH_4 + B_{10}H_{14}$ heat treated at different conditions in comparison with $MgB_{12}H_{12}$. ($2LiBH_4 + B_{10}H_{14}$: 5h BM, HT at 200 °C for 15 h; $2NaBH_4 + B_{10}H_{14}$: 5h BM, HT at 450 °C for 20 h; $2KBH_4 + B_{10}H_{14}$: 5h BM, HT at 450 °C for 20 h)

Small amount of impurities from $M_2B_{10}H_{10}$ (~ 0 ppm and -30 ppm) and residual MBH_4 (about -38 ppm) can be observed in our synthesized $M_2B_{12}H_{12}$ samples. The residual MBH_4 would exist in nano size being confronted with different environment from that of the pure crystalline MBH_4, which results in 3-4 ppm upfield in comparison with those of $LiBH_4$ (-41 ppm)[92, 96] or $NaBH_4$ (-42 ppm)[103] as reported. There is another small resonance (< ~ 3% of total ^{11}B resonance) at -17.8 ppm is observed in the synthesized $Li_2B_{12}H_{12}$ sample, and it has not yet identified. I attribute this resonance to a contaminant but not from $Li_2B_{12}H_{12}$ in physically different environment, because mobile phase of $Li_2B_{12}H_{12}$ exhibits sharp peak at -15.6 ppm. The existence of contaminants is also observed in ^{1}H MAS NMR. The observed small amount of $M_2B_{10}H_{10}$ is suggested to originate from the reaction between MBH_4 and small molecules of boranes which may be produced from the complicated decomposition processes of $B_{10}H_{14}$.[178] Relative amount of the B-H species in the synthesized $Li_2B_{12}H_{12}$, $Na_2B_{12}H_{12}$ and $K_2B_{12}H_{12}$ is listed in Table 3.1 based on peak fitting using ^{11}B MAS NMR (Figure 3.6). Further improvement of the synthesis condition is pursued at present to increase the purity of $M_2B_{12}H_{12}$ obtained from HT of $2MBH_4 + B_{10}H_{14}$ as starting materials.

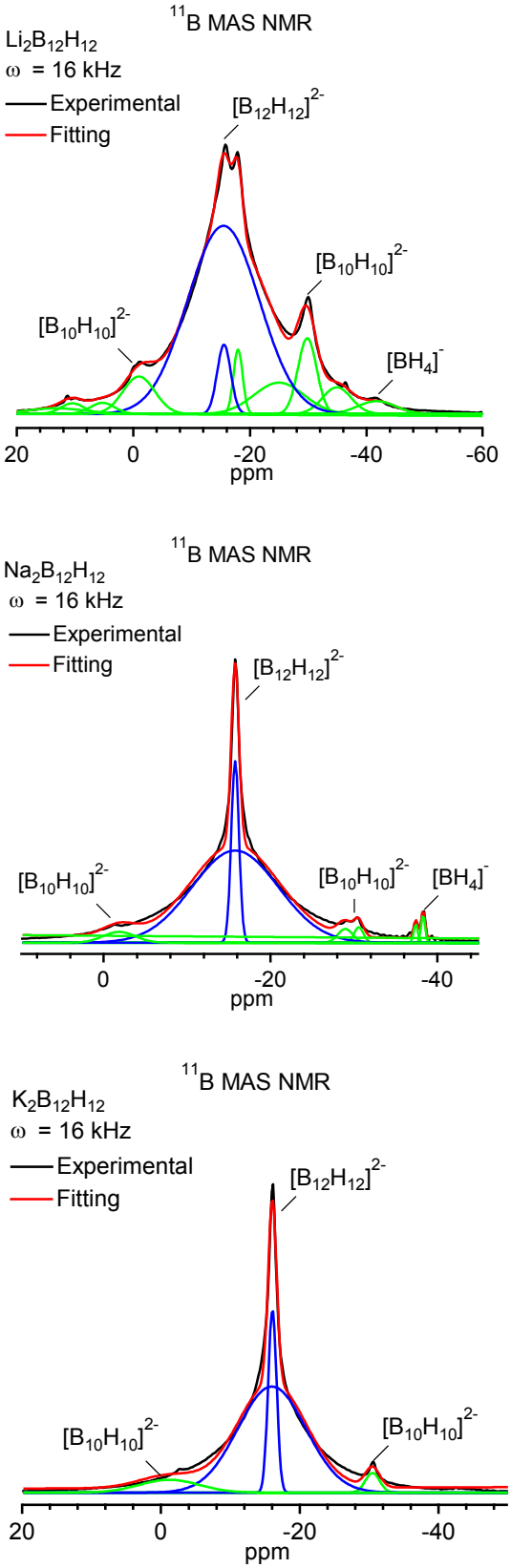

Figure 3.6 ^{11}B MAS NMR peak fitting of as synthesized $Li_2B_{12}H_{12}$, $Na_2B_{12}H_{12}$ and $K_2B_{12}H_{12}$.

Table 3.1 Relative amount of the B-H species in the synthesized $Li_2B_{12}H_{12}$, $Na_2B_{12}H_{12}$ and $K_2B_{12}H_{12}$.

Compounds	$[B_{12}H_{12}]^{2-}$	$[B_{10}H_{10}]^{2-}$	$[BH_4]^-$	Others
$Li_2B_{12}H_{12}$	67.67%	12.25%	2.27%	17.81%
$Na_2B_{12}H_{12}$	91.40%	4.78%	1.09%	2.73%
$K_2B_{12}H_{12}$	89.31%	10.69%	0	0

3.3.3 Comparison of the Two Reaction Routes

From the abovementioned experiments, $M_2B_{12}H_{12}$ (M = Li, Na, K) can be feasibly synthesized from both reaction routes via HT of $2MH + 1.2B_{10}H_{14}$ and $2MBH_4 + B_{10}H_{14}$. The reactivity between MBH_4 and $B_{10}H_{14}$ is better than that between MH and $B_{10}H_{14}$ when I carefully compare the yield of $M_2B_{12}H_{12}$ synthesized from $2MH + 1.2B_{10}H_{14}$ and $2MBH_4 + B_{10}H_{14}$.

For example, in the case of $Li_2B_{12}H_{12}$ synthesis, the single phase of $Li_2B_{12}H_{12}$ can be easily identified in XRD patterns from 200 °C with 10 h HT of $2LiBH_4 + B_{10}H_{14}$ sample. At the same condition, no diffraction from $Li_2B_{12}H_{12}$ can be detected from HT of $2LiH + 1.2B_{10}H_{14}$ sample. Only very weak XRD peaks of $Li_2B_{12}H_{12}$ begins to come out accompanying with large amount of residual starting materials even the HT time was increased to 15 h for $2LiH + 1.2B_{10}H_{14}$ (Figure 3.7).

To clarify the different reactivity from the viewpoint of thermodynamics, the reaction enthalpy and free energy of equations (3.4) of $2MH + 1.2B_{10}H_{14}$ and (3.5) of $2MBH_4 + B_{10}H_{14}$ are compared. Table 3.2 list the standard formation enthalpy ΔH_f^{298K} of relative starting materials referred to the NIST Chemistry WebBook,[5] and ΔH_f^{298K} of $M_2B_{12}H_{12}$ (M= Li, Na, K) recently calculated to by Lee.[185]

I subsequently calculate the enthalpy changes and Gibbs free energies of equations (3.4) and (3.5) using the values of standard formation enthalpy ΔH_f^{298K} listed in Table 3.2, the results are listed in Table 3.3. The ΔG is decided at 298K by equation $\Delta G = \Delta H - T\Delta S$, the entropy change ΔS is thought to be a constant (0.13 kJ• K^{-1} mol^{-1} H_2) mainly from production of H_2.[72] Both equations (3.4) and (3.5) show negative values of Gibbs free energy which supply the possibility in thermodynamics to synthesize $M_2B_{12}H_{12}$ from routes of $2MH + 1.2B_{10}H_{14}$ and $2MBH_4 + B_{10}H_{14}$.

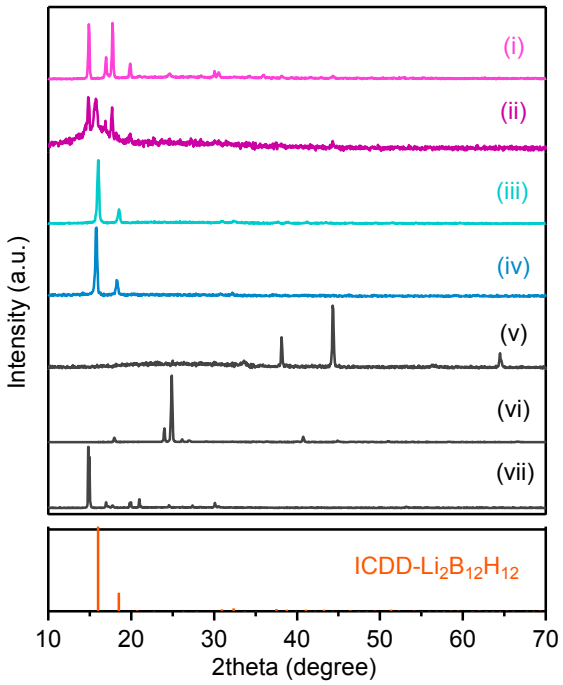

Figure 3.7 XRD patterns of $Li_2B_{12}H_{12}$ synthesized from different routes and conditions. (i) and (ii) are 5h BM of $2LiH + 1.2B_{10}H_{14}$ followed by HT at 200 °C for 10 h and at 200 °C for 15 h; (iii) and (iv) are 5h BM of $2LiBH_4 + B_{10}H_{14}$ followed by HT at 200 °C for 10 h and at 200 °C for 15 h; (v), (vi) and (vii) are LiH, $LiBH_4$ and $B_{10}H_{14}$, respectively. (BM = ball milling, HT = heat treatment)

Table 3.2 Standard formation enthalpies of relative compounds at 298K.[a]

Compounds	ΔH_f^{298K}
$B_{10}H_{14}$	-28.87
LiH	-90.63
NaH	-56.44
KH	-57.82
$LiBH_4$	-190.46
$NaBH_4$	-191.84
KBH_4	-226.90
$Li_2B_{12}H_{12}$	-711.18
$Na_2B_{12}H_{12}$	-658.43
$K_2B_{12}H_{12}$	-714.52

[a] Unit of formation enthalpies is given in kJ/mol.

Table 3.3 Enthalpy changes ΔH^{298K} and Gibbs free energy ΔG^{298K} of relative reactions.[a]

	Reaction	ΔH^{298K}	ΔG^{298K}
Equation (3.4)	$2LiH + 1.2B_{10}H_{14} \rightarrow Li_2B_{12}H_{12} + 3.4H_2$	-495.28	-627.00
	$2NaH + 1.2B_{10}H_{14} \rightarrow Na_2B_{12}H_{12} + 3.4H_2$	-510.91	-642.63
	$2KH + 1.2B_{10}H_{14} \rightarrow K_2B_{12}H_{12} + 3.4H_2$	-564.24	-695.96
Equation (3.5)	$2LiBH_4 + B_{10}H_{14} \rightarrow Li_2B_{12}H_{12} + 5H_2$	-301.39	-495.09
	$2NaBH_4 + B_{10}H_{14} \rightarrow Na_2B_{12}H_{12} + 5H_2$	-245.88	-439.58
	$2KBH_4 + B_{10}H_{14} \rightarrow K_2B_{12}H_{12} + 5H_2$	-231.85	-425.55

[a] Unit of enthalpy changes is given in kJ/(mol $[B_{12}H_{12}]^{2-}$).

In addition, equation (3.4) with larger ΔG than those of equation (3.5) for the same cations (Li, Na, K), indicates that equation (3.4) is more feasible for $M_2B_{12}H_{12}$ production in thermodynamics. This comparison means the higher yield of $M_2B_{12}H_{12}$ in equation (3.5) of $2MBH_4 + B_{10}H_{14}$ than equation (3.4) of $2MH + 1.2B_{10}H_{14}$ would be dominated by reaction kinetics.

The structural rearrangement as shown in Figure 3.8 is considered to contribute to the different reaction kinetics of equations (3.4) of $2MH + 1.2B_{10}H_{14}$ and (3.5) of $2MBH_4 + B_{10}H_{14}$. For $2MH + 1.2B_{10}H_{14}$, part of $B_{10}H_{14}$ has to be decomposed into small boranes as B source in order to supply B atoms to the residual $B_{10}H_{14}$ for production of bigger framework of $[B_{12}H_{12}]^{2-}$. On the other hand, for $2MBH_4 + B_{10}H_{14}$, MBH_4 as B source can directly supply B atom and combine to $B_{10}H_{14}$ for $[B_{12}H_{12}]^{2-}$ framework production, in which the decomposition of $B_{10}H_{14}$ may be not necessary.

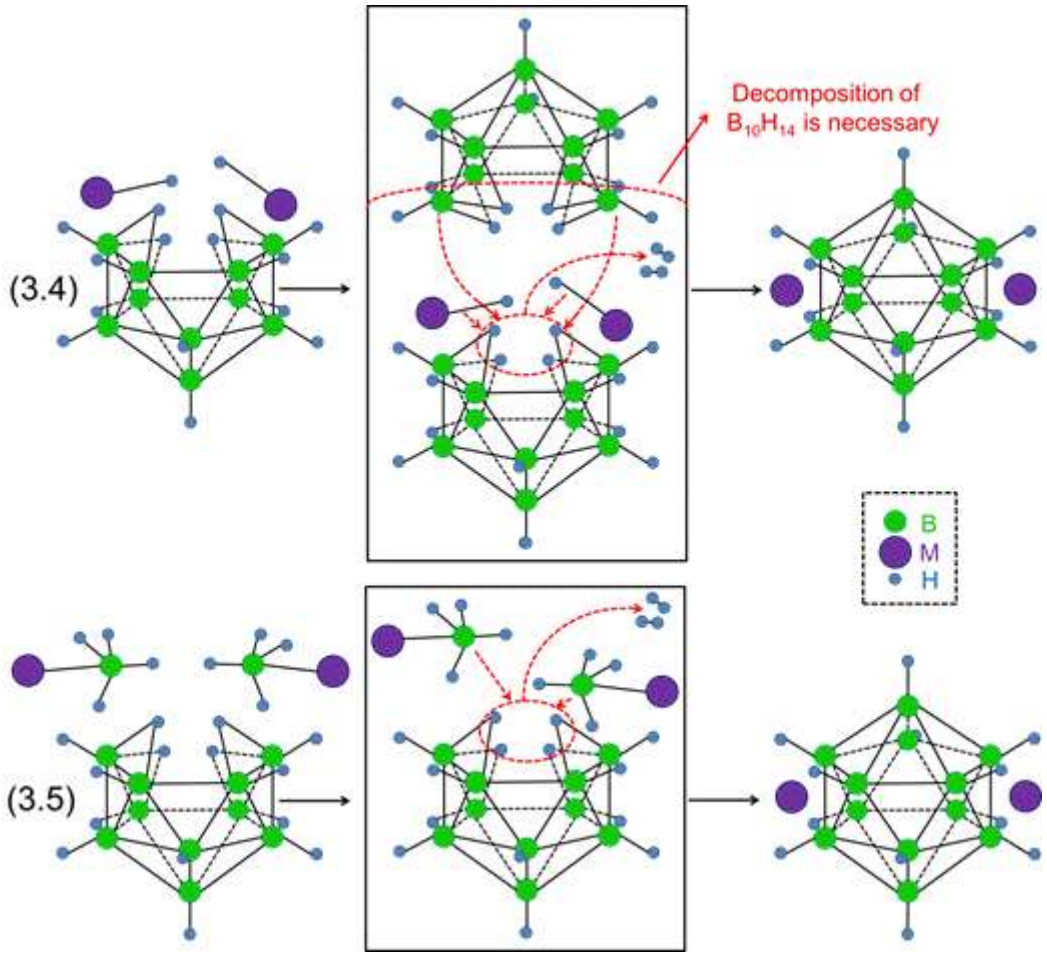

Figure 3.8 Schematic illustrations of reactions in equation (3.4) and equation (3.5).

3.3.4 Thermal Decomposition of Anhydrous $M_2B_{12}H_{12}$ (M = Li, Na, K)

3.3.4.1 $Li_2B_{12}H_{12}$

Thermal decomposition behaviors of anhydrous $Li_2B_{12}H_{12}$ measured using TG and MS are shown in Figure 3.9. Only hydrogen is detected in MS, indicating the weight loss upon heating is originated from the dehydrogenation process of $Li_2B_{12}H_{12}$. The dehydrogenation starts at approximately 200 °C and the dehydrogenation amount accumulates to 5.1 mass% (approximately 66% of theoretical hydrogen capacity in $Li_2B_{12}H_{12}$) when heated up to 700 °C via a multistep decomposition pathway as shown in TG and MS results. The initial decomposition of $Li_2B_{12}H_{12}$ is prior to that of $LiBH_4$ starts at ca.300 °C as shown in Figure 3.10.

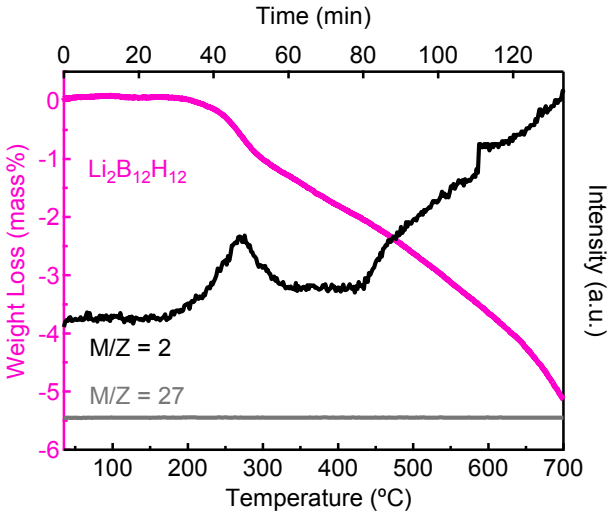

Figure 3.9 TG curve and MS signals of anhydrous $Li_2B_{12}H_{12}$ (mass numbers 2 and 27 represent H_2 and B_2H_6).

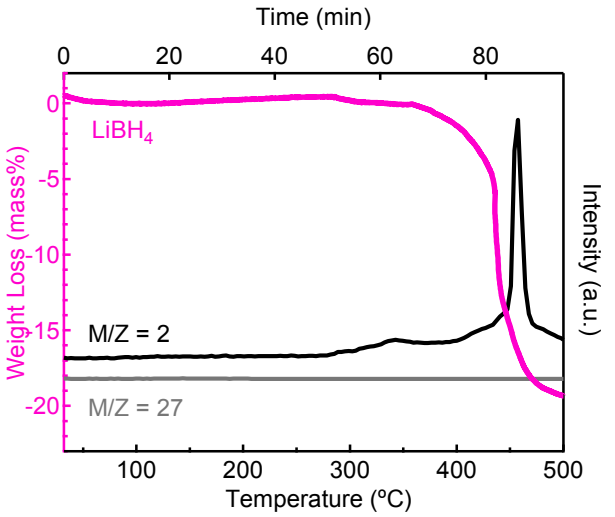

Figure 3.10 TG curve and MS signals of Aldrich $LiBH_4$ (mass numbers 2 and 27 represent H_2 and B_2H_6).

In order to elucidate the decomposition pathway of anhydrous $Li_2B_{12}H_{12}$, the sample was heated to respective temperatures and subsequently cooled down to room temperature, and followed by systematic analyses of XRD, Raman and ^{11}B NMR, the results are shown in Figure 3.11 and Figure 3.12, respectively.

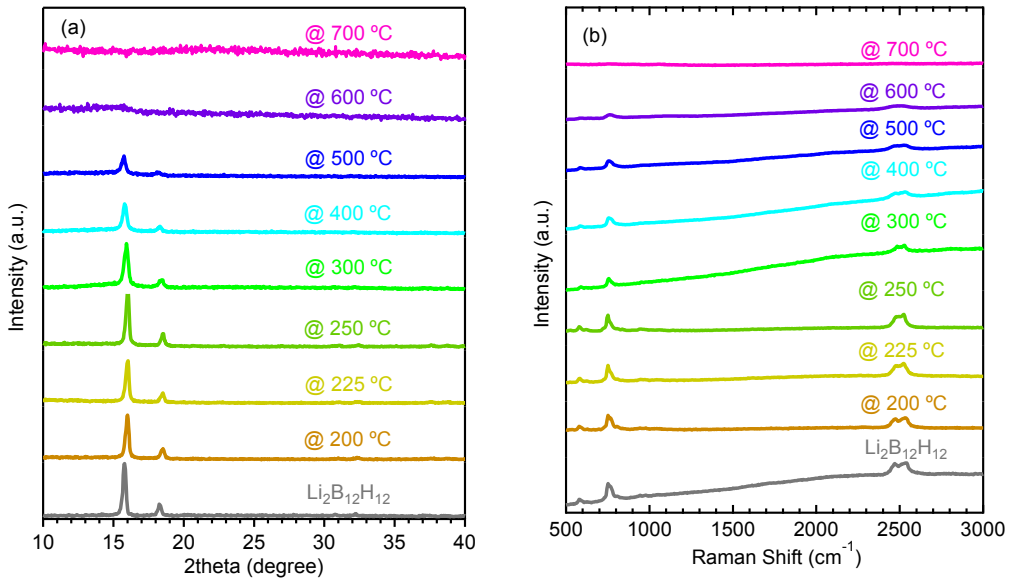

Figure 3.11 Ex-situ (a) XRD patterns and (b) Raman spectra of anhydrous $Li_2B_{12}H_{12}$ as synthesized and heated up to respective temperatures.

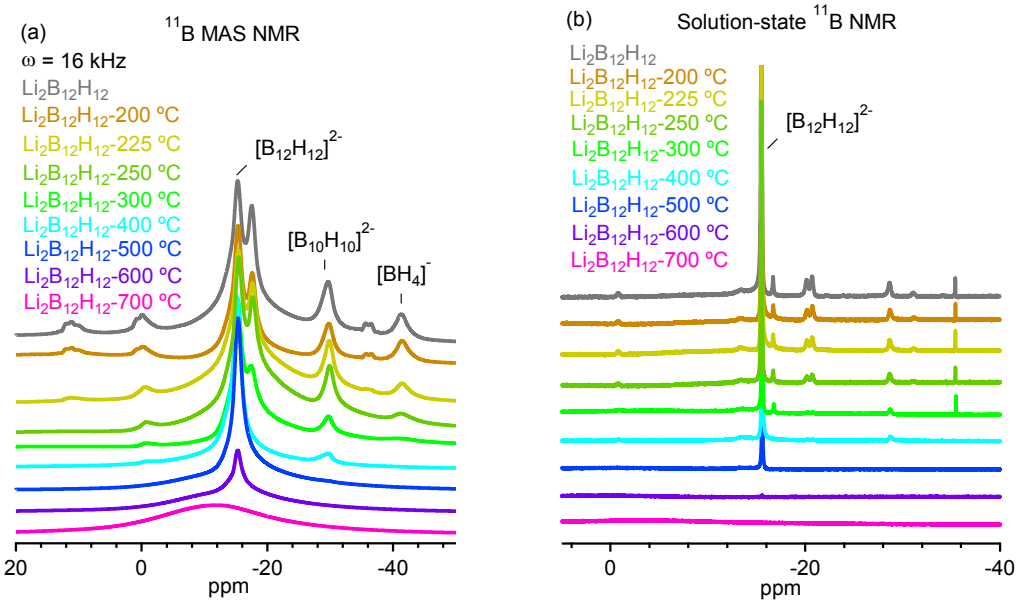

Figure 3.12 ^{11}B NMR spectra of anhydrous $Li_2B_{12}H_{12}$ as synthesized and heated up to respective temperatures: (a) solid-state ^{11}B MAS NMR spectra and (b) solution-state ^{11}B NMR spectra measured in DMSO-d_6. Resonance assignments: -15.6 ppm $[B_{12}H_{12}]^{2-}$, -35.6 ppm $[BH_4]^-$, -0.9 & -28.8 ppm $[B_{10}H_{10}]^{2-}$, -16.8 ppm $[B_{11}H_{11}]^{2-}$, -20.3 (-20.8) ppm $[B_9H_9]^{2-}$.[186]

When the $Li_2B_{12}H_{12}$ sample is heated to 200 °C, no an changes in XRD patterns,

Raman spectra and ^{11}B NMR which indicates the synthesized $Li_2B_{12}H_{12}$ sample is stable at 200 °C. Considering the as-synthesized $Li_2B_{12}H_{12}$ sample includes small amount of impurities (Table 3.1), it is further heated to 225 and 250 °C to investigate the really initial decomposition temperature of $Li_2B_{12}H_{12}$. At both temperatures, still no obvious changes of $Li_2B_{12}H_{12}$ in XRD patterns, Raman spectra and ^{11}B NMR which elucidates that $Li_2B_{12}H_{12}$ is stable up to 250 °C. However, the ^{11}B MAS NMR clearly shows the significant weakening of $[BH_4]^-$ (-41.3 ppm) and disappearance of other unknown impurity phases (11.2 and -36.0 ppm) at 250 °C, which reveals the weight loss (0.3 mass%) in TG below 250 is originated from decomposition of impurities. When the temperature is increased up to 300 °C, both diffraction peaks (2θ = 15.8° and 18.4°) and Raman vibrations (between 500-1000 cm^{-1} and around 2500 cm^{-1}) of $Li_2B_{12}H_{12}$ fall off, consistently indicating the partial decomposition of $Li_2B_{12}H_{12}$ above 250 °C to release hydrogen.[149] When heated to higher temperatures, the diffraction peaks and Raman vibrations further weaken and ultimately nearly disappear at 600 °C, the main resonance in ^{11}B MAS NMR at -15.3 ppm attributed to $Li_2B_{12}H_{12}$ becomes significantly weak but without any change in chemical shift, which consistently indicate that a major part of B-H bond in the icosahedral $[B_{12}H_{12}]^{2-}$ has been broken to release hydrogen at 600 °C. Taking into account the impurity-included dehydrogenation amount (3.7 mass%) of $Li_2B_{12}H_{12}$ heated up to 600 °C, I believe that the decomposition product mainly forms H-deficiency $Li_2B_{12}H_{12-x}$ ($x < 5.3$) that keeps the icosahedral B_{12} skeletons.[149] No signals in solution-state ^{11}B NMR were detected which implies that the formed $Li_2B_{12}H_{12-x}$ at 600 °C is DMSO insoluble. When the temperature is further increased up to 700 °C, the dehydrogenation amount reaches 5.1 mass% and the major resonance of $Li_2B_{12}H_{12}$ at -15.3 ppm in ^{11}B MAS NMR shifts to -11.9 ppm, which suggest $Li_2B_{12}H_{12-x}$ continuously releases hydrogen accompanying with the polymerization of the icosahedral B_{12} skeletons and the formation of $(Li_2B_yH_z)_n$ polymers[187-188] those are water and DMSO insoluble. No amorphous B was detected at 700 °C which implies higher temperature is needed for decomposition of $(Li_2B_yH_z)_n$ polymers.

Based on the abovementioned experimental results, thermal decomposition pathway of anhydrous $Li_2B_{12}H_{12}$ could be briefly summarized as the following steps:

Step 1: $Li_2B_{12}H_{12} \rightarrow Li_2B_{12}H_{12-x} + x/2H_2$ (3.6)

Step 2: $nLi_2B_{12}H_{12-x} \rightarrow (Li_2B_yH_z)_n + z'H_2$ (3.7)

The similar polymerization phenomenon has been also observed in decomposition of anhydrous $MgB_{12}H_{12}$ and $CaB_{12}H_{12}$ in our recent work. It is worth emphasizing that the thermal decomposition behaviors of the single phase $Li_2B_{12}H_{12}$ are different from that in-situ formed during dehydrogenation of $LiBH_4$: the single phase $Li_2B_{12}H_{12}$ exhibits a lower initial decomposition temperature and a wider decomposition temperature range of 250 ~ >700 °C than those of $LiBH_4$. Those differences may result from the concurrent formation of LiH together with $Li_2B_{12}H_{12}$, since destabilization of $M_{2/n}B_{12}H_{12}$ by MH_x has been predicted by first-principles calculations.[89]

3.3.4.2 $Na_2B_{12}H_{12}$

Similar to the anhydrous $Li_2B_{12}H_{12}$, thermal decomposition behaviors of anhydrous $Na_2B_{12}H_{12}$ are also systematically investigated using the same way and their TG and MS results are shown in Figure 3.13. Only hydrogen is detected in MS, indicating the weight loss upon heating is originated from the dehydrogenation of $Na_2B_{12}H_{12}$. The dehydrogenation starts at ca. 580 °C and the dehydrogenation amount reaches 1.6 mass% (approximately 25% of theoretical hydrogen capacity in $Na_2B_{12}H_{12}$), comparable to the reported value (~ 1.5 mass% at 697 °C),[154] when heated up to 700 °C. The dehydrogenation of $NaBH_4$ is shown in Figure 3.14 for comparison.

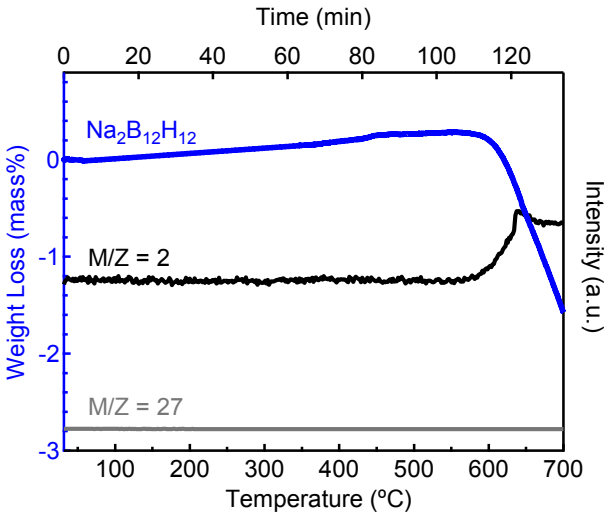

Figure 3.13 TG curve and MS signals of anhydrous $Na_2B_{12}H_{12}$ (mass numbers 2 and 27 represent H_2 and B_2H_6).

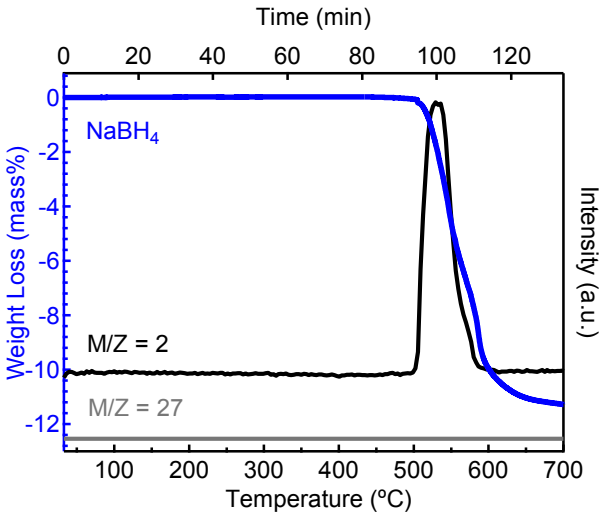

Figure 3.14 TG curve and MS signals of Aldrich $NaBH_4$ (mass numbers 2 and 27 represent H_2 and B_2H_6).

XRD patterns, Raman spectra and ^{11}B NMR spectra of anhydrous $Na_2B_{12}H_{12}$ heated to respective temperatures and subsequently cooled down to room temperature are shown in Figures 3.15 and 3.16, respectively. When $Na_2B_{12}H_{12}$ is heated up to 500 °C, no obvious changes of diffraction peaks, Raman spectra and the major resonance for $Na_2B_{12}H_{12}$ are observed, whereas the resonances of $[BH_4]^-$ and $[B_{10}H_{10}]^{2-}$ nearly disappear in solid and solution-state ^{11}B NMR, suggesting that the very small amount of impurities decompose below 500 °C without detected weight loss in TG curve. When $Na_2B_{12}H_{12}$ is heated up to 600 °C, diffraction peaks and Raman spectra attributed to $Na_2B_{12}H_{12}$ slightly weaken, the main resonance of $[B_{12}H_{12}]^{2-}$ shows no obvious change, indicating small amount of preliminary decomposition of $Na_2B_{12}H_{12}$ at 600 °C. When further heated up to 700 °C, diffraction peaks and Raman spectra from $Na_2B_{12}H_{12}$ are hardly observed, the main resonance of $[B_{12}H_{12}]^{2-}$ at -15.7 ppm in ^{11}B MAS NMR significantly weakens and overlaps with a broad resonance between -12.4 and -14.8 ppm, indicating that the dehydrogenation of $Na_2B_{12}H_{12}$ to $Na_2B_{12}H_{12-x}$ as well as the polymerization of $Na_2B_{12}H_{12-x}$ to water and DMSO insoluble $(Na_2B_yH_z)_n$ polymers starts to happen at 700 °C.[187-188] Still weak resonance from $[B_{12}H_{12}]^{2-}$ is found in solution-state ^{11}B NMR which reveals the existence of small amount of residual $Na_2B_{12}H_{12}$ at 700 °C and confirms the higher stability of $Na_2B_{12}H_{12}$ than that of $Li_2B_{12}H_{12}$. The intermediate decomposition product at 700 °C would be decided as $Na_2B_{12}H_9$ by means of weight loss in TG curve if without considering the small amount of residual $Na_2B_{12}H_{12}$ and overlaps originated

from $(Na_2B_yH_z)_n$.

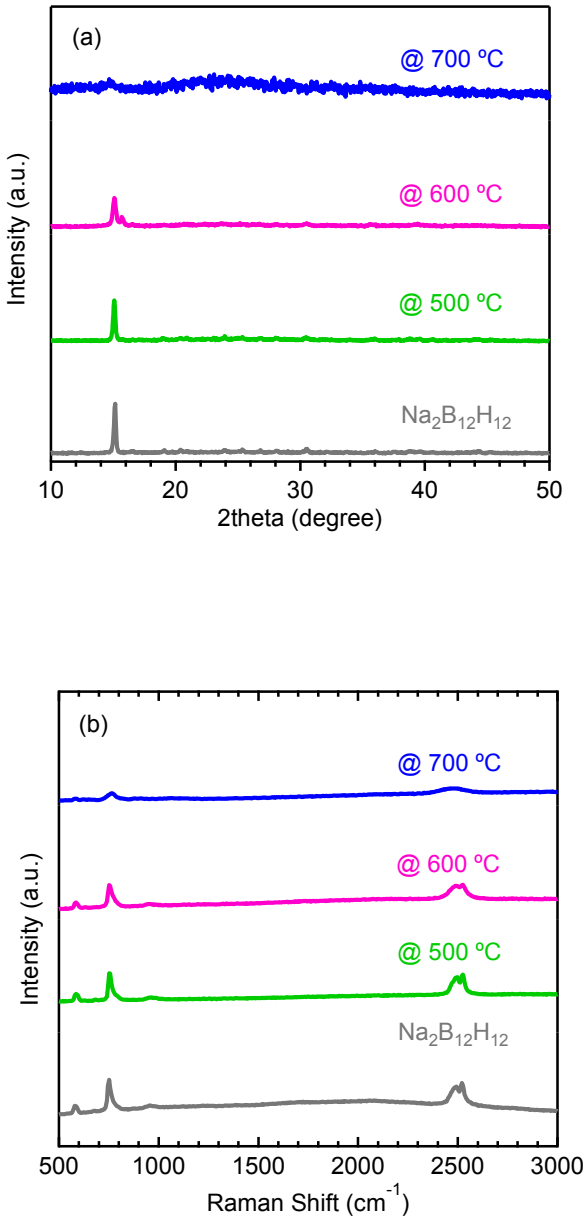

Figure 3.15 Ex-situ (a) XRD patterns and (b) Raman spectra of anhydrous $Na_2B_{12}H_{12}$ as synthesized and heated up to respective temperatures.

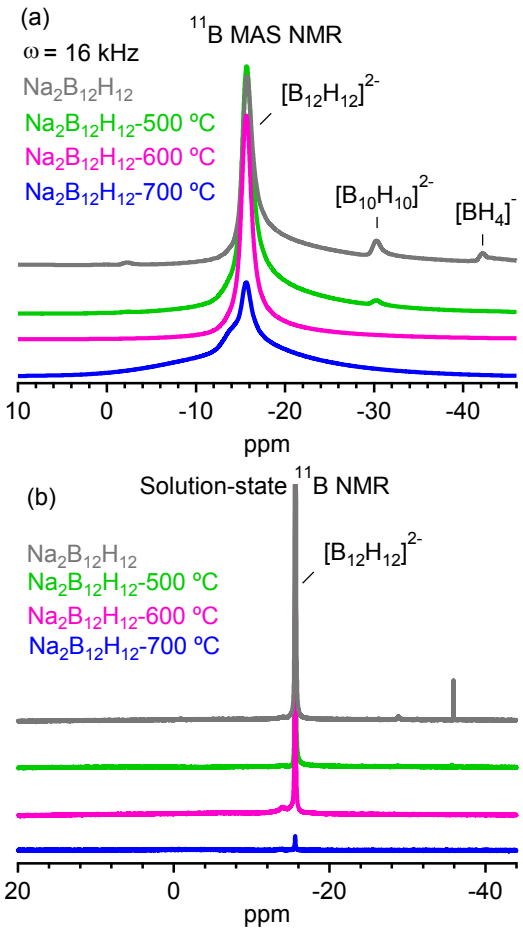

Figure 3.16 ^{11}B NMR spectra of anhydrous $Na_2B_{12}H_{12}$ as synthesized and heated up to respective temperatures: (a) solid-state ^{11}B MAS NMR spectra and (b) solution-state ^{11}B NMR spectra measured in DMSO-d_6. Resonance assignments: -15.6 ppm $[B_{12}H_{12}]^{2-}$, -35.9 ppm $[BH_4]^-$, -28.8 ppm $[B_{10}H_{10}]^{2-}$.[189]

The decomposition pathway of single phase anhydrous $Na_2B_{12}H_{12}$ via multistep processes is considered to be the same as that of $Li_2B_{12}H_{12}$ as summarized in equation (3.6) and (3.7). Similar to that of $Li_2B_{12}H_{12}$, the decomposition behavior of single phase $Na_2B_{12}H_{12}$ may be different from that formed as a dehydrogenation intermediate of $NaBH_4$ for the coexisting NaH may play a crucial role in facilitating the decomposition of $[B_{12}H_{12}]^{2-}$ similar to MgH_2.[89] However, the formation of $Na_2B_{12}H_{12}$ intermediate is only confirmed in $2NaBH_4+MgH_2$ system,[103] the $Na_2B_{12}H_{12}$ formation as intermediate during decomposition of pure $NaBH_4$ is still to be confirmed and studied[190].

3.3.4.3 $K_2B_{12}H_{12}$

Thermal decomposition behaviors of anhydrous $K_2B_{12}H_{12}$ are also systematically investigated following the used methods and the TG and MS results are shown in Figures 3.17. Hydrogen as the unique gas component in decomposition products is detected in MS, indicating the weight loss upon heating is originated from the dehydrogenation of $K_2B_{12}H_{12}$. The dehydrogenation starts at ca. 480 °C and the dehydrogenation amount reaches 4.2 mass% (approximately 76% of theoretical hydrogen capacity in $K_2B_{12}H_{12}$) via multistep decomposition processes, when heated up to 700 °C. The dehydrogenation of KBH_4 is shown in Figure 3.18 for comparison.

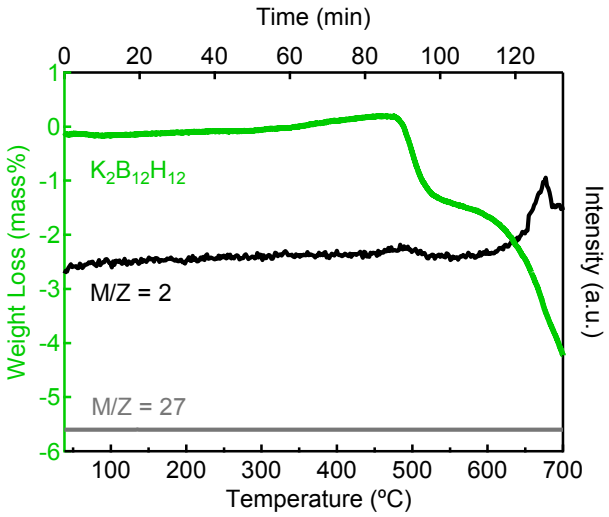

Figure 3.17 TG curve and MS signals of anhydrous $K_2B_{12}H_{12}$ (mass numbers 2 and 27 represent H_2 and B_2H_6).

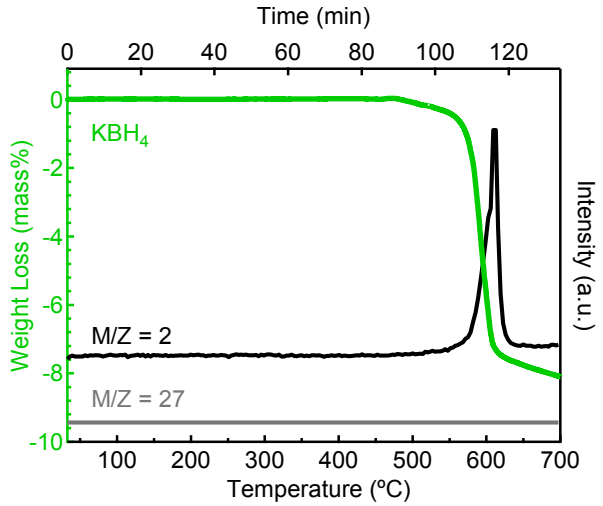

Figure 3.18 TG curve and MS signals of Aldrich KBH_4 (mass numbers 2 and 27 represent H_2 and B_2H_6).

XRD patterns, Raman spectra and ^{11}B NMR spectra of anhydrous $K_2B_{12}H_{12}$ heated up to respective temperatures and subsequently cooled down to room temperature are shown in Figure 3.19 and Figure 3.20, respectively. No obvious changes of diffraction peaks, Raman spectra and the major resonance for $K_2B_{12}H_{12}$ are observed at 475 °C which is consistent with TG result. When $K_2B_{12}H_{12}$ is heated up to 550 °C, still no obvious changes of diffraction peaks, Raman spectra and the major resonance for $K_2B_{12}H_{12}$ are detected, whereas the resonance originated from $[BH_4]^-$ (-38.2 ppm in solid-state and -35.6 ppm in solution-state ^{11}B NMR) disappears in both solid-state and solution-state ^{11}B NMR, suggesting that the weight loss bellow 550 °C is responsible for the dehydrogenation of residual KBH_4. When $K_2B_{12}H_{12}$ is heated up to 625 °C, XRD peaks and Raman spectra attributed to $K_2B_{12}H_{12}$ weaken, the main resonance of $[B_{12}H_{12}]^{2-}$ in ^{11}B MAS NMR slightly falls off without chemical shift change, indicating small amount of decomposition of $K_2B_{12}H_{12}$ at 625 °C. When $K_2B_{12}H_{12}$ is further heated up to 700 °C, diffraction peaks and Raman spectra from $K_2B_{12}H_{12}$ are hardly observed, the main resonance of $[B_{12}H_{12}]^{2-}$ at -15.4 ppm in ^{11}B MAS NMR falls off intensively and overlaps with a broad resonance between -12.2 and -14.2 ppm (similar to what happens in $Na_2B_{12}H_{12}$ at the same temperature), indicating that the significant dehydrogenation of $K_2B_{12}H_{12}$ to $K_2B_{12}H_{12-x}$ accompanying with the polymerization of $K_2B_{12}H_{12-x}$ to $(K_2B_yH_z)_n$ polymers starts to happen at 700 °C.[187-188] The produced $(K_2B_yH_z)_n$ polymers are water and DMSO insoluble as being confirmed in water and solution-state ^{11}B NMR using DMSO as solvent. The decomposition pathway of single phase anhydrous $K_2B_{12}H_{12}$ is suggested to be the same to that of $Li_2B_{12}H_{12}$ and $Na_2B_{12}H_{12}$ as summarized in equation (3.6) and (3.7), too. The decomposition behaviors of single phase $K_2B_{12}H_{12}$ are different from that formed as a dehydrogenation intermediate of KBH_4 as theoretically predicted[191], suggesting that the coexisting KH may be in favor of the decomposition of $[B_{12}H_{12}]^{2-}$.

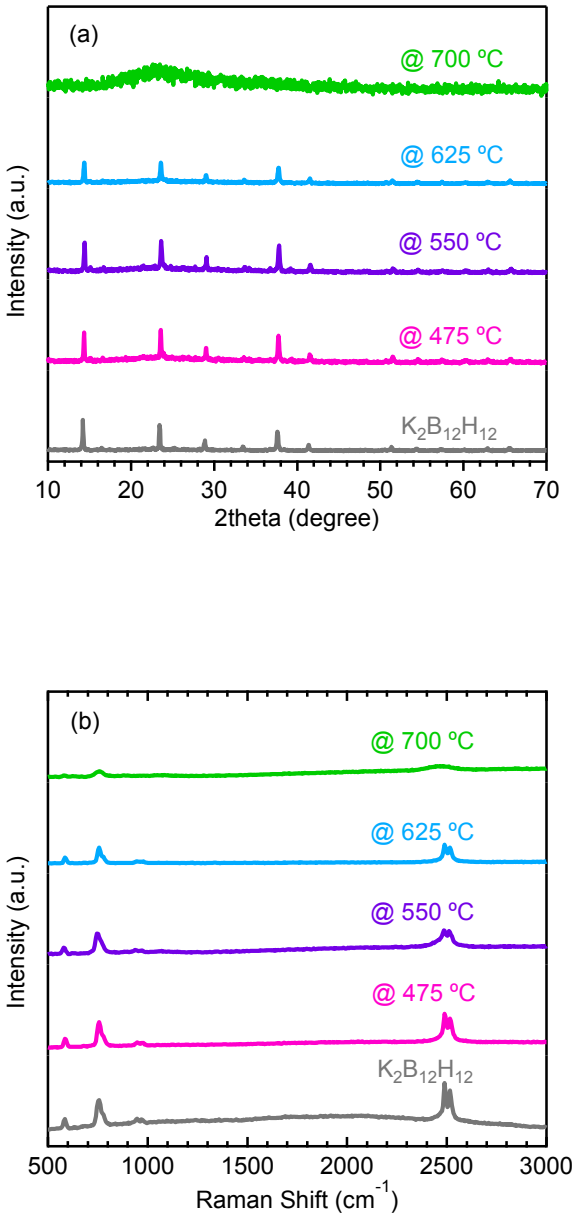

Figure 3.19 Ex-situ (a) XRD patterns and (b) Raman spectra of anhydrous $K_2B_{12}H_{12}$ as synthesized and heated up to respective temperatures.

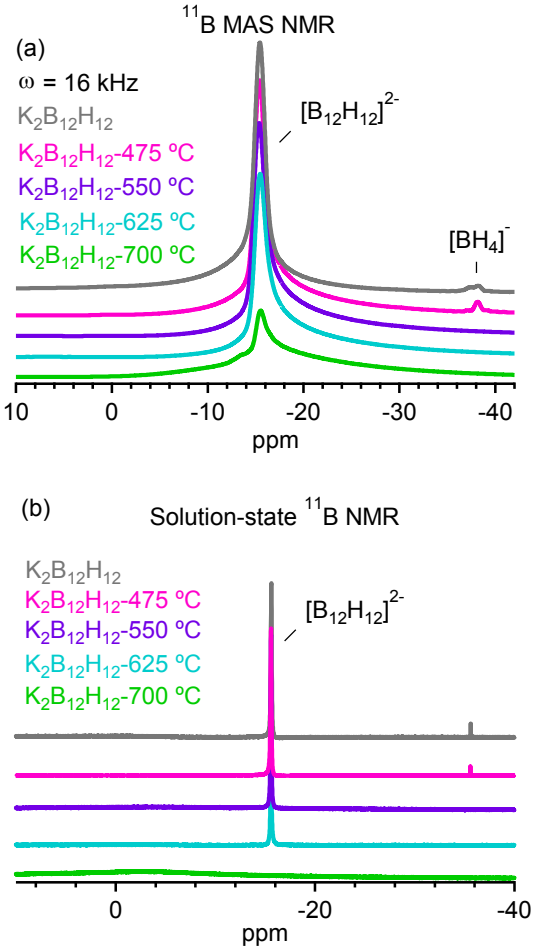

Figure 3.20 ^{11}B NMR spectra of anhydrous $K_2B_{12}H_{12}$ as synthesized and heated up to respective temperatures: (a) solid-state ^{11}B MAS NMR spectra and (b) solution-state ^{11}B NMR spectra measured in DMSO-d_6. Resonance assignments: -15.6 ppm $[B_{12}H_{12}]^{2-}$, -35.6 ppm $[BH_4]^-$.[189]

In summary, thermal decomposition of all single phase alkali metal dodecaborates $M_2B_{12}H_{12}$ (M = Li, Na, K) experiences two steps of a) dehydrogenation to produce H-deficiency $M_2B_{12}H_{12-x}$ and b) polymerization of $M_2B_{12}H_{12-x}$ to form $(M_2B_yH_z)_n$, which is also observed in the dehydrogenation processes of anhydrous $MgB_{12}H_{12}$ and $CaB_{12}H_{12}$,[192] would be the major obstacle to be overcome for rehydrogenation to borohydrides. $M_2B_{12}H_{12}$ formed in-situ during the dehydrogenation of MBH_4 would be facilitated by the coexisting MH.[102, 193] In other words, an appropriate composition of $M_{2/n}B_{12}H_{12}$ and MH_x is expected to be designed to improve the rehydrogenation and the cycled reversibility of borohydrides. All the $M_2B_{12}H_{12}$ (M = Li, Na, K) samples include small amount of $[BH_4]^-$ as impurity which will be further eliminated

by tuning stoichiometric molar ratio of starting reaction materials of MBH_4 and $B_{10}H_{14}$ though no obvious effect of small amount of $[BH_4]^-$ to the dehydrogenation of $M_2B_{12}H_{12}$ is observed in current experiments.

3.4 Conclusions

In this chapter, solvent-free reaction processes via heat treatment of $2MH + 1.2B_{10}H_{14}$ or $2MBH_4 + B_{10}H_{14}$ have been developed for successful synthesis of anhydrous alkali metal dodecaborates $M_2B_{12}H_{12}$ (M = Li, Na, K). Interaction between MH or MBH_4 with $B_{10}H_{14}$ did not happen if only with ball milling process at room temperature, but it was substantially improved if heat treating MH or MBH_4 with $B_{10}H_{14}$ higher than 99.6 °C (melting point of $B_{10}H_{14}$). MBH_4 exhibited better reactivity with $B_{10}H_{14}$ than that of MH when I compared the $M_2B_{12}H_{12}$ yields of reactions $2MH + 1.2B_{10}H_{14}$ and $2MBH_4 + B_{10}H_{14}$, which suggests that heat treatment of $2MBH_4 + B_{10}H_{14}$ would be a practicable solvent-free method for anhydrous $M_2B_{12}H_{12}$ synthesis.

Systematic thermal decomposition behaviors of anhydrous alkali metal dodecaborates $M_2B_{12}H_{12}$ (M = Li, Na, K) have been investigated, the results demonstrate that all $M_2B_{12}H_{12}$ release hydrogen to form H-deficiency $M_2B_{12}H_{12-x}$ with the icosahedral B_{12} skeletons followed by polymerization processes to produce $(M_2B_yH_z)_n$ polymers. No amorphous B was detected in all $M_2B_{12}H_{12}$ samples at 700 °C which means higher temperature is needed for complete dehydrogenation of $(M_2B_yH_z)_n$ with high stability. The synergistic interaction of electronegativity[111] and size[150] of cations in $Na_2B_{12}H_{12}$ is considered to be responsible for the higher stability of $Na_2B_{12}H_{12}$ than that of $Li_2B_{12}H_{12}$ and $K_2B_{12}H_{12}$. Distinct from those of the single phase $M_2B_{12}H_{12}$, thermal decomposition of those in-situ formed $M_2B_{12}H_{12}$ during the dehydrogenation of MBH_4 could be facilitated by the coexisting MH, suggesting that designing an appropriate composition of $M_{2/n}B_{12}H_{12}$ and MH_x would be a promising way to substantially improve the rehydrogenation and reversibility of borohydrides.

Chapter 4

Synthesis and Decomposition Behaviors of Anhydrous Alkaline Earth Metal Dodecaborates $MB_{12}H_{12}$ (M = Mg, Ca)

The chapter is based on the submitted paper:

He L, Li H-W, Tumanov N, Filinchuk Y, Akiba E, Facile Synthesis of Anhydrous Alkaline Earth Metal Dodecaborate $MB_{12}H_{12}$ (M = Mg, Ca) from $M(BH_4)_2$. Submitted to *Dalton Transactions*.

In this chapter, anhydrous alkaline earth metal dodecaborates $MB_{12}H_{12}$ (M= Mg, Ca) are successfully synthesized using the recently developed solvent-free process, i.e. heat treatment of $Mg(BH_4)_2$ and $Ca(BH_4)_2$ with $B_{10}H_{14}$. Like those of $M_2B_{12}H_{12}$ (M= Li, Na, K), anhydrous $MgB_{12}H_{12}$ and $CaB_{12}H_{12}$ exhibit similar decomposition behaviors, i.e. multistep decomposition accompanied with the formation of H-deficiency $MB_{12}H_{12-x}$ followed by $(MB_yH_z)_n$ polymers.

4.1 Introduction

In Chapter 3, I have developed a new solvent-free synthesis method, i.e. sintering of $M(BH_4)_n$ with $B_{10}H_{14}$, by which high purity of anhydrous alkali metal dodecaborates $M_2B_{12}H_{12}$ (M = Li, Na, K) have been successfully synthesized.[157] Comparison on the yield of $M_2B_{12}H_{12}$ between two routes of $2MH + 1.2B_{10}H_{14}$ and $2MBH_4 + B_{10}H_{14}$ indicates that heat treatment of $2MBH_4 + B_{10}H_{14}$ is a facile way to synthesize anhydrous metal dodecaborates. Decomposition of the synthesized $M_2B_{12}H_{12}$ exhibits different behaviors with those in-situ formed $M_2B_{12}H_{12}$ during the dehydrogenation of MBH_4. Therefore, it is of great importance to systematically investigate the thermal decomposition behavior of anhydrous alkaline earth metal

dodecaborates $MB_{12}H_{12}$ (M = Mg, Ca) in order to elucidate the decomposition mechanism.

In this chapter, I apply my recently developed solvent free process to the syntheses of anhydrous alkaline earth metal dodecaborates $MgB_{12}H_{12}$ and $CaB_{12}H_{12}$.[157] Anhydrous $MgB_{12}H_{12}$ and $CaB_{12}H_{12}$ have been successfully synthesized by sintering of $Mg(BH_4)_2$ and $Ca(BH_4)_2$ with $B_{10}H_{14}$, based on the following equation (4.1):

$$M(BH_4)_2 + B_{10}H_{14} \rightarrow MB_{12}H_{12} + 5H_2 \, (M = Mg, Ca) \quad (4.1)$$

Deliquescence and thermal decomposition behaviors of thus synthesized anhydrous $MgB_{12}H_{12}$ and $CaB_{12}H_{12}$ have been carefully investigated using Raman spectra, X-ray diffraction (XRD), thermogravimetry (TG), mass spectrometry (MS), and solid-state magic angle spinning (MAS) nuclear magnetic resonance (NMR) spectra. Furthermore, the decomposition pathways of $MgB_{12}H_{12}$ and $CaB_{12}H_{12}$ are discussed in comparison with those in-situ formed during the dehydrogenation of $Mg(BH_4)_2$ and $Ca(BH_4)_2$, in order to obtain insightful hints for substantial improvement of reversibility of borohydrides.

4.2 Experimental Section

Commercial $B_{10}H_{14}$ (99%, Wako), γ-$Mg(BH_4)_2$ (95%, Aldrich) and $Ca(BH_4)_2$ (95%, Aldrich) were all stored in glove box under Ar gas protection and utilized without further purification. The same mole ratio 1:1 of $Mg(BH_4)_2 + B_{10}H_{14}$ and $Ca(BH_4)_2 + B_{10}H_{14}$ as starting materials were firstly mechanically milled by Fritsch P-7 ball milling machine at room temperature with 10 steel balls (7 mm in diameter) in a hardened steel vial (30 cm^3 in volume) under 0.1 MPa Ar for 5 h (15 min milling, 5 min pausing). Subsequently, the samples $Mg(BH_4)_2 + B_{10}H_{14}$ and $Ca(BH_4)_2 + B_{10}H_{14}$ after ball milling were sealed into stainless steel crucibles (~ 0.7 cm^3 in volume, 38.3 g in weight for every set) for sintering at 300 °C with 1 h and 380 °C with 2 h, respectively.

For deliquescence experiments, samples were firstly put into the 5 mm Al pots in glove box and then transferred into air in laboratory with relatively humidity of 35% at 20 °C. The samples were put in Raman spectrometer for in-situ observation for 1 h, and then they were sealed using Scotch tape for X-ray diffraction measurement. Powder X-ray diffraction (XRD) patterns were obtained from Rigaku Ultima IV X-ray diffractometer with Cu-Kα radiation (λ = 1.54 Å) with accelerating voltage and

tube current as 40 kV and 40 mA. The powder state of samples was paved in a glass plate sealed by Scotch tape to prohibit contamination by air during the measurement. Powder XRD patterns of the as-synthesized $MgB_{12}H_{12}$ were measured in a glass capillary, on MAR345 diffractometer, with Mo Kα (λ = 0.71 Å) rotating anode generator and a focusing mirror. The synchrotron radiation powder XRD pattern for the as-synthesized $CaB_{12}H_{12}$ was measured on the Materials Science Beamline X04SA at the Swiss Light Source (transmission geometry in capillary, MYTHEN detector, λ = 1.00117 Å). Raman spectra were collected on RAMAN-11 VIS-SS (Nanophoton) machine via a laser with 532 nm wavelength (green). Analysis of gas release was performed using TG linked to MS, using 5 °C/min of heating ramp under 1 bar of He with 200 ml/min flow. TG and MS were recorded by Rigaku Thermo Plus Evo II TG-DTA 8120/S AEMK and quadrupole mass spectrometer, respectively. Solid-state MAS NMR spectra were recorded using a Bruker Ascend-600 spectrometer at room temperature. ^{11}B NMR peak simulation was carried out using Gaussian functions by Peakfit v4.12 software. NMR sample preparations were always finished in glove box protected with pure Ar and sample spinning was achieved using dry N_2 gas. ^{11}B MAS NMR spectra were obtained at excitation pulses of 6.5 μs（π/2 pulse) and with strong ^{1}H decoupling pulses. BF_3OEt_2 (δ = 0.00 ppm) was used as external standard for confirmation of ^{11}B NMR chemical shifts.

4.3 Results and Discussion

4.3.1 Synthesis of Anhydrous $MgB_{12}H_{12}$ and $CaB_{12}H_{12}$

Figure 4.1 shows XRD patterns and Raman spectra of $Mg(BH_4)_2$ + $B_{10}H_{14}$ after sintering at 300 °C for 1 h. The observed broad peak between 2θ = 3° and 15° (between 2θ = 10° and 18° using Cu-Kα radiation) distinct from starting materials of $Mg(BH_4)_2$ and $B_{10}H_{14}$, could be ascribed to the formation of amorphous $MgB_{12}H_{12}$ which has been theoretically predicted by First-principle Calculations.[194] In the Raman spectra, two peaks ascribed to B-H bending and stretching vibrations of $[B_{12}H_{12}]^{2-}$ are observed at 751 and 2569 cm^{-1}, respectively, together with the high level of baseline due to the fluorescent effect. Furthermore, no trace of O-H bond of water is observed in the Raman spectra, which prove the successful synthesis of anhydrous $MgB_{12}H_{12}$.

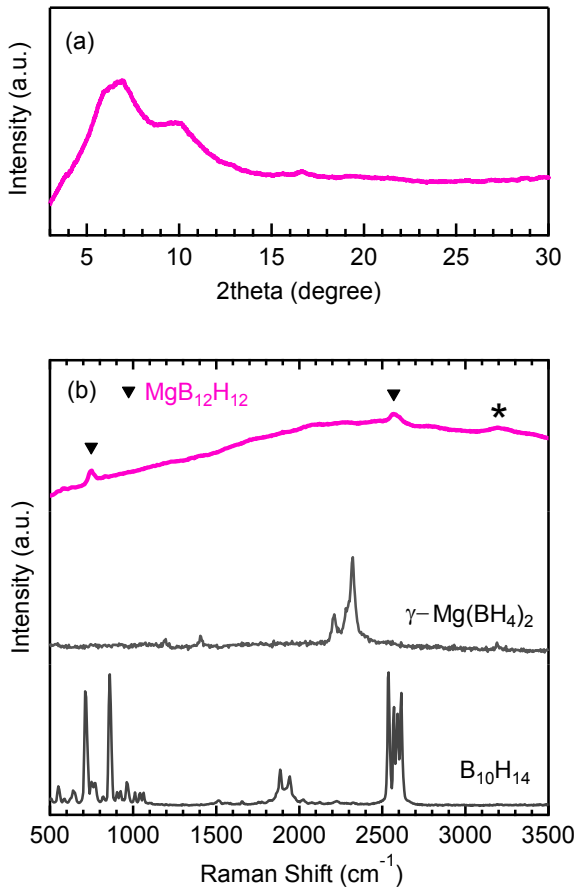

Figure 4.1 (a) XRD pattern (Mo Kα) and (b) Raman spectra of 5 h ball milled $Mg(BH_4)_2$ + $B_{10}H_{14}$ followed by sintering at 300 °C for 1 h. (Starting materials of $Mg(BH_4)_2$ and $B_{10}H_{14}$ are also shown as references, asterisk indicates the systematic error)

Anhydrous $CaB_{12}H_{12}$ is also synthesized by sintering of $Ca(BH_4)_2$ + $B_{10}H_{14}$ at 380 °C for 2h, its XRD and Raman results are shown in Figure 4.2. Three representative diffraction peaks at 2θ = 9.3°, 9.5° and 10.5° (2θ = 14.3°, 14.7° and 16.4° using Cu-Kα radiation) originated from $CaB_{12}H_{12}$ with a monoclinic (C2/*c*) crystal structure are clearly observed in the XRD patterns.[176] In the Raman spectra, vibration peaks assigned to B-H bending and stretching modes of $[B_{12}H_{12}]^{2-}$ are observed at 585, 751 and 2485, 2547 cm^{-1}, respectively.[182] No O-H vibration peak of water is detected in Raman spectra, which indicate the successful synthesis of anhydrous $CaB_{12}H_{12}$.

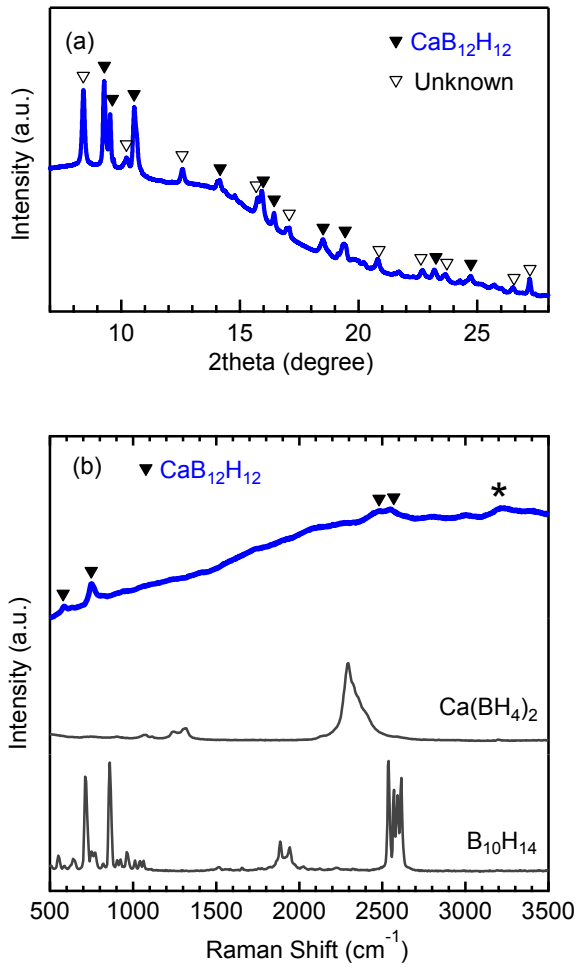

Figure 4.2 (a) Synchrotron XRD pattern and (b) Raman spectra of 5 h ball milled $Ca(BH_4)_2$ + $B_{10}H_{14}$ followed by sintering at 380 °C for 2 h. (Starting materials of $Ca(BH_4)_2$ and $B_{10}H_{14}$ are indicated as references, asterisk indicates the systematic error)

The successful synthesis of anhydrous $MgB_{12}H_{12}$ and $CaB_{12}H_{12}$ is further proved by solid state ^{11}B MAS NMR spectra, as shown in Figure 4.3. The main resonances at -15.0 and -14.0 ppm are assigned to $[B_{12}H_{12}]^{2-}$ in $MgB_{12}H_{12}$ and $CaB_{12}H_{12}$, respectively.[176] A small amount of $[B_{10}H_{10}]^{2-}$ (-28.3 ppm for Mg, -26.3 ppm for Ca),[96] $[BH_4]^-$ (-41.9 ppm for Mg, -32.2 ppm for Ca)[189] and unknown phases (-6.0 and -46.3 ppm) are detected in the synthesized $MgB_{12}H_{12}$ or $CaB_{12}H_{12}$ samples as impurities. In addition, the synthesized anhydrous $MgB_{12}H_{12}$ and $CaB_{12}H_{12}$ samples display homogenous yellow color, which is distinct from those of the starting materials of $Mg(BH_4)_2$ (white), $Ca(BH_4)_2$ (white) and $B_{10}H_{14}$ (white). All the above mentioned results, therefore, consistently indicate that sintering of metal borohydrides $M(BH_4)_2$

with $B_{10}H_{14}$ is a feasible method to synthesize anhydrous alkaline earth metal dodecaborates. The relative amount of the B-H species in the synthesized $MgB_{12}H_{12}$ and $CaB_{12}H_{12}$ is listed in Table 4.1 according to ^{11}B MAS NMR peak fitting (Figure 4.4).

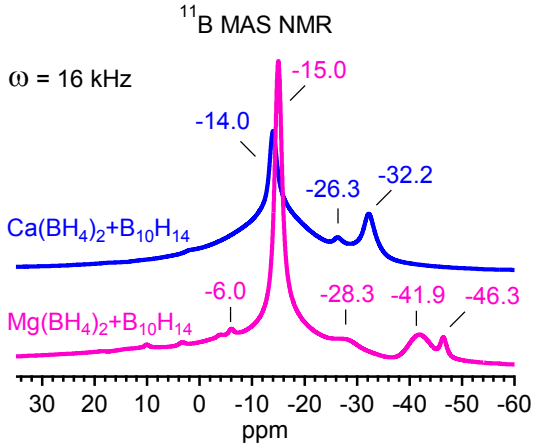

Figure 4.3 ^{11}B MAS NMR spectra of synthesized samples from $M(BH_4)_2$ + $B_{10}H_{14}$ (M = Mg: 5 h ball milling followed by sintering at 300 °C for 1 h; M = Ca: 5 h ball milling followed by sintering at 380 °C for 2 h).

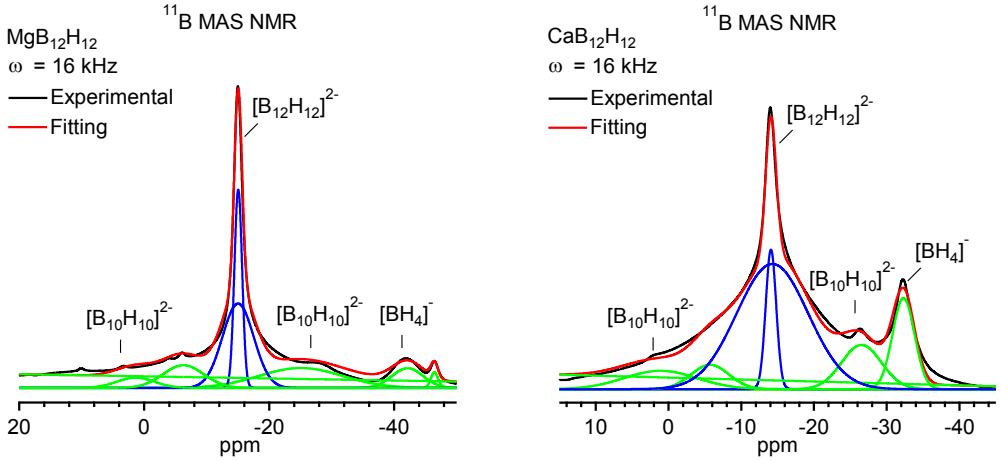

Figure 4.4 ^{11}B MAS NMR peak fitting of as synthesized $MgB_{12}H_{12}$ and $CaB_{12}H_{12}$.

Table 4.1 Relative amount of the B-H species in the synthesized $MgB_{12}H_{12}$ and $CaB_{12}H_{12}$.

Compounds	$[B_{12}H_{12}]^{2-}$	$[B_{10}H_{10}]^{2-}$	$[BH_4]^-$	Others
$MgB_{12}H_{12}$	52.98%	26.02%	7.81%	13.19%
$CaB_{12}H_{12}$	63.44%	18.79%	12.18%	5.59%

4.3.2 Deliquescence of Anhydrous $MgB_{12}H_{12}$ and $CaB_{12}H_{12}$

As the anhydrous $MgB_{12}H_{12}$ is hard to obtain, its reaction properties are barely to known.[151, 189] To comprehensively understand the reaction properties of dodecaborate intermediates for further improvement of hydrogen storage performance of borohydrides, I here firstly pay attention to investigate the deliquescence processes of anhydrous $MgB_{12}H_{12}$ and $CaB_{12}H_{12}$ based on our synthesized samples.

As shown in Figure 4.5, the deliquescence process of $MgB_{12}H_{12}$ was clearly observed using in-situ Raman spectra. With exposure in air for 5 min, the intensities of B-H vibration increased which implies the formation of $MgB_{12}H_{12}$•xH_2O with better crystal feature than amorphous $MgB_{12}H_{12}$. The Raman peak of B-H stretching mode shifted from 2590 to ca. 2510 cm^{-1} and a new peak at ca. 3500 cm^{-1} appeared which means the deliquescence process happened.[101, 189] When the exposure time was prolonged to 10, 20 and 60 min, no obvious change was observed, which means the swift deliquescence process of anhydrous $MgB_{12}H_{12}$. The 60 min of deliquescence product of anhydrously amorphous $MgB_{12}H_{12}$ has been identified as $Mg(H_2O)_6B_{12}H_{12}$•$6H_2O$ with apparent crystalline structure based on X-ray diffraction analysis (Figure 4.6).[151]

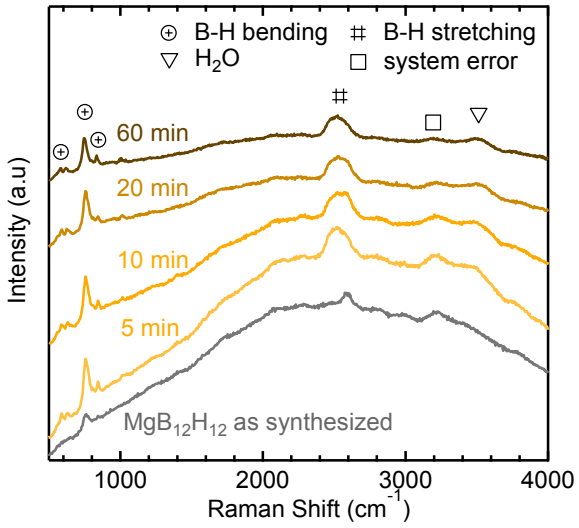

Figure 4.5 In-situ Raman spectra observation of the deliquescence processes of anhydrous $MgB_{12}H_{12}$ at 20 °C in air.

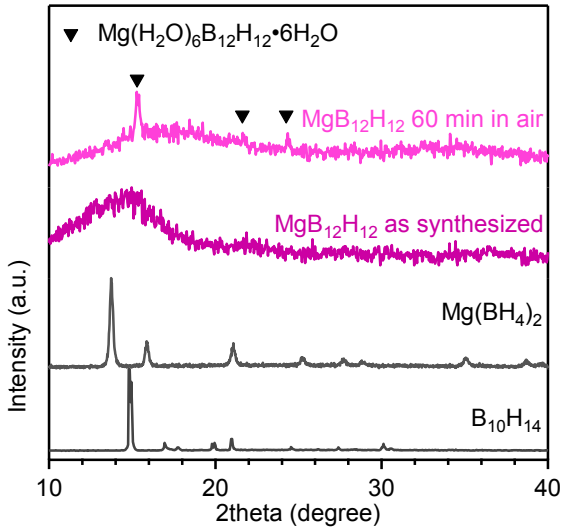

Figure 4.6 XRD patterns of as synthesized and 60 min exposure in air of $MgB_{12}H_{12}$.

The deliquescence process of anhydrous $CaB_{12}H_{12}$ is shown in Figure 4.7, there is no apparent change of peak location or appearance of O-H vibration, this phenomenon is caused by the high fluorescence background of synthesized sample.[137] In fact, the XRD patterns of anhydrous $CaB_{12}H_{12}$ after 60 min exposure in air indicates completely new crystal structure which is from $Ca(H_2O)_7[B_{12}H_{12}]•H_2O$ (Figure 4.8).[195]

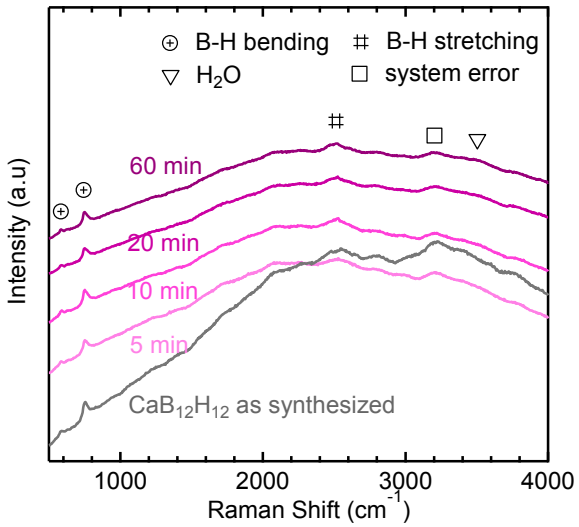

Figure 4.7 In-situ Raman spectra observation of the deliquescence processes of anhydrous $CaB_{12}H_{12}$ at 20 °C in air.

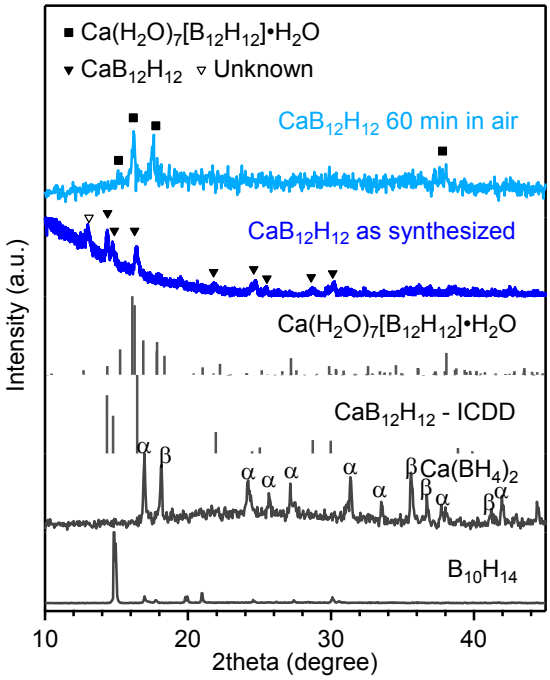

Figure 4.8 XRD patterns of $CaB_{12}H_{12}$ as synthesized and 60 min exposure in air. (The XRD pattern of $Ca(H_2O)_7[B_{12}H_{12}]\bullet H_2O$ is calculated based on its reported crystal structure by I Tiritiris et al for reference)[195]

Both of anhydrous $MgB_{12}H_{12}$ and $CaB_{12}H_{12}$ inflated and became fleecy when they were exposed in air, the sample of $MgB_{12}H_{12}$ remained yellow while $CaB_{12}H_{12}$ turn to pale from yellow (Figure 4.9). To make the dodecaborate samples deliquesce absolutely, both of anhydrous $MgB_{12}H_{12}$ and $CaB_{12}H_{12}$ were put in air for 4 h. Thermogravimetric analyses indicated apparent weight loss below 200 °C ascribed to the loss of absorbed water during deliquescence process (Figure 4.10) which couldn't be observed in as synthesized anhydrous $MgB_{12}H_{12}$ or $CaB_{12}H_{12}$.

In summary, both anhydrous $MgB_{12}H_{12}$ and $CaB_{12}H_{12}$ are apt to deliquesce in air to form crystalline hydrates, the anhydrous $MgB_{12}H_{12}$ exhibits better water adsorption ability to form $Mg(H_2O)_6B_{12}H_{12}\bullet 6H_2O$ than that of anhydrous $CaB_{12}H_{12}$ to produce $Ca(H_2O)_7[B_{12}H_{12}]\bullet H_2O$ under 1 h exposure in air. The finding that $MgB_{12}H_{12}$ combines with H_2O tighter than that of $MgB_{12}H_{12}$ may explain why anhydrous $MgB_{12}H_{12}$ is unavailable but anhydrous $CaB_{12}H_{12}$ is available from liquid-state processes.

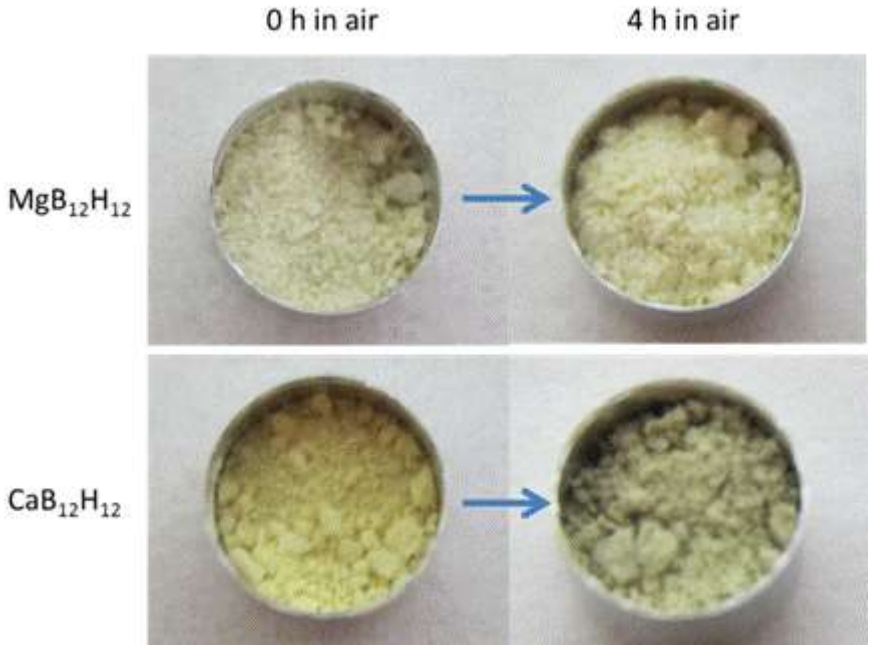

Figure 4.9 Photographical comparisons of $MgB_{12}H_{12}$ and $CaB_{12}H_{12}$ with/without 4 h exposure in air.

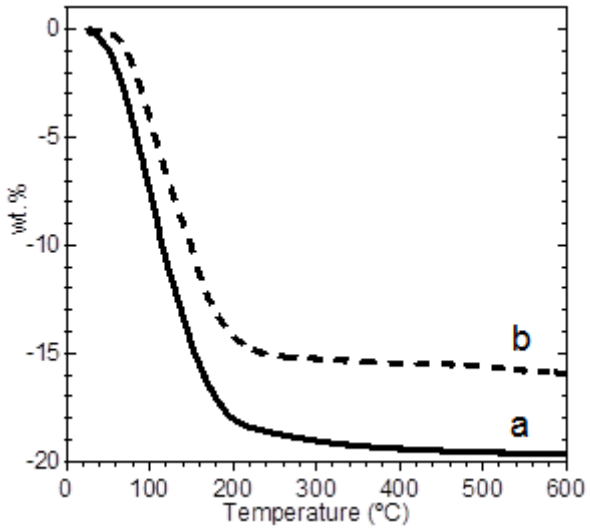

Figure 4.10 Thermogravimetric curves of synthesized $MgB_{12}H_{12}$ (a) and $CaB_{12}H_{12}$ (b) samples after 4 h of exposure in air (He 200 ml/min, 5 °C/min temperature ramp).

4.3.3 Thermal Decomposition of Anhydrous $MgB_{12}H_{12}$ and $CaB_{12}H_{12}$

4.3.3.1 $MgB_{12}H_{12}$

Thermal decomposition behaviors of anhydrous $MgB_{12}H_{12}$ examined by TG and MS are shown in Figure 4.11. Only hydrogen is detected by MS, indicating the weight loss upon heating is originated from the dehydrogenation of $MgB_{12}H_{12}$. The

dehydrogenation starts at approximately 190 °C and the dehydrogenation amount accumulates to 5.6 mass% (approximately 77% of theoretical hydrogen capacity in $MgB_{12}H_{12}$) when heated up to 800 °C via a multistep decomposition pathway as shown in TG and MS results.

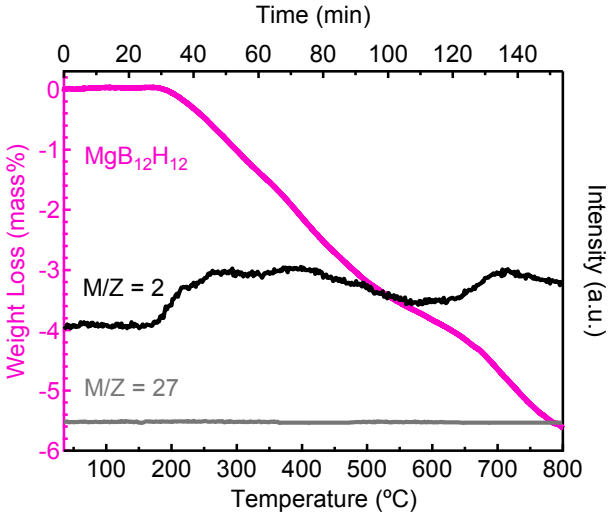

Figure 4.11 TG curve and MS signals of the synthesized $MgB_{12}H_{12}$ (mass numbers of 2 and 27 represent H_2 and B_2H_6).

In order to elucidate the decomposition pathway of anhydrous $MgB_{12}H_{12}$, the sample was heated to respective temperatures and subsequently cooled down to room temperature, and followed by systematic analyses of XRD, Raman and solid state ^{11}B NMR, their results are shown in Figure 4.12 and Figure 4.13, respectively.

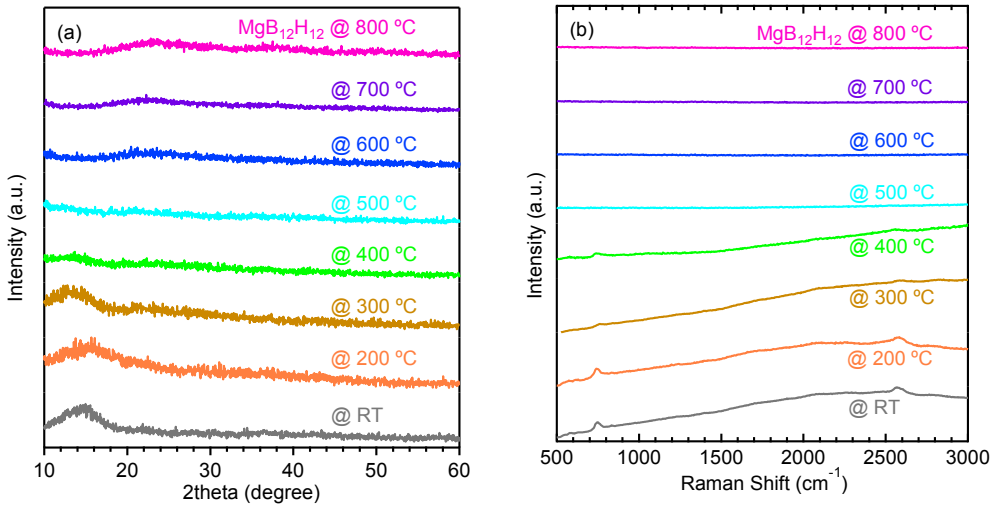

Figure 4.12 Ex-situ (a) XRD patterns and (b) Raman spectra of $MgB_{12}H_{12}$ at room temperature and heated up to respective temperatures.

When the temperature is increased up to 200 °C, the main resonance at -15.0 ppm attributed to $MgB_{12}H_{12}$ becomes weak, while the peak intensity for impurities of $Mg(BH_4)_2$ and $MgB_{10}H_{10}$ does not change obviously, which indicates that the decomposition of $MgB_{12}H_{12}$ starts at 190 °C, prior to that of $Mg(BH_4)_2$ as shown in Figure 4.14. When the temperature is increased up to 400 °C, the broad diffraction peak between 2θ = 10° and 18° disappears, and the B-H stretching mode of $MgB_{12}H_{12}$ at 2569 cm^{-1} becomes almost invisible, the main resonance of $MgB_{12}H_{12}$ at -15.0 ppm reduces significantly without any change in the chemical shift, which consistently indicate that a major part of B-H bond in the icosahedral $[B_{12}H_{12}]^{2-}$ has been broken to release hydrogen. Taking into account the dehydrogenation amount (2.1 mass%) of $MgB_{12}H_{12}$ up to 400 °C, I believe that the decomposition product mainly forms H-deficiency $MgB_{12}H_{12-x}$ (x = 3.5) that keeps the icosahedral B_{12} skeletons.[149] When the temperature is further increased up to 500, 600 and 700 °C, the dehydrogenation amount reaches 3.2, 3.8 and 4.6 mass% and the major resonance of $[B_{12}H_{12}]^{2-}$ at -15.0 ppm shifts to -13.1, -9.4 and -5.6 ppm, which suggest $MgB_{12}H_{12-x}$ continuously releases hydrogen accompanying with the polymerization of the icosahedral B_{12} skeletons and the formation of $(MgB_yH_z)_n$ polymers[187-188] those are water and DMSO insoluble. When the sample is heated up to 800 °C, the major resonance shifts to 0.9 ppm, which indicates the formation of amorphous boron at 800 °C, which is higher than that (600 °C) observed from the reported $MgB_{12}H_{12}$/Carbon nanocomposite,[189] suggesting that the carbon nanocomposite contributes to the temperature reduction.

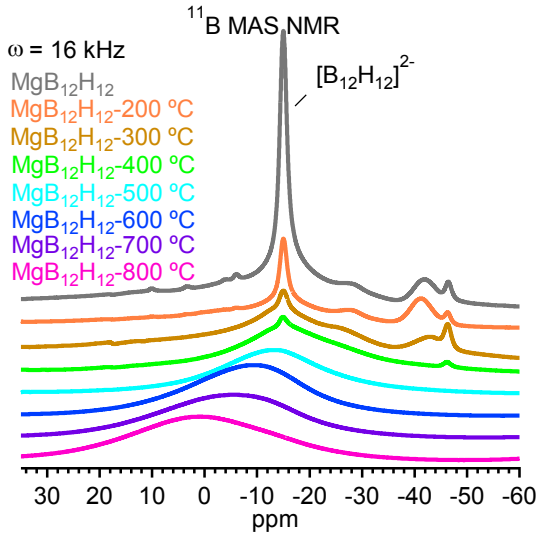

Figure 4.13 ^{11}B MAS NMR spectra of $MgB_{12}H_{12}$ as synthesized and heated up to respective temperatures.

Based on the abovementioned experimental results, thermal decomposition pathway of anhydrous $MgB_{12}H_{12}$ could be briefly summarized as the following steps:

Step 1: $MgB_{12}H_{12} \rightarrow MgB_{12}H_{12-x} + x/2H_2$ (4.2)

Step 2: $nMgB_{12}H_{12-x} \rightarrow (MgB_yH_z)_n + z'H_2$ (4.3)

Step 3: $(MgB_yH_z)_n \rightarrow$ amorphous B + Mg + z''H_2 (4.4)

It is worth emphasizing that the thermal decomposition behavior of the single phase

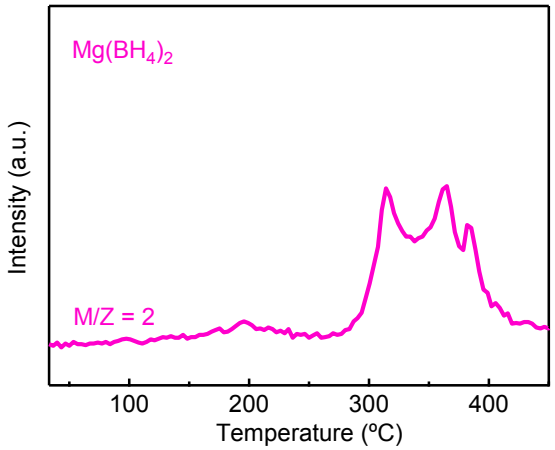

Figure 4.14 MS spectra of $Mg(BH_4)_2$ (mass numbers 2 represents H_2).

$MgB_{12}H_{12}$ is different from that in-situ formed during dehydrogenation of $Mg(BH_4)_2$: a) the single phase $MgB_{12}H_{12}$ exhibits a lower initial decomposition temperature and a wider decomposition temperature range of 190 ~ 800 °C than those of $Mg(BH_4)_2$, b) the single phase $MgB_{12}H_{12}$ decomposes into amorphous boron rather than MgB_2 formed as the decomposition product of $Mg(BH_4)_2$ at 600 °C.[196] Those differences may result from the concurrent formation of MgH_2 together with $MgB_{12}H_{12}$, since $MgB_{12}H_{12}$ can be facilitated by MgH_2 to form MgB_2 as predicted by first-principles calculations.[89]

4.3.3.2 $CaB_{12}H_{12}$

Like those of the anhydrous $MgB_{12}H_{12}$, thermal decomposition behaviors of anhydrous $CaB_{12}H_{12}$ are also systematically studied in the same way and their TG and MS results are shown in Figures 4.15. Only hydrogen is detected by MS, indicating the weight loss upon heating is originated from the dehydrogenation of $CaB_{12}H_{12}$. The dehydrogenation starts at ca. 320 °C and the dehydrogenation amount reaches 2.5

mass% (approximately 38% of theoretical hydrogen capacity in $CaB_{12}H_{12}$), comparable to the reported value (1.5 mass% at 600 °C),[176] via multistep reactions when heated up to 750 °C.

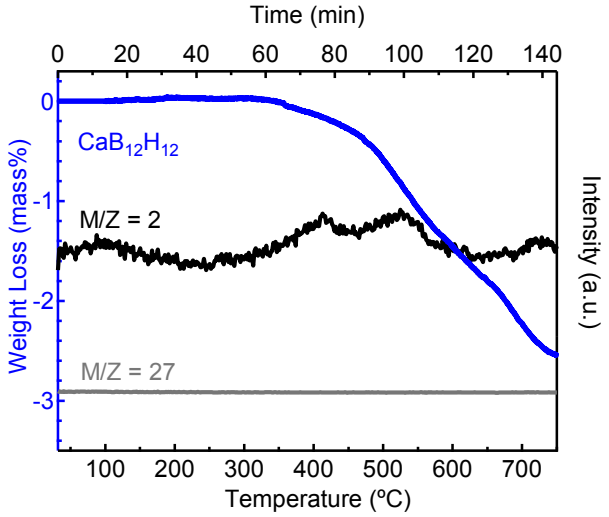

Figure 4.15 TG curve and MS signals of the synthesized $CaB_{12}H_{12}$ (mass numbers of 2 and 27 represent H_2 and B_2H_6).

XRD patterns, Raman spectra and solid-state ^{11}B MAS NMR spectra of anhydrous $CaB_{12}H_{12}$ heated to respective temperatures and subsequently cooled down to room temperature are shown in Figures 4.16 and 4.17, respectively. When $CaB_{12}H_{12}$ is heated up to 400 °C, no obvious changes of diffraction peaks, Raman spectra and the major resonance for $CaB_{12}H_{12}$ are confirmed, whereas the resonance at -32.2 ppm originated from the residual $Ca(BH_4)_2$ nearly disappears at 375 °C, suggesting that the weight loss below 400 °C is responsible for the dehydrogenation of residual $Ca(BH_4)_2$. When $CaB_{12}H_{12}$ is heated up to 500 °C, diffraction peaks and Raman spectra attributed to $CaB_{12}H_{12}$ disappear, the major resonance at -14.0 ppm becomes significantly weak and overlaps with a broad resonance between 0 and -13 ppm, suggesting that the dehydrogenation of $CaB_{12}H_{12}$ to $CaB_{12}H_{12-x}$ as well as the polymerization of $CaB_{12}H_{12-x}$ to water and DMSO insoluble $(CaB_yH_z)_n$ polymers starts to happen at 500 °C.[187-188] When $CaB_{12}H_{12}$ is further heated up to 600 °C and 750 °C, the major resonance shifts to -11.2 and -7.0 ppm, indicating the continuous polymerization of $(CaB_yH_z)_n$, similar to that of $MgB_{12}H_{12}$ heated up to 500 ~ 700 °C. Unlike $MgB_{12}H_{12}$, no obvious NMR spectra originated from amorphous boron is observed when $CaB_{12}H_{12}$ is heated up to 750 °C.

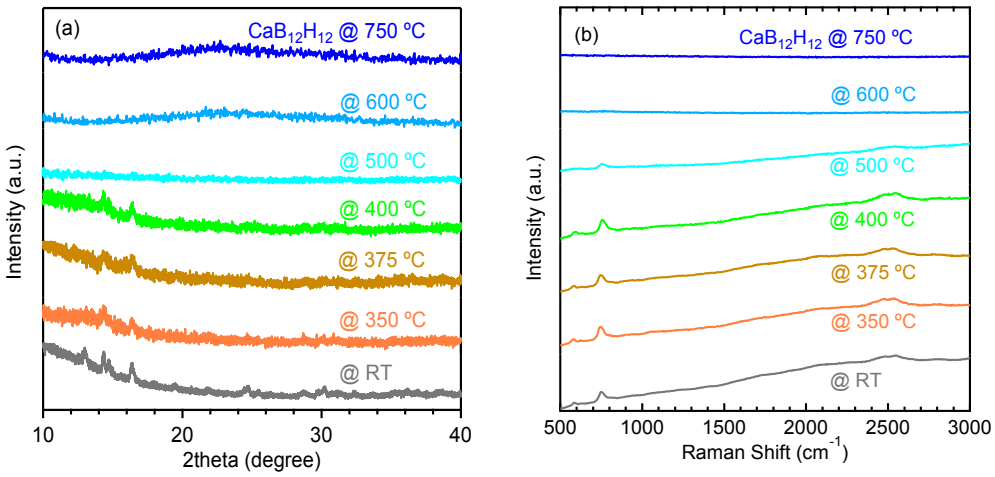

Figure 4.16 Ex-situ (a) XRD patterns and (b) Raman spectra of $CaB_{12}H_{12}$ at room temperature and heated up to respective temperatures.

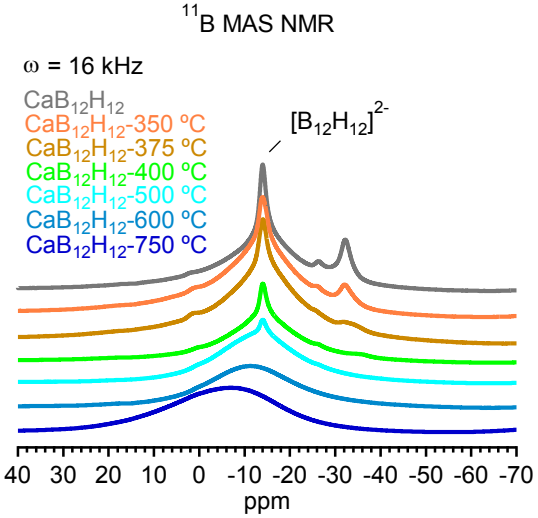

Figure 4.17 ^{11}B MAS NMR spectra of $CaB_{12}H_{12}$ as synthesized and heated up to respective temperatures.

The decomposition pathway of single phase anhydrous $CaB_{12}H_{12}$ is briefly summarized as the following steps (below 750 °C):

Step 1 : $CaB_{12}H_{12} \rightarrow CaB_{12}H_{12-x} + x/2H_2$ (4.5)

Step 2 : $nCaB_{12}H_{12-x} \rightarrow (CaB_yH_z)_n + z'H_2$ (4.6)

Similar to that of $MgB_{12}H_{12}$, the decomposition behavior of single phase $CaB_{12}H_{12}$ is different from that formed as a dehydrogenation intermediate of $Ca(BH_4)_2$, suggesting

that the coexist CaH_2 facilitates the decomposition of $CaB_{12}H_{12}$ to produce CaB_6 that is not detected even $CaB_{12}H_{12}$ was heated up to 750 °C.[89]

In summary, thermal decomposition of single phase $MgB_{12}H_{12}$ and $CaB_{12}H_{12}$ tends to experience two steps of 1) dehydrogenation to produce H-deficiency $MB_{12}H_{12-x}$ and 2) polymerization of $MB_{12}H_{12-x}$ to form $(MB_yH_z)_n$, which would be the major obstacle to be overcome for rehydrogenation. On the other hand, $MB_{12}H_{12}$ formed in-situ during the dehydrogenation of $Mg(BH_4)_2$ and $Ca(BH_4)_2$ can be facilitated by the co-exist MH_2 to form MB_x that improves the rehydrogenation.[102, 193] In other words, an appropriate composition of $M_{2/n}B_{12}H_{12}$ and MH_x is expected to be designed to improve the rehydrogenation as well as the reversibility of borohydrides.

4.4 Conclusions

In this chapter, anhydrous alkaline earth metal dodecaborates $MgB_{12}H_{12}$ and $CaB_{12}H_{12}$ have been successfully synthesized through sintering of ball milled $M(BH_4)_2 + B_{10}H_{14}$ (M = Mg, Ca). This study again proves that sintering of borohydrides with $B_{10}H_{14}$ is a facile method to synthesize anhydrous metal dodecaborates. Both anhydrous $MgB_{12}H_{12}$ and $CaB_{12}H_{12}$ are apt to deliquesce in air to form $Mg(H_2O)_6B_{12}H_{12}\bullet 6H_2O$ and $Ca(H_2O)_7[B_{12}H_{12}]\bullet H_2O$ under 1 h exposure. The better water combining ability of anhydrous $MgB_{12}H_{12}$ than that of $CaB_{12}H_{12}$ may be the reason why anhydrous $MgB_{12}H_{12}$ is unavailable but anhydrous $CaB_{12}H_{12}$ is available from liquid-state processes. Systematic thermal decomposition investigations demonstrate that both $MgB_{12}H_{12}$ and $CaB_{12}H_{12}$ firstly release hydrogen to form H-deficiency $MB_{12}H_{12-x}$ with the icosahedral B_{12} skeletons followed by a polymerization process to produce $(MB_yH_z)_n$. The single phase anhydrous $MgB_{12}H_{12}$ decomposes into amorphous B at 800 °C, whereas $CaB_{12}H_{12}$ may require much higher temperature to complete the decomposition. The lower electronegativity of Ca than that of Mg is considered to be responsible for the higher stability of $CaB_{12}H_{12}$ than that of $MgB_{12}H_{12}$.[111] Distinct from those of the single phase $MgB_{12}H_{12}$ and $CaB_{12}H_{12}$, thermal decomposition of those in-situ formed during the dehydrogenation of $Mg(BH_4)_2$ and $Ca(BH_4)_2$ could be facilitated by the co-exist MgH_2 and CaH_2, suggesting that designing an appropriate composition of $M_{2/n}B_{12}H_{12}$ and MH_x would be a promising way to substantially improve the rehydrogenation of borohydrides.

Chapter 5

Synthesis and Thermal Stabilities of Bimetallic Dodecaborates

This chapter is based on the submitted paper:

He L, Li H-W, Filinchuk Y, Nakajima H, Tumanov N, Filinchuk Y, Huang S, Sharma M, Hagemann H, Akiba E, Synthesis of a Bimetallic Dodecaborate $LiNaB_{12}H_{12}$ with Outstanding Super Ionic Conductivity. Submitted to *Chemistry of Materials*.

In this chapter, bimetallic dodecaborates $LiNaB_{12}H_{12}$, $Li_6K_4(B_{12}H_{12})_5$ and $Na_8K_2(B_{12}H_{12})_5$ are synthesized for the first time using the solvent-free synthesis process. All of bimetallic dodecaborates $LiNaB_{12}H_{12}$, $Li_6K_4(B_{12}H_{12})_5$ and $Na_8K_2(B_{12}H_{12})_5$ exhibit different decomposition temperatures with their single counterparts ($Li_2B_{12}H_{12}$, $Na_2B_{12}H_{12}$ and $K_2B_{12}H_{12}$), suggesting that designing bimetallic dodecaborates is an effective way to tune the thermal stabilities of their single counterparts.

5.1 Introduction

In borohydrides $M(BH_4)_n$, the formation enthalpy ΔH_f can be estimated by the Pauling electronegativity χ_p of the corresponding M. The good linear relationship between ΔH_f of $M(BH_4)_n$ and χ_p of M, as well as the negative correlation between the decomposition temperature T_d of $M(BH_4)_n$ and χ_p of M was discovered.[111] According to this finding, improving χ_p of the metal cations in borohydrides can be applied to decrease the decomposition temperature of corresponding borohydrides. As a result, producing bimetallic borohydrides $MM'(BH_4)_n$ in which M and M' with different electronegativities, is suggested to tune the thermodynamic stability of borohydrides.[112] Successful synthesis of bimetallic borohydrides such as $LiK(BH_4)_2$, $Na_2Mn(BH_4)_4$ and $KSc(BH_4)_4$ have been reported.[113, 115-116] All $MM'(BH_4)_n$ present

different thermodynamic stabilities from those of $M(BH_4)_n$ and $M'(BH_4)_n$.

Though bimetallic borohydrides have been studied, no study on bimetallic dodecaborate synthesis and property investigation has been reported at present, how to tune the stability of dodecaborate still remains a crucial issue to be investigated and resolved for both improvement hydrogen storage properties of borohydrides and development of potential superionic conductor for battery application. Herein in this chapter, I attempt to tune thermal stabilities of dodecaborates by designing bimetallic dodecaborates. Anhydrous bimetallic dodecaborates $LiNaB_{12}H_{12}$, $Li_6K_4(B_{12}H_{12})_5$ and $Na_8K_2(B_{12}H_{12})_5$ are successfully synthesized for the first time via heat treatment of decaborane with two monometallic borohydrides. Their thermal stabilities are subsequently discussed through comparison with their single counterparts.

5.2 Experimental Section

Commercial $B_{10}H_{14}$ (99%, Wako), $LiBH_4$ (95%, Aldrich), $NaBH_4$ (99.99%, Aldrich) and KBH_4 (98%, Aldrich) were all purchased from chemical companies and stored in glove box protected by purified Ar and used without purification. $NaAl(BH_4)_4$ and $KAl(BH_4)_4$ were supplied by Prof. Y. Filinchuk from Université catholique de Louvain. Different proportions of starting materials were firstly mechanically milled by Fritsch P-7 ball milling machine at room temperature with 10 steel balls (7 mm in diameter) in a hardened steel vial (30 cm^3 in volume) under 0.1 MPa Ar for 5 h (15 min milling, 5 min pausing). To avoid decomposition during mechanical milling, $NaAl(BH_4)_4 + 2B_{10}H_{14}$ and $KAl(BH_4)_4 + 2B_{10}H_{14}$ were hand milled for only 10 min in glove box protected with pure Ar. Subsequently, the ball milled products were sealed into stainless steel crucibles (~ 0.7 cm^3 in volume, 38.3 g in weight for every set) for heat treatment at 110-450 °C with time range from 10 to 20 h, respectively.

Powder X-ray diffraction (XRD) patterns were obtained from Rigaku Ultima IV X-ray diffractometer with Cu-Kα radiation (λ = 1.54 Å) with accelerating voltage and tube current as 40 kV and 40 mA. The powder state of samples was placed in a glass plate sealed by Scotch tape to prevent contamination by air during the measurement. Raman spectra were obtained on RAMAN-11 VIS-SS (Nanophoton) machine via a laser with 532 nm wavelength (green). Solid-state magic angle spinning (MAS) nuclear magnetic resonance (NMR) spectra were measured by a Bruker DSX-500 spectrometer and 4mm Bruker MAS probe without boron background at room

temperature. NMR sample preparations were always finished in glove box protected with pure Ar and sample spinning was achieved using dry N_2 gas. ^{11}B MAS NMR spectra were obtained at excitation pulses of 0.5 μs（π/12 pulse) and with strong ^{1}H decoupling pulses. BF_3OEt_2 (δ = 0.00 ppm) was used as external standard for confirmation of ^{11}B NMR chemical shifts. TG was recorded by Rigaku Thermo Plus Evo II TG-DTA 8120/S AEMK using 5 °C/min of heating ramp under 1 bar of He with 200 ml/min flow.

5.3 Results and Discussion

5.3.1 Monometallic Borohydrides for Bimetallic Dodecaborate Synthesis

As a case study to investigate the synthesis of bimetallic dodecaborates from monometallic borohydrides, alkali metal borohydrides $LiBH_4$, $NaBH_4$ and KBH_4 are firstly used as starting materials and the reaction equation is shown as follows:

$$aMBH_4 + bM'BH_4 + cB_{10}H_{14} \rightarrow M_aM'_b(B_{12}H_{12})_c + dH_2$$

(M, M' = Li, Na, K; a + b = 2c) (5.1)

$LiNaB_{12}H_{12}$ was prepared through sintering of $LiBH_4$, $NaBH_4$ and $B_{10}H_{14}$ with a stoichiometric molar ratio of 1:1:1 at 400 °C for 10 h. The successful synthesis was proved by X-ray diffraction, Raman spectra and solid state nuclear magnetic resonance (NMR) measurements (Figure 5.1 and Figure 5.2). As shown in Figure 5.1, when sintering of $LiBH_4$ + $NaBH_4$ + $B_{10}H_{14}$ was performed at 400 °C for 10 h, four new diffraction peaks different from those of $Li_2B_{12}H_{12}$ or $Na_2B_{12}H_{12}$ at 2θ = 15.64°, 18.08°, 20.24° and 22.20° were clearly observed in the product, which means the formation of new compound. Raman spectra of synthesized sample exhibits similar B-H bending and stretching of $[B_{12}H_{12}]^{2-}$ cluster from ca. 500 to 1000 cm^{-1} and around 2500 cm^{-1} to those of $Li_2B_{12}H_{12}$ and $Na_2B_{12}H_{12}$. Careful comparison of B-H stretching modes indicates that two Raman peaks of the synthesized sample at 2490 cm^{-1} (H_g) and 2534 cm^{-1} (A_g) are both at locations between that of $Li_2B_{12}H_{12}$ (2476 cm^{-1} for H_g and 2543 cm^{-1} for A_g) and $Na_2B_{12}H_{12}$ (2494 cm^{-1} for H_g and 2521 cm^{-1} for A_g) which means the successful synthesis of $LiNaB_{12}H_{12}$. The successful synthesis of $LiNaB_{12}H_{12}$ is also confirmed by ^{11}B and ^{23}Na MAS NMR (Figure 5.2). Diffraction peaks at approximately -16 ppm are ascribed to $[B_{12}H_{12}]^{2-}$, two small peaks at ~ 2 ppm and -32 ppm are ascribed to small amount of $[B_{10}H_{10}]^{2-}$ inpurity.[96, 103, 176, 178, 183]

In ^{23}Na MAS NMR, the -15 ppm peak is assigned to $Na_2B_{12}H_{12}$ phase, the rest broad peak can be assigned to the $LiNaB_{12}H_{12}$ phase with the yield over 90%.

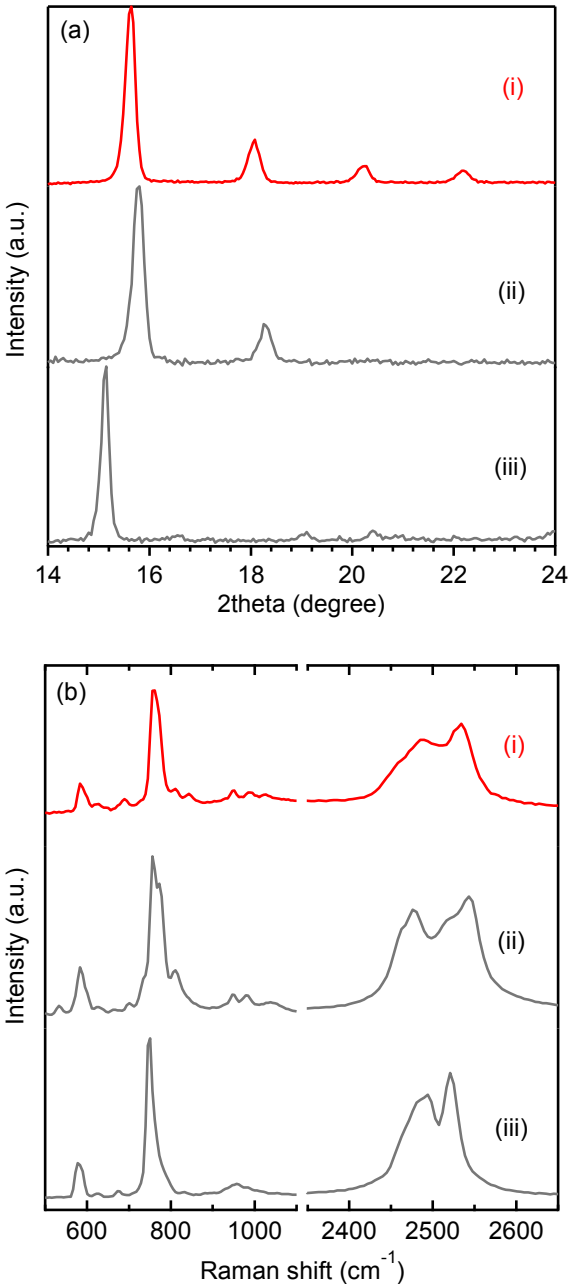

Figure 5.1 (a) XRD diffraction patterns and (b) Raman spectra of (i) 5 h ball milled $LiBH_4$ + $NaBH_4$ + $B_{10}H_{14}$ followed by heat treatment at 400 °C for 10 h; (ii) $Li_2B_{12}H_{12}$ and (iii) $Na_2B_{12}H_{12}$.

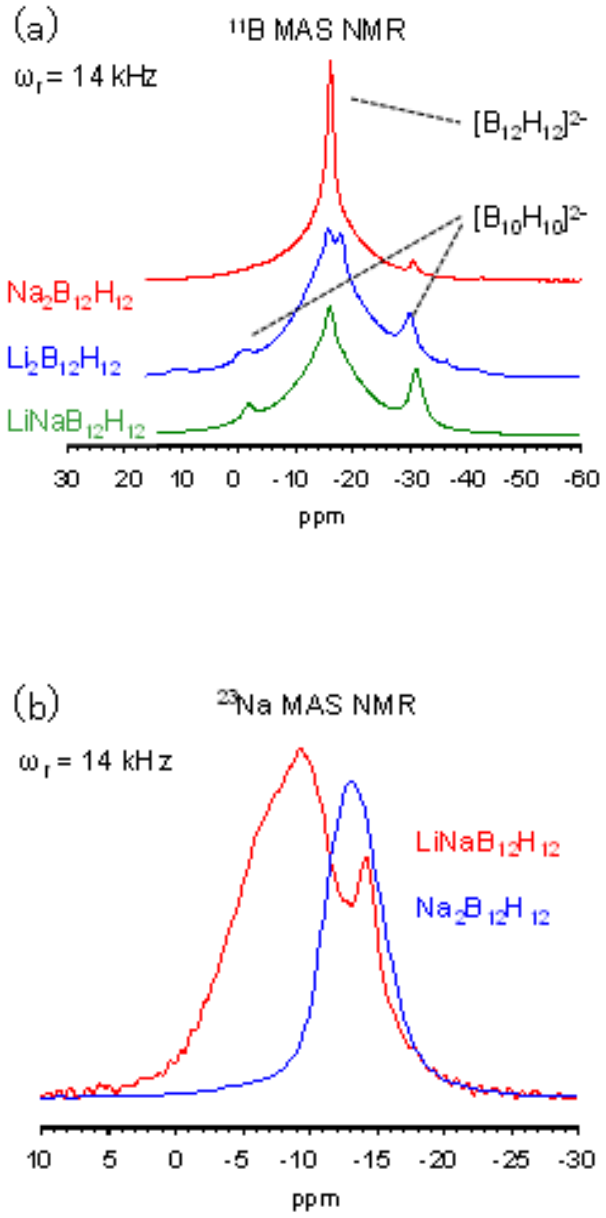

Figure 5.2 (a) ^{11}B and (b) ^{23}Na MAS NMR profiles of (i) 5 h ball milled $LiBH_4$ + $NaBH_4$ + $B_{10}H_{14}$ followed by heat treatment at 400 °C for 10 h; (ii) $Li_2B_{12}H_{12}$ and (iii) $Na_2B_{12}H_{12}$.

The synthesis of bimetallic dodecaborates including Li and K as cations is shown in Figure 5.3. $LiBH_4$, KBH_4 and $B_{10}H_{14}$ with mole ratio 1:1:1 is firstly adopted based on the synthesis experience of $LiNaB_{12}H_{12}$. When the starting materials of $LiBH_4$ + KBH_4 + $B_{10}H_{14}$ is heat treated at 300 °C for 10 h, two diffraction peaks different from those of $Li_2B_{12}H_{12}$ and $K_2B_{12}H_{12}$ at 2θ = 16.7° and 21.1° are obviously observed

which is ascribed to the formation of new phase. Raman spectra compared with those of $Li_2B_{12}H_{12}$ and $K_2B_{12}H_{12}$ indicate the formation of $[B_{12}H_{12}]^{2-}$ cluster. However, large amount of $K_2B_{12}H_{12}$ formation as impurity has also been observed. To improve the yield of the possible $LiKB_{12}H_{12}$ new phase, the starting materials of $LiBH_4$ + KBH_4 + $B_{10}H_{14}$ is also heat treated at 400 °C for 10 h and 400 °C for 20 h, the XRD patterns show significant increase of new phase and two low diffraction peaks at 2θ = 25.7° and 29.9° ascribed to new phase are also observed, which means 400 °C is more efficient for synthesis of new phase than 300 °C. Nevertheless, the existence of $K_2B_{12}H_{12}$ as impurity is still clearly observed in these two improved synthesis conditions. Then I consider the bimetallic dodecaborate including Li and K may not be comprised with a proportion of 1:1.

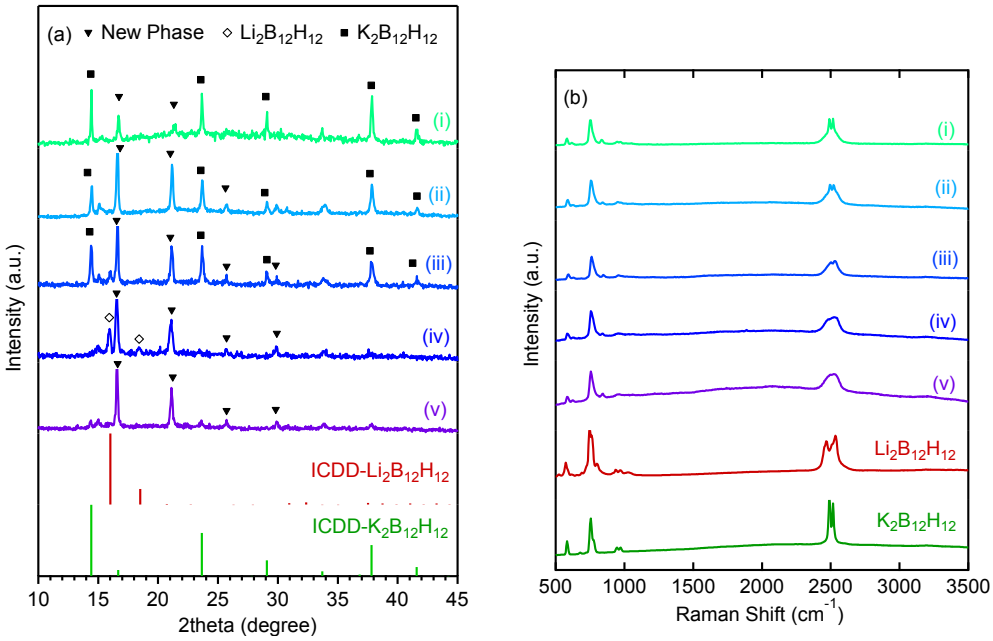

Figure 5.3 (a) XRD patterns and (b) Raman spectra of synthesized samples from 5h ball milled a$LiBH_4$ + bKBH_4 + (a+b)/2$B_{10}H_{14}$ at different reaction conditions: (i) a:b=1:1, 300 °C 10 h HT; (ii) a:b=1:1, 400 °C 10 h HT; (iii) a:b=1:1, 400 °C 20 h HT; (iv) a:b=2:1, 400 °C 10 h HT; (v) a:b=3:2, 400 °C 10 h HT; $Li_2B_{12}H_{12}$ and $K_2B_{12}H_{12}$ are shown for comparison, respectively. (HT = Heat treatment)

The starting material is then changed to be 4$LiBH_4$ + 2KBH_4 + 3$B_{10}H_{14}$ with 2:1 mole ratio of $LiBH_4$ and KBH_4 and heat treated at 400 °C for 10 h. In this case, the new phase is also obviously observed but with formation of small amount of

$Li_2B_{12}H_{12}$. I attribute this phenomenon to the excess of $LiBH_4$ in the starting material. Therefore, the starting material is further changed as $6LiBH_4 + 4KBH_4 + 5B_{10}H_{14}$ with 3:2 mole ratios of $LiBH_4$ and KBH_4. The diffraction of $6LiBH_4 + 4KBH_4 + 5B_{10}H_{14}$ after 400 °C heat treatment for 10 h almost exhibits complete new phase. Raman specatra show the similar B-H bending and stretching peaks from $[B_{12}H_{12}]^{2-}$ cluster between 500-100 cm^{-1} and around 2500 cm^{-1}, which indicates the new phase is $Li_6K_4(B_{12}H_{12})_5$. Taking into account the similar XRD patterns of synthesized $Li_6K_4(B_{12}H_{12})_5$ to those of $LiNaB_{12}H_{12}$, they may own same symmetric structures.

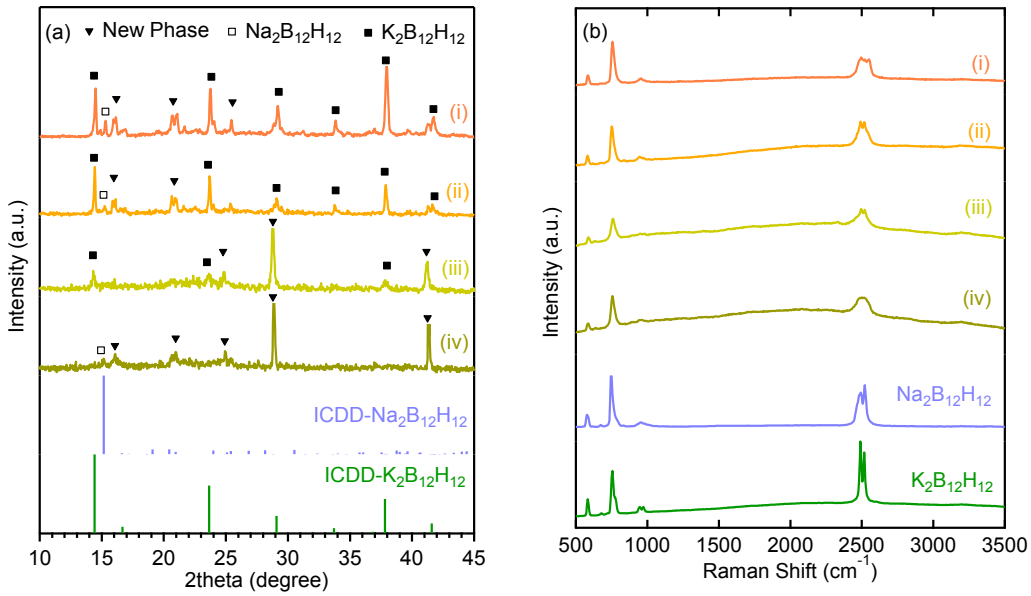

Figure 5.4 (a) XRD patterns and (b) Raman spectra of synthesized samples from 5h ball milled $aNaBH_4 + bKBH_4 + (a+b)/2B_{10}H_{14}$ at different reaction conditions: (i) a:b=1:1, 450 °C 20 h HT; (ii) a:b=1:1, 400 °C 10 h HT; (iii) a:b=3:1, 400 °C 10 h HT; (iv) a:b=4:1, 400 °C 10 h HT; $Na_2B_{12}H_{12}$ and $K_2B_{12}H_{12}$ are shown for comparison, respectively. (HT = Heat treatment)

The synthesis information of bimetallic dodecaborates including Na and K as cations is shown in Figure 5.4. The exploration process of synthesis conditions is similar to that of synthesis of $Li_6K_4(B_{12}H_{12})_5$. Finally, the starting material of $8NaBH_4 + 2KBH_4 + 5B_{10}H_{14}$ with 4:1 mole ratio of $NaBH_4$ and KBH_4 heat treated at 400 °C for 10 h exhibits formation of almost complete new phase at 2θ = 16.1°, 21.0°, 25.0°, 28.8° and 41.3°. Raman spectra compared with those of $Na_2B_{12}H_{12}$ and $K_2B_{12}H_{12}$ indicate the formation of $[B_{12}H_{12}]^{2-}$ cluster with similar B-H bending and stretching

peaks between 500-100 cm^{-1} and around 2500 cm^{-1}. Therefore, the single phase of bimetallic dodecaborates including Na and K can be decided as $Na_8K_2(B_{12}H_{12})_5$.

5.3.2 Bimetallic Borohydrides for Bimetallic Dodecaborate Synthesis

To investigate the synthesis of bimetallic dodecaborates from bimetallic borohydrides, bimetallic borohydrides $NaAl(BH_4)_4$, $KAl(BH_4)_4$ and $B_{10}H_{14}$ are used as starting materials and the reaction equations are conceived as follows:

$$NaAl(BH_4)_4 + 2B_{10}H_{14} \rightarrow NaAl(B_{12}H_{12})_2 + 10H_2 \quad (5.2)$$

$$KAl(BH_4)_4 + 2B_{10}H_{14} \rightarrow KAl(B_{12}H_{12})_2 + 10H_2 \quad (5.3)$$

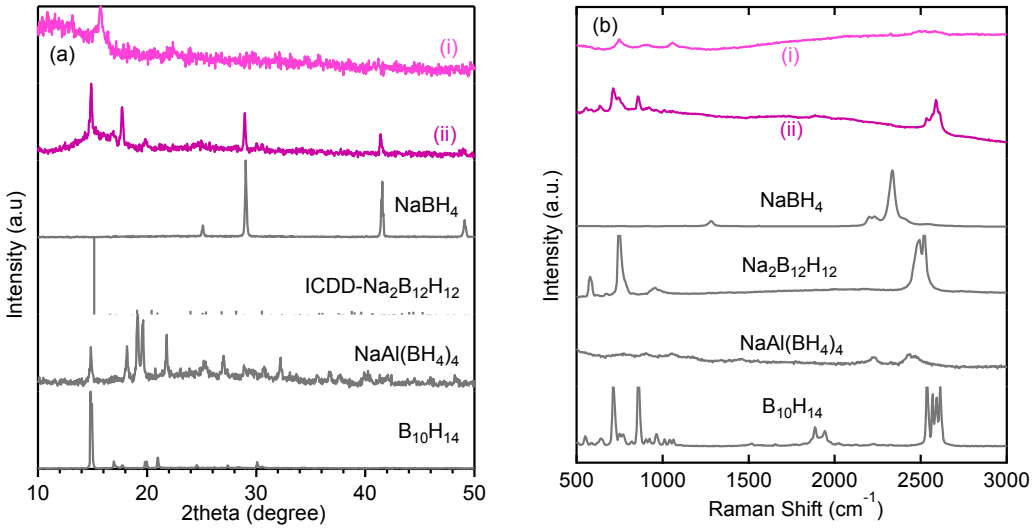

Figure 5.5 (a) XRD patterns and (b) Raman spectra of synthesized samples from 10 min hand milled $NaAl(BH_4)_4 + 2B_{10}H_{14}$ at different reaction conditions: (i) 300 °C 10 h HT; (ii) 110 °C 10 h HT; $NaBH_4$, $Na_2B_{12}H_{12}$, $NaAl(BH_4)_4$ and $B_{10}H_{14}$ are shown for comparison, respectively. (HT = Heat treatment)

As shown in Figure 5.5, when starting materials $NaAl(BH_4)_4 + 2B_{10}H_{14}$ are heat treated at 300 °C for 10 h, XRD patterns show a new peak at $2\theta \approx 16$, but Raman spectra show no $[B_{12}H_{12}]^{2-}$ formation. The product turns to yellow and black with heterogeneous features, the product reacts with water violently which may be ascribed to the formed $Al(BH_4)_3$ not detected in XRD patterns and Raman spectra; when starting materials are heat treated at 110 °C for 10 h, the product turns to yellow. XRD patterns indicate the large amount residual of $B_{10}H_{14}$ and formation of $NaBH_4$ which means $NaAl(BH_4)_4$ has already decomposed into $NaBH_4$ at even 110 °C. Raman

spectra indicate the existence of residual of $B_{10}H_{14}$ but without formation of $[B_{12}H_{12}]^{2-}$ at 110 °C, too.

Starting materials $KAl(BH_4)_4$ + $2B_{10}H_{14}$ was heat treated at 300 °C for 10 h, the product turn to gray and polyporous block. As shown in Figure 5.6, XRD pattern shows the formation of KBH_4, but Raman spectra show the residual $B_{10}H_{14}$ and potential small amount of $K_2B_{12}H_{12}$. Both $NaAl(BH_4)_4$ and $KAl(BH_4)_4$ turn to decompose during the heat treatment processes and no formation of bimetallic $NaAl(B_{12}H_{12})_2$ or $KAl(B_{12}H_{12})_2$ were achieved.

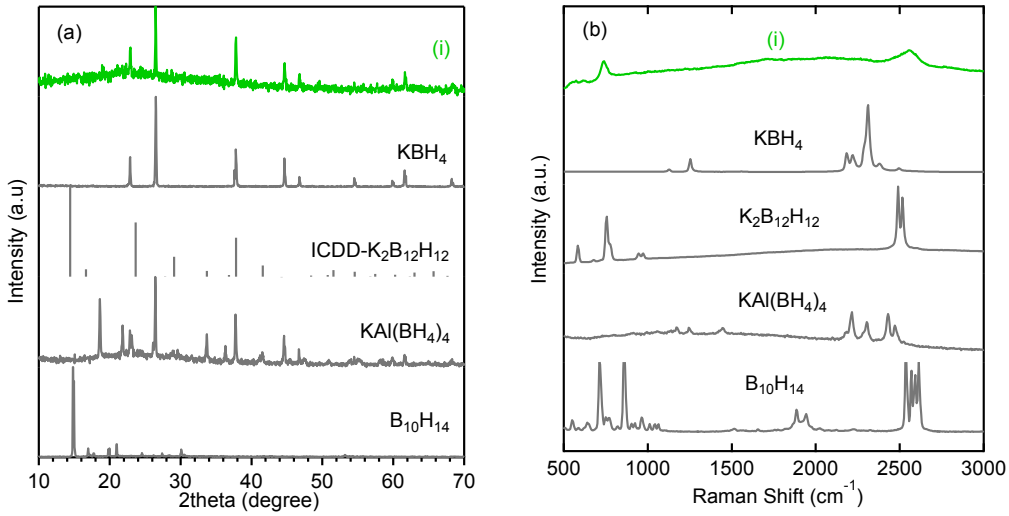

Figure 5.6 (a) XRD patterns and (b) Raman spectra of 10 min hand milled $KAl(BH_4)_4$ + $2B_{10}H_{14}$ followed by 300 °C 10 h HT; KBH_4, $K_2B_{12}H_{12}$, $KAl(BH_4)_4$ and $B_{10}H_{14}$ are shown for comparison, respectively. (HT = Heat treatment)

5.3.3 Thermal Stabilities of Synthesized Bimetallic Dodecaborates

The thermal stabilities of the successfully synthesized bimetallic dodecaborates are preliminarily investigated by TG to compare with their single counterparts. As shown in Figure 5.7, $LiNaB_{12}H_{12}$ starting to decompose at ca. 300 °C with overall 2.54 mass % weight loss at 700 °C exhibits compromised thermal stability between that of $Li_2B_{12}H_{12}$ and $Na_2B_{12}H_{12}$. This fact indicates it is feasible to stabilize $Li_2B_{12}H_{12}$ or destabilize $Na_2B_{12}H_{12}$ via $LiNaB_{12}H_{12}$ obtained by partial cationic substitution of $Li_2B_{12}H_{12}$ or $Na_2B_{12}H_{12}$.

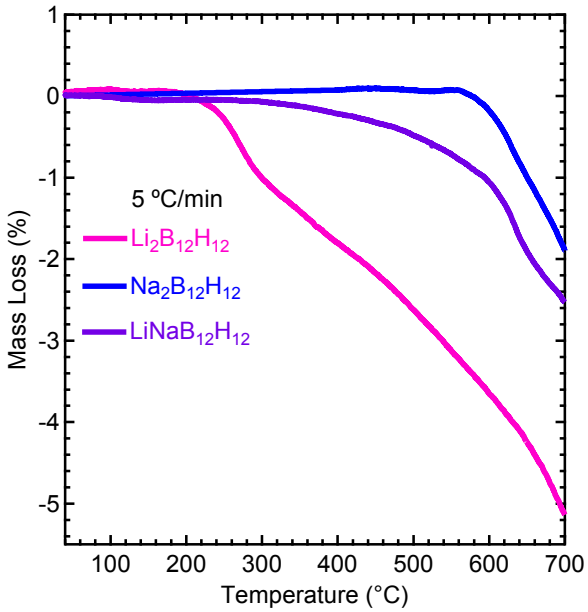

Figure 5.7 TG curve of synthesized $LiNaB_{12}H_{12}$ ($LiBH_4$ + $NaBH_4$ +$B_{10}H_{14}$: 5h ball milling, heat treatment at 400 °C for 10 h) compared with that of $Li_2B_{12}H_{12}$ and $Na_2B_{12}H_{12}$. (200 ml/min He flow, 5 °C/min)

Figure 5.8 shows the stability of $Li_6K_4(B_{12}H_{12})_5$ in comparison with that of $Li_2B_{12}H_{12}$ and $K_2B_{12}H_{12}$. $Li_6K_4(B_{12}H_{12})_5$ starting to decompose at ca. 300 °C with overall 1.66 mass% weight loss at 700 °C exhibits compromised thermal stability between that of $Li_2B_{12}H_{12}$ and $K_2B_{12}H_{12}$ below 500 °C. At temperature higher than 500 °C, $Li_6K_4(B_{12}H_{12})_5$ presents higher stability than that of $Li_2B_{12}H_{12}$ and $K_2B_{12}H_{12}$.

In Figure 5.9, the stability of $Na_8K_2(B_{12}H_{12})_5$ in comparison with that of $Na_2B_{12}H_{12}$ and $K_2B_{12}H_{12}$ is exhibited. $Na_8K_2(B_{12}H_{12})_5$ starting to decompose at ca. 380 °C with overall 3.2 mass% weight loss at 500 °C exhibits lower thermal stability than those of $Li_2B_{12}H_{12}$ and $K_2B_{12}H_{12}$. This phenomenon indicates bimetallic dodecaborates may also exhibit lower stability than those of both counterparts.

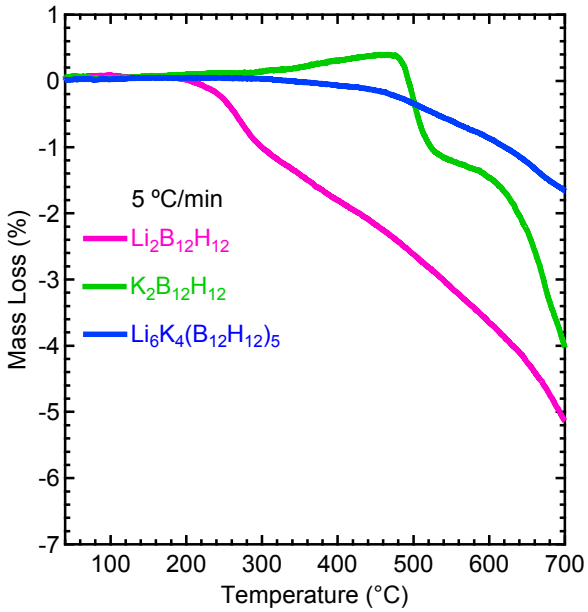

Figure 5.8 TG curve of synthesized $Li_6K_4(B_{12}H_{12})_5$ ($6LiBH_4 + 4KBH_4 + 5B_{10}H_{14}$: 5h ball milling, heat treatment at 400 °C for 10 h) compared with that of $Li_2B_{12}H_{12}$ and $K_2B_{12}H_{12}$. (200 ml/min He flow, 5 °C/min)

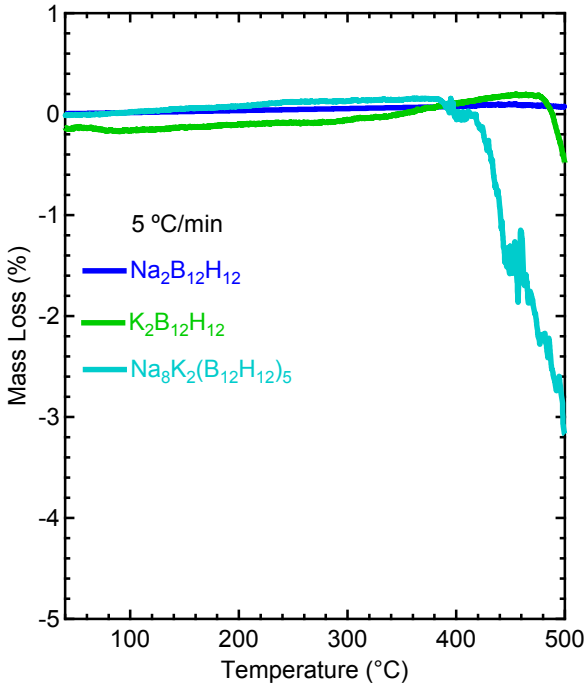

Figure 5.9 TG curve of synthesized $Na_8K_2(B_{12}H_{12})_5$ ($8NaBH_4 + 2KBH_4 + 5B_{10}H_{14}$: 5h ball milling, heat treatment at 400 °C for 10 h) compared with that of $Na_2B_{12}H_{12}$ and $K_2B_{12}H_{12}$. (200 ml/min He flow, 5 °C/min)

In summary, two routes by heat treatment of two kinds of monometallic

borohydrides or one kind of bimetallic borohydride with decaborane for dodecaborate synthesis have been investigated. Single phase of bimetallic dodecaborates including $LiNaB_{12}H_{12}$, $Li_6K_4(B_{12}H_{12})_5$ and $Na_8K_2(B_{12}H_{12})_5$ were successfully synthesized via heat treatment reactions as shown in equation (5.1). On the other hand, the synthesis of $NaAl(B_{12}H_{12})_2$ and $KAl(B_{12}H_{12})_2$ via heat treatment of $NaAl(BH_4)_4$ and $KAl(BH_4)_4$ with $B_{10}H_{14}$ did not succeed. The possible reason is the great differences of stabilities between $Na_2B_{12}H_{12}$ and $K_2B_{12}H_{12}$ with that of $Al_2(B_{12}H_{12})_3$, as I know that $Al(BH_4)_3$ is liquid at room and starts to decompose at 150 °C.[24] All of single phase of bimetallic dodecaborates including $LiNaB_{12}H_{12}$, $Li_6K_4(B_{12}H_{12})_5$ and $Na_8K_2(B_{12}H_{12})_5$ exhibit different thermal stabilities with those of their corresponding counterparts, which indicate the feasibility to tune stability of dodecaborates through partial substitution of metal cations via synthesis of bimetallic dodecaborates.

5.4 Conclusions

In this chapter, I attempted to tune the stabilities of dodecaborates via synthesis of bimetallic dodecaborates from two routes: a) heat treatment of two kinds of monometallic borohydrides with $B_{10}H_{14}$; b) heat treatment of one kind of bimetallic borohydride with $B_{10}H_{14}$. Route a) is a feasible synthesis method by which I have successfully synthesized bimetallic dodecaborates $LiNaB_{12}H_{12}$, $Li_6K_4(B_{12}H_{12})_5$ and $Na_8K_2(B_{12}H_{12})_5$ for the first time, their thermal stabilities were subsequently investigated. All of them exhibit different stabilities with their corresponding single counterparts, which indicate the feasibility to stabilize/destabilize dodecaborates by synthesis of bimetallic dodecaborates. The detailed property investigation is on way and some bimetallic dodecaborates such as $LiNaB_{12}H_{12}$ with outstanding superionic conductivity is available in the Chapter 6.

Chapter 6

Bimetallic Dodecaborate $LiNaB_{12}H_{12}$ with Outstanding Superionic Conductivity

This chapter is based on the submitted paper:

He L, Li H-W, Filinchuk Y, Nakajima H, Tumanov N, Filinchuk Y, Huang S, Sharma M, Hagemann H, Akiba E, Synthesis of a Bimetallic Dodecaborate $LiNaB_{12}H_{12}$ with Outstanding Super Ionic Conductivity. Submitted to *Chemistry of Materials*.

In this chapter, phase transition and ionic conductivity of the synthesized bimetallic dodecaborate $LiNaB_{12}H_{12}$ are investigated. $LiNaB_{12}H_{12}$ exhibits reversible phase transition at 215 ºC which is lower than the phase transition temperatures in both $Li_2B_{12}H_{12}$ (342 ºC) and $Na_2B_{12}H_{12}$ (256 ºC) as reported.[154] The ionic conductivity of $LiNaB_{12}H_{12}$ reaches 0.79 S/cm at around 280 ºC, which is approximately 8 times higher than that for the recent remarkable system $Na_2B_{12}H_{12}$.[155]

6.1 Introduction

Metal dodecaborates $M_{2/n}B_{12}H_{12}$ containing icosahedral polyatomic anion $[B_{12}H_{12}]^{2-}$, have been attracting increasing interest as potential energy materials, especially in the context of hydrogen storage[72, 197] and superionic conductivity.[155] $M_{2/n}B_{12}H_{12}$ are commonly forming as dehydrogenation intermediates from metal borohydrides $M(BH_4)_n$, like $LiBH_4$ and $Mg(BH_4)_2$,[87, 96, 178, 198-199] which are well known as potential high-density hydrogen storage materials.[85, 200-201] The strong B-B bond in the icosahedral $[B_{12}H_{12}]^{2-}$, however, is regarded to be the key factor which prevents the rehydrogenation of dodecaboranes.[138] In order to elucidate the mechanism as well as to provide effective solutions to these problems, a new solvent-free synthesis route of

anhydrous $M_{2/n}B_{12}H_{12}$ (here M means Li, Na and K) was developed.[157] Thermal stability of the anhydrous single phase $Li_2B_{12}H_{12}$ suggested the formation of the high temperature polymorph of $Li_2B_{12}H_{12}$ during the dehydrogenation of $LiBH_4$, while concurrently emphasized the importance of further investigation on the decomposition mechanism of metal borohydrides and metal dodecaborates.[149] The high stability of icosahedral $[B_{12}H_{12}]^{2-}$, on the other hand, favors its potential application as solid electrolyte. Li^+ conductivity of $Li_2B_{12}H_{12}$ was indicated by Paskevicius et al via careful phase transition study to $Li_2B_{12}H_{12}$.[153] Recently, Na^+ conductivity of $Na_2B_{12}H_{12}$ was reported to be 0.1 S/cm above its order-disorder phase-transition at ~256 °C,[155] which is comparable to that of a polycrystalline β"-Al_2O_3 (0.24 S/cm at 573 K) solid state Na-electrolyte.[202] Mechanistic understanding on the diffusion behavior of cation and further improvement of ionic conductivity at a lower temperature, however, are important in order to facilitate the practical applications of metal dodecaborates as superionic conductors.

Bimetallic compounds composed of two different metal elements, often show different crystal structures and interesting chemical and physical properties, which are often distinguished from those of the monometallic counterparts. For example, bimetallic borohydride has been proven as a way to tune the thermodynamics of metal borohydride decomposition.[112-113, 203] To our knowledge, there has been no report of improving the ionic conductivity of $M_{2/n}B_{12}H_{12}$ by introducing another metal to form a bimetallic dodecaborate, and I hypothesized that the coexistence of bimetallic elements could have a synergetic effect on the mobility of each ion. In this chapter, I report for the first time that a bimetallic dodecaborate $LiNaB_{12}H_{12}$ exhibits lower phase transition temperature (215 °C) than its single counterparts of $Li_2B_{12}H_{12}$ (342 °C) and $Na_2B_{12}H_{12}$ (256 °C),[154] and the ionic conductivity of $LiNaB_{12}H_{12}$ reaches a value of 0.79 S/cm at 277 °C, which is approximately 8 times higher as that for $Na_2B_{12}H_{12}$.[155]

6.2 Experimental Section

Differential scanning calorimetry profiles are examined by Thermo Plus2 DSC8230HP AEMK under 0.1 MPa He with a gas flow rate of 200 ml/min. In-situ Raman spectra were observed on RAMAN-11 VIS-SS (Nanophoton) machine via a laser with 532 nm wavelength (green).

High-resolution X-ray powder diffraction patterns were measured at variable temperature using a synchrotron radiation source at BM1A station at the Swiss-Norwegian Beam Lines at the ESRF (λ = 0.68857 and 0.698509 Å, Pilatus 2M hybrid pixel detector). Nominal sample-to-detector distances (344 mm), coordinates of beam center and detector tilts were calibrated using LaB_6 (NIST standard 660b). A powdered sample of $LiNaB_{12}H_{12}$ was filled in the sapphire single crystal capillary for the experiment with H_2 pressure and in the quartz capillary for the experiment without pressure load. All manipulations were done in the argon-filled glove box ($p(O_2, H_2O)$ < 1 ppm). First capillary was placed in a specially developed *in situ* sample cell for investigation of solid-gas reactions.[164] The samples were heated with a rate of 5 °C/min between RT and 350 °C in P(Ar) ≈ 1 bar and P(H_2) ≈ 160 bar. Raw powder diffraction data were processed (calibration, integration) using the Fit2D program.[165] Uncertainties of the integrated intensities were calculated at each 2θ-point by applying Poisson statistics to the intensity data, considering the geometry of the 2D detector.[166-167] The structures were refined by the Rietveld method using a Fullprof Suite software.[168] The final refinement of $LiNaB_{12}H_{12}$ low temperature phase was done in *Pa*-3 space group .The background was described by linear interpolation between selected points. The final discrepancy factors are: R_B = 6.10%, R_F = 9.50%, R_p = 10.0%, and R_{wp} = 9.97% (corrected for background). High temperature phase of $LiNaB_{12}H_{12}$ was modeled in *Fm*-3*m* space group, *Z*= 4, *a* = 9.82707(9) Å, *V* = 1040.204(11) $Å^3$ at 240 K. Li and Na are located on *x*, *x*, *x* position (x =0.29683), centered around the 8-fold 1/4 1/4 1/4 position, and the presumably disordered dodecaborate is located near the 0, 0, 0 position. The final discrepancy factors are: R_B = 1.55%, R_F = 12.7%, R_p = 9.10%, and R_{wp} = 6.74% (corrected for background).

Ionic conductivities were measured with electrochemical impedance spectroscopy[169] for the sample pressed into a pellet with a diameter of 8 mm and a thickness of approximately 2 mm. Cu foils with a thickness of 20 μm were used as electrodes, which were mechanically fixed on both sides of the pellet sample in an air-tight cell (Hohsen, HS-cell). Impedance plots were measured at the open circuit potential between 27 and 277 °C using a frequency response analyzer (Ono Sokki, DS-2100/DS-266/DS-273) combined with a potentio/galvanostat (Hokuto Denko, HA-301) in a frequency range from 0.1 MHz to 1 Hz. Ionic conductivities of the sample were derived from the high frequency resistances obtained by the complex

nonlinear least-squares fitting (Scribner, Z-View) for the impedance spectra[169]. The spectra did not exhibit clear separation of overlapping contributions of the bulk and grain boundary. All the sample preparations and the air-tight cell assembly were always operated in a glove box protected by purified Ar gas. Transport number of Lithium ion was measured by potentiostatic polarization measurement[170-171]. Time variations of the current were recorded by a data logger (GRAPHTEC, midi LOGGER GL820) for the sample sandwiched by Li foil electrodes with a thickness of 100 μm in the air-tight cell under constant potential differences with time applied between the electrodes by the potentio/galvanostat. In current transient measurement, the initial i_0 and steady-state currents i_∞ give the transport number of Li ion, t_{Li}, from the following equation with the constant potential differences of ΔV[170-171].

$$t_{\mathrm{Li}^+} = \frac{\Delta V/i_0 - R_{\mathrm{ct}}}{\Delta V/i_\infty - R_{\mathrm{ct}}} \tag{6.1}$$

where the charge transfer resistance, R_{ct}, assumed constant with time was negligibly small compared with the other resistances in the impedance spectra for the sample with the Li electrodes.

Computational studies were performed with the Gaussian 09 program using Density Functional Theory (DFT) with the B3LYP functional and 6-31G(d, p) basis set.[204]

6.3 Results and Discussion

6.3.1 Reversible Phase Transition in $LiNaB_{12}H_{12}$

Phase transition of $LiNaB_{12}H_{12}$ examined by differential scanning calorimetry (Figure 6.1) occurs at approximately 215 °C, which is substantially lower than those reported for pure $Li_2B_{12}H_{12}$ (342 °C) and $Na_2B_{12}H_{12}$ (256 °C).[154] It is worth emphasizing that there is no obvious hysteresis of the phase transition temperature in $LiNaB_{12}H_{12}$ even after 20 cycles of heating and cooling measurement (Figure 6.2), whereas large hysteresis is clearly observed in $Li_2B_{12}H_{12}$ and $Na_2B_{12}H_{12}$.[154]

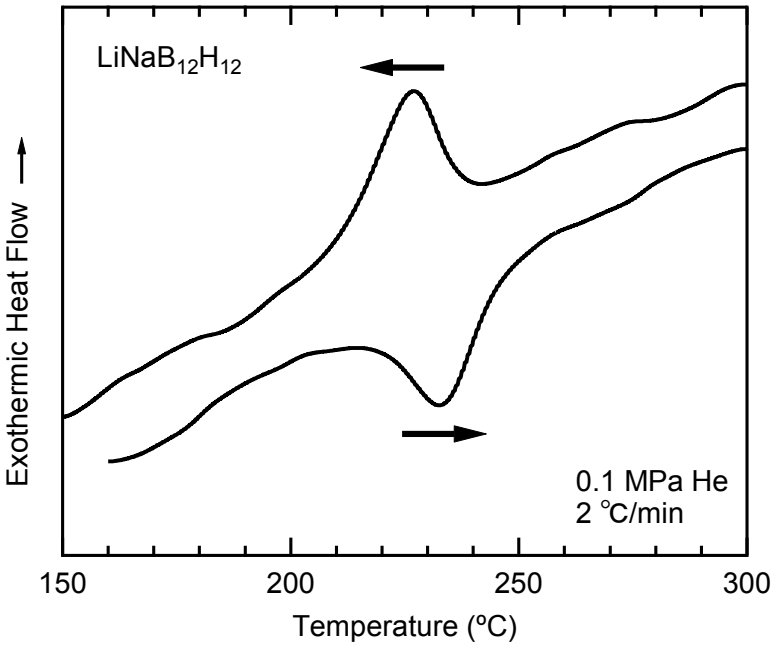

Figure 6.1 Differential scanning calorimetry curves showing the reversible phase transition in $LiNaB_{12}H_{12}$ with small hysteresis.

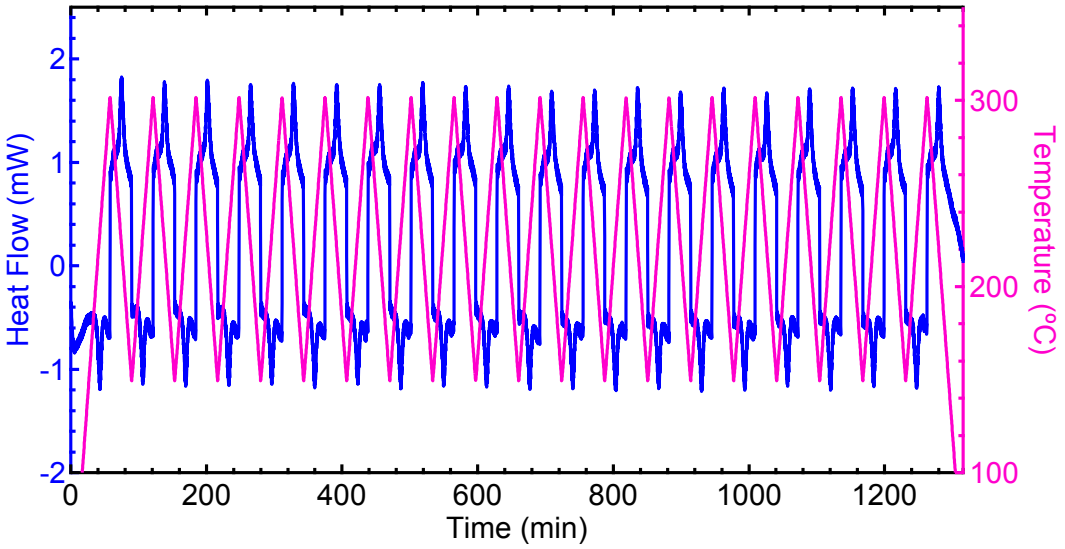

Figure 6.2 DSC measurement of $LiNaB_{12}H_{12}$ between 150 and 300 °C for 20 cycles (5 °C/min in 0.1 MPa He).

The structural investigation of $LiNaB_{12}H_{12}$ by synchrotron X-ray powder diffraction (Figures 6.3 and 6.4) reveals the cubic *Pa-3* space group symmetry and the cell parameter a = 9.8009(1) Å at room temperature (RT). Experimental structural parameters for $LiNaB_{12}H_{12}$ at 30 °C are shown in Table 6.1. Upon heating it turns to a

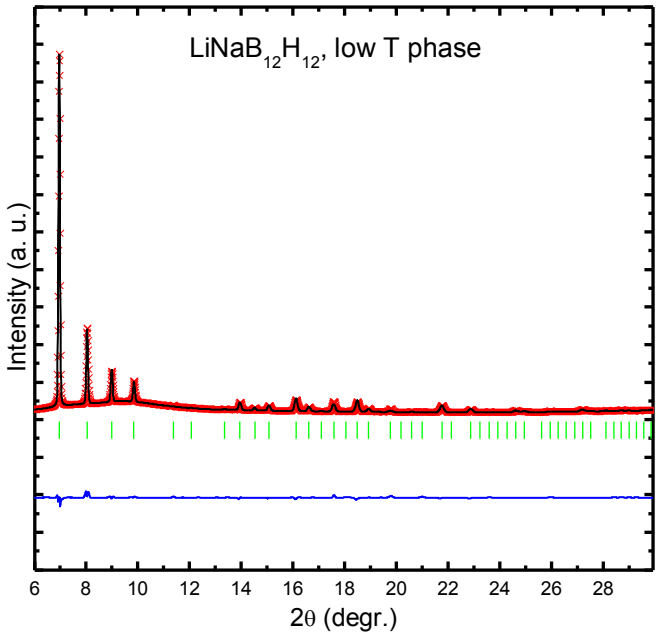

Figure 6.3 Rietveld refinement plot for $LiNaB_{12}H_{12}$ at 30 °C (low temperature phase). Red crosses and black line show the experimental and calculated data, respectively. Blue line is the difference profile, and green marks indicate Bragg positions. λ = 0.68857 Å.

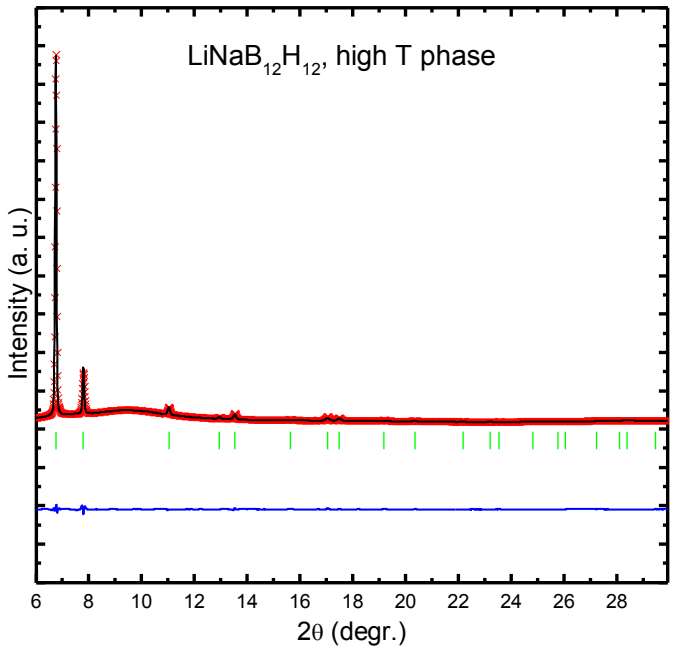

Figure 6.4 Rietveld refinement plot for $LiNaB_{12}H_{12}$ at 240 °C (high temperature phase). Red crosses and black line show the experimental and calculated data, respectively. Blue line is the difference profile, and green marks indicate Bragg positions. λ = 0.68857 Å.

Table 6.1 Experimental structural parameters for $LiNaB_{12}H_{12}$ at 30 °C (low temperature phase). Space group *Pa*-3, $Z = 4$, $a = 9.82707(9)$ Å, $V = 949.01(3)$ Å^3. The refined fractional site occupancy for Na1 is 0.377, for Li 0.623, close to the nominal composition (0.5/0.5), all other atoms fully occupy their crystallographic positions.

Atom	x	y	z
Li1	0.63644	0.63644	0.63644
Na1	0.63644	0.63644	0.63644
B1	-0.09125	-0.09102	0.12363
B2	-0.03597	-0.03888	-0.17056
H1	-0.15556	-0.15515	0.21074
H2	-0.06132	-0.06628	-0.29074

high-temperature phase, which is similar to the transition behavior seen for $Li_2B_{12}H_{12}$ (Figure 6.5).[153] Despite in the earlier work [153], the high-temperature $Li_2B_{12}H_{12}$ phase was modeled in the primitive parent cubic cell, the unit cell of the high-temperature $LiNaB_{12}H_{12}$ is clearly cubic *F*-centered. I searched for a better structural model, as the Li/Na mixed-metal site is a stronger scatterer, allowing characterizing it easier. The resulting structure has the space group symmetry *Fm*-3*m* where both metal and $[B_{12}H_{12}]^{2-}$ sites are disordered. Our refinements show a significant positional disorder of the Li/Na site centered around the 8-fold 1/4 1/4 1/4 position; the dodecaborane anions are centered around the 4-fold 0 0 0 position. The anions may be positionally ordered, especially in the *F*-centered cubic subgroups of *Fm*-3*m*. The phase transition is reversible, a sequential refinement was done on 313 powder patterns collected, and the cell parameters of the two phases are plotted as a function of T in Figure 6.5. The unit cell parameters show practically linear T dependences. The phase transition happens at ca. 241 °C on heating and 208 °C on cooling, the cell parameters exhibit nearly the same values (ca. 0.13 Å) of expansion or shrink on heating or cooling. Thus, I can state that no dehydrogenation/hydrogenation occurs at 16.0 MPa H_2 and temperatures up to 500 °C. A similar experiment without hydrogen back pressure shows that hydrogen has no significant effect on the phase transition, the phase

transition occurs at ca. 241 °C on heating and at 208 °C on cooling and no dehydrogenation/hydrogenation was observed.

The reversible phase transition is also examined by the in-situ Raman spectroscopy measurements as shown in Figure 6.6. When the temperature is increased above the phase transition temperature, the B-H bending modes at 618, 680, and 980 cm-1 start to disappear at 240 °C and two B-H stretching mode peaks at around 2500 cm^{-1} starts to degenerate and a single peak is observed at 280 °C due to the disordered structure of the high-temperature phase. When the temperature is decreased below the phase transition temperature, the bending modes at 618, 680, and 980 cm^{-1} reappear, and the stretching around 2500 cm^{-1} splits into two peaks.

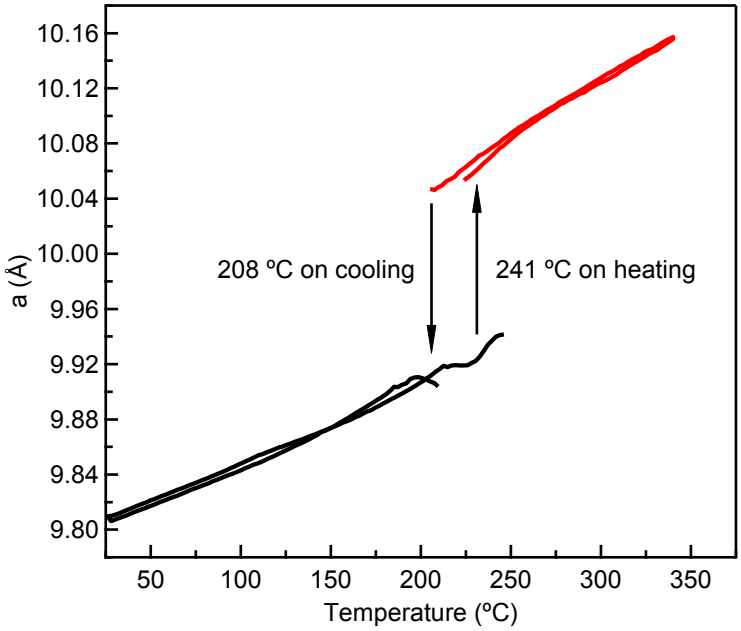

Figure 6.5 Unit cell dimension of $LiNaB_{12}H_{12}$ as a function of temperature, refined from the in-situ synchrotron X-ray diffraction profiles measured at 16.0 MPa H_2.

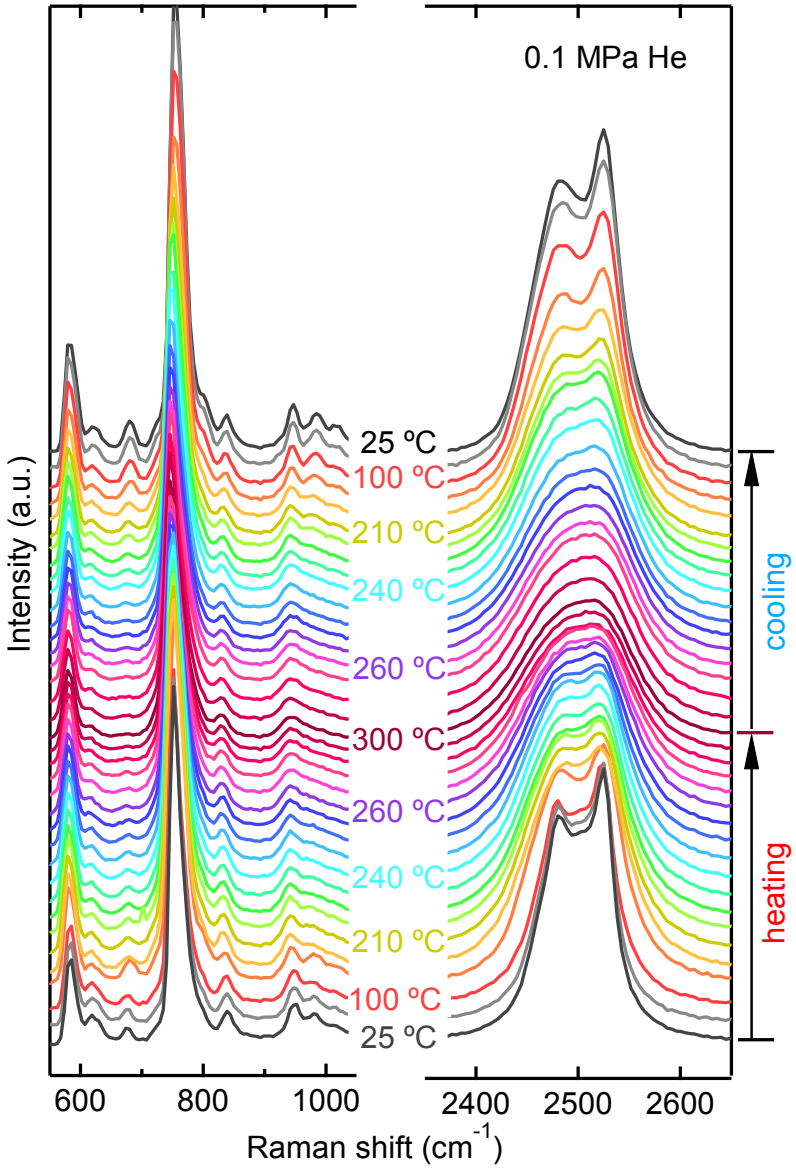

Figure 6.6 In-situ Raman spectra of $LiNaB_{12}H_{12}$ upon heating and cooling at 0.1 MPa He.

DFT calculations on isolated $B_{12}H_{12}^{2-}$ and $Li_2B_{12}H_{12}$ (with D_{3d} symmetry, to be as close as possible to the S_6 local symmetry in the $LiNaB_{12}H_{12}$ crystal) were performed to further analyze the origin of these bands. It appears in particular that the band at 680 cm^{-1}, which is not observed in the Raman spectrum of the cubic $Cs_2B_{12}H_{12}$,[205] originates from a Raman inactive mode with G_g symmetry for the icosahedral $B_{12}H_{12}^{2-}$ anion (gif animation available). The calculated frequencies and experimental Raman frequencies are summarized in Tables 6.2 and 6.3. It is also important to note that the space groups *Fm*-3*m* and *Pa-3* do not have a direct group-subgroup relation. This fact

leads to the hysteresis shown in Figure 6.1, but is also reflected by the fact that the band at 680 cm^{-1} disappears suddenly at the phase transition with increasing temperature.

Table 6.2 Calculated vibrational frequencies for isolated $[B_{12}H_{12}]^{2-}$ and $Li_2B_{12}H_{12}$ (molecule with D_{3d} symmetry) and experimental vibrational frequencies for solid $Cs_2B_{12}H_{12}$[205] and $LiNaB_{12}H_{12}$ [this work]. In I_h symmetry, A_g and H_g are Raman active, and T_{1u} IR active. In D_{3d} symmetry, A_{1g} and E_g are Raman active, and A_{2u} and E_u IR active.

$B_{12}H_{12}$ calc DFT	I_h	$Cs_2B_{12}H_{12}$ Allis	$Li_2B_{12}H_{12}$ calc DFT	D_{3d}	Raman $LiNaB_{12}H_{12}$
			223,223,259,260,436,475		
516 (x5)	H_u	**531**	514, 514, 523, 545, 545	$A_{1u}+2E_u$	
572 (x5)	H_g	581 (R),586 (R)	564,565,579,580,619	$A_{1g}+2E_g$	579,618
652 (x4)	G_g		655,662 (A_{2g}),671,672	$A_{1g}+A_{2g}+E_g$	679
702 (x3)	T_{1u}	**708,718**	707,722,722	$A_{2u}+E_u$	
734 (x4)	G_u	**757**	725,743,743,754	$A_{1u}+A_{2u}+E_u$	
737 (x1)	A_g	747	749	A_{1g}	751
753 (x5)	H_g	762,787	761,761,795,795,830	$A_{1g}+2E_g$	801,834
758 (x3?)	T_{2u}		792,792,811	$A_{2u}+E_u$	
862 (x4)	G_u	**860**	857 (A_{1u}),872,872,944	$A_{1u}+A_{2u}+E_u$	
937 (x4)	G_g	940	930,930,939,955	$A_{1g}+A_{2g}+E_g$	942
941 (x5)	H_u	**950**	945,946,950,998,998	$A_{1u}+2E_u$	
943 (x5)	H_g	972	946,947,947,962,963	$A_{1g}+2E_g$	979
957 (x3)	T_{1g}		1025,1069,1069	$A_{2g}+E_g$	
1063 (x3)	T_{1u}	**1057,1073**	1089,1124, 1124	$A_{2u}+E_u$	
2476 (x3)	T_{2u}		2421,2421,2446	$A_{2u}+E_u$	
2483 (x5)	H_g		2420,2420, 2455,2635,2635	$A_{1g}+2E_g$	2485
2504 (x3)	T_{1u}		2632,2642,2642	$A_{2u}+E_u$	
2542 (x1)	A_g		2650	A_{1g}	2525

Table 6.3 Correlation table for selected subgroups of I_h.

I_h	T_h	T	D_{2h}	D_{3d}	C_{3v}	D_{5d}	C_{5v}
A_g	A_g	A	A_g	A_{1g}	A_1	A_{1g}	A_1
T_{1g}	T_g	T	$B_{1g}+B_{2g}+B_{3g}$	$A_{2g}+E_g$	A_2+E	$A_{2g}+E_{1g}$	A_2+E_1
T_{2g}	T_g	T	$B_{1g}+B_{2g}+B_{3g}$	$A_{2g}+E_g$	A_2+E	$A_{2g}+E_{2g}$	A_2+E_1
G_g	A_g+T_g	$A+T$	$A_g+B_{1g}+B_{2g}+B_{3g}$	$A_{1g}+A_{2g}+E_g$	A_1+A_2+E	$E_{1g}+E_{2g}$	E_1+E_2
H_g	E_g+T_g	$E+T$	$2A_g+B_{1g}+B_{2g}+B_{3g}$	$A_{1g}+2E_g$	A_1+2E	$A_{1g}+E_{1g}+E_{2g}$	$A_1+E_1+E_2$
A_u	A_u	A	A_u	A_{1u}	A_2	A_{1u}	A_2
T_{1u}	T_u	T	$B_{1u}+B_{2u}+B_{3u}$	$A_{2u}+E_u$	A_1+E	$A_{2u}+E_{1u}$	A_1+E_1
T_{2u}	T_u	T	$B_{1u}+B_{2u}+B_{3u}$	$A_{2u}+E_u$	A_1+E	$A_{2u}+E_{2u}$	A_1+E_1
G_u	A_u+T_u	$A+T$	$A_u+B_{1u}+B_{2u}+B_{3u}$	$A_{1u}+A_{2u}+E_u$	A_1+A_2+E	$E_{1u}+E_{2u}$	E_1+E_2
H_u	E_u+T_u	$E+T$	$2A_u+B_{1u}+B_{2u}+B_{3u}$	$A_{1u}+2E_u$	A_2+E+E	$A_{1u}+E_{1u}+E_{2u}$	$A_2+E_1+E_2$

The phase transition of $LiNaB_{12}H_{12}$ at different back pressures does not show distinct change, as shown in Figure 6.7. The ΔH of phase transition is evaluated to be ~ 9 kJ/mol $LiNaB_{12}H_{12}$ with/without different H_2 back pressures, this value is compromise of that of $Li_2B_{12}H_{12}$ and $Na_2B_{12}H_{12}$,[154] ΔS is then calculated as ~ 18 J/(K•mol) based on ΔH and corresponding peak temperatures (Table 6.4). Subsequently, the phase transition activation energy E_a was evaluated as 376.4 kJ/mol through Kissinger's method[206] using equation 6.2:

$$\ln\left(\frac{\emptyset}{Tp2}\right) = -\frac{Ea}{RTp} + C \qquad (6.2)$$

(where T_p is the peak temperature, Φ is temperature ramp, R = 8.314 $J \cdot mol^{-1} \cdot K^{-1}$ and C is a constant) in 0.1 MPa He atmosphere (Figure 6.8), which is much higher than 75 kJ/mol of low-temperature phase transition E_a of $Na_2B_{12}H_{12}$ as reported.[140]

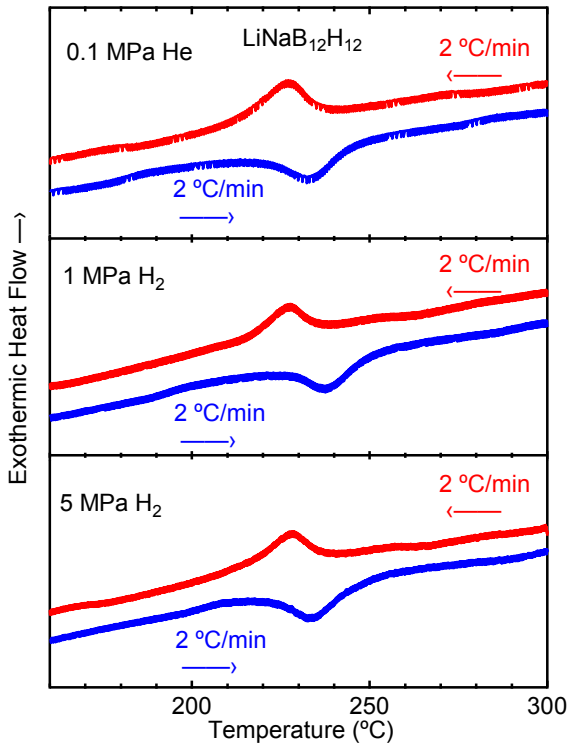

Figure 6.7 The DSC measurement of $LiNaB_{12}H_{12}$ at different back pressures (2 °C /min).

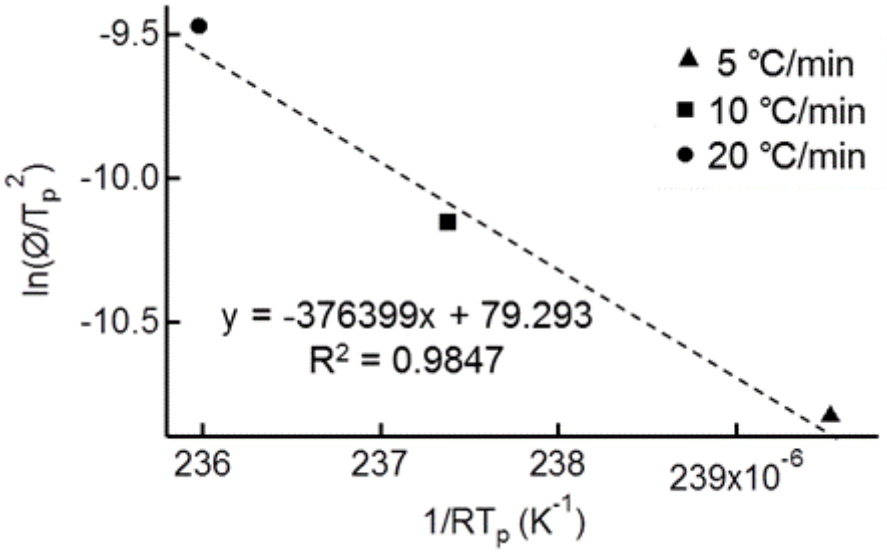

Figure 6.8 Kissinger's plot of $\ln(\Phi/Tp^2)$ versus $1/RT_p$.

Table 6.4 The enthalpy and entropy changes of $LiNaB_{12}H_{12}$ phase transition (heating) evaluated at different back pressures (ramp = 2 °C /min).

Back pressure	ΔH (kJ/mol)	ΔS (J/(K•mol))
0.1 MPa He	8.83	17.47
1 MPa H_2	9.48	18.57
5 MPa H_2	9.74	19.24

6.3.2 Superionic Conductivity in $LiNaB_{12}H_{12}$

Ionic conductivities are measured by electrochemical impedance spectroscopy (Figure 6.9) followed by complex non-linear squares fitting using equivalent circuits (Figure 6.10). The impedance Z is composed of a real part (Z') on X-axis and an imaginary part (Z') on Y-axis. In the plots, every point is the impedance at one frequency and the higher frequency points are on the left.[207] At low temperatures, the diameter of the semicircle in the impedance plots is equal to the ion conducting resistance determined by the ionic conductivity of $LiNaB_{12}H_{12}$ sample, which is simulated using R_2 in Figure 6.10 (a). R_1 is adopted to represent the inner contact resistance which can be ignored by comparing with R_2 because the $LiNaB_{12}H_{12}$ sample at low temperature exhibits properties of non-conductor with far larger resistance than R_1. At temperature higher than phase transition temperature of $LiNaB_{12}H_{12}$, it transforms to typical conductor. The impedance plots appear as one straight line and the intercept of this line on X-axis is used to evaluate the resistance of $LiNaB_{12}H_{12}$. Warburg element without practical meaning here is used only for the linear curve fitting. Ionic conductivities of $LiNaB_{12}H_{12}$ as a function to temperature shown in Figure 6.11 display a significant increase with temperature: above the phase transition temperature it is 6 orders of magnitude higher than that at room temperature (3.62×10^{-7} S/cm at 32 °C). At 277 °C the ionic conductivity reaches 0.79 S/cm, which is approximately 8 times higher than that for the recent remarkable system $Na_2B_{12}H_{12}$; at 77 °C the ionic conductivity is approximately 3 orders of magnitude higher than that for $Na_2B_{12}H_{12}$.[155]

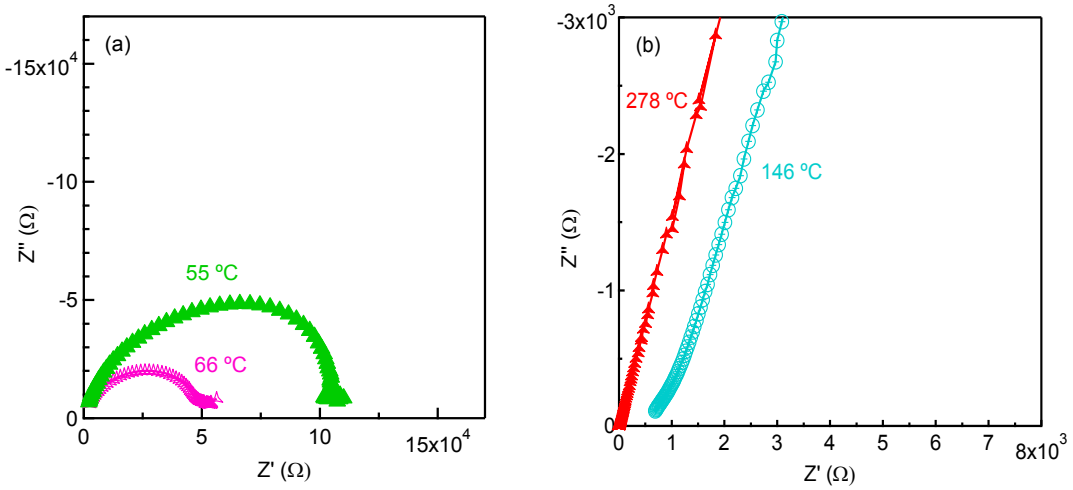

Figure 6.9 Impedance plots for $LiNaB_{12}H_{12}$ measured at various temperatures during heating run.

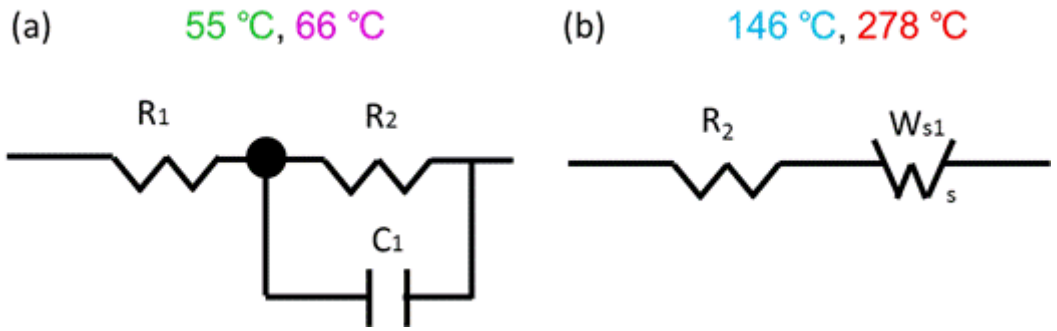

Figure 6.10 Equivalent circuits used for impedance simulation. (R_1= Inner contact resistance, R_2= Ion conducting resistance, C_1= Capacitor, W_{s1}= Warburg element, s= short)

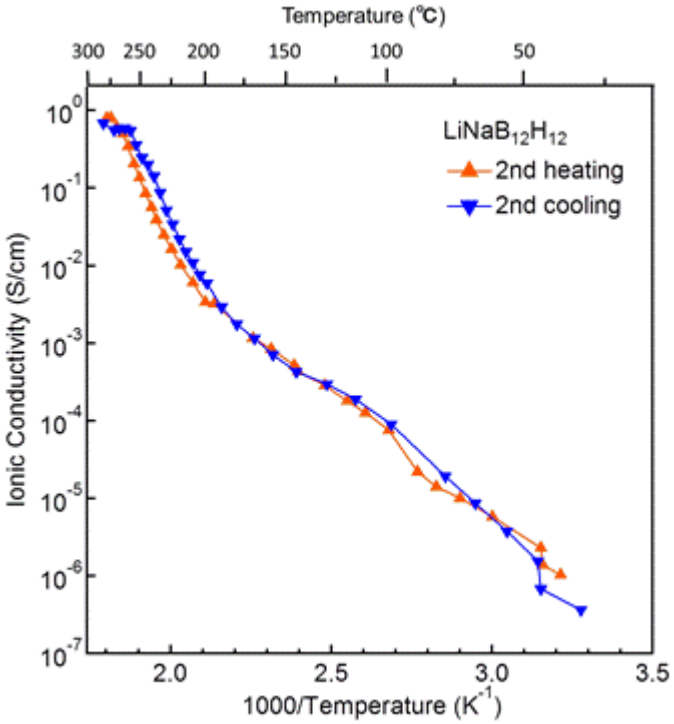

Figure 6.11 Ionic conductivity measurements for $LiNaB_{12}H_{12}$ as a function of temperature.

In the preliminary experiments, Li ionic transport number estimated using polarization responses (Figure 6.12) decreases from 0.92 to 0.72 with temperature increased from 120 °C to 160 °C, implying that Li^+ contributes much more than Na^+ to the superionic conductivity, but decreases with elevated temperatures. In addition, unlike $Na_2B_{12}H_{12}$,[155] no clear hysteretic behavior is observed during the cooling process. The significantly improved ionic conductivity and the minimal hysteresis behavior demonstrated by the $LiNaB_{12}H_{12}$, therefore, prove the synergistic effects of employing the bimetallic dodecaborates. The demonstration further opens up the feasibility of designing bimetallic dodecaborates to tune geometric structure and to improve the ion mobility. Further investigation on $LiNaB_{12}H_{12}$ with different molar ratios of Li/Na, as well as various bimetallic systems with different ionic radius and valence, is of great importance for the clarification of the detailed mechanism and the improvement of ionic conductivity at moderate temperature for the application of metal dodecaborates as solid electrolyte for batteries.

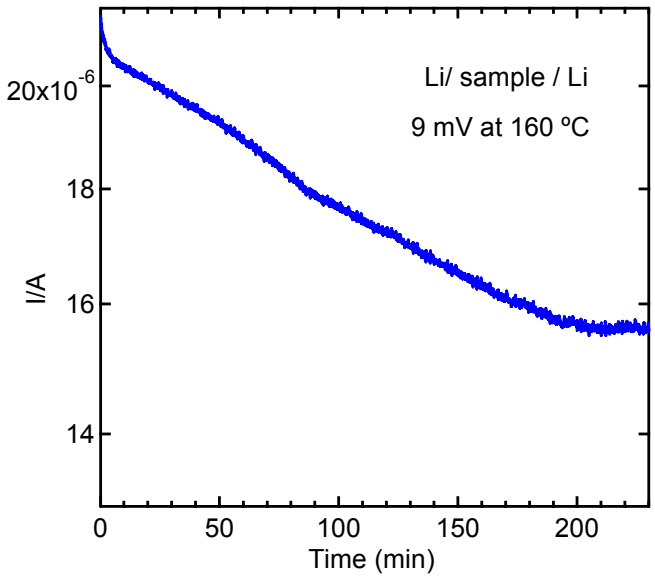

Figure 6.12 Time variation of the current with the potentiostatic polarization of a Li|$LiNaB_{12}H_{12}$|Li cell at 160 °C and applied potential difference of 9 mV.

6.4 Conclusions

The bimetallic dodecaborate $LiNaB_{12}H_{12}$ exhibits lower phase transition temperature, smaller hysteresis and significantly higher ionic conductivity than its monometallic counterparts, i.e. $Li_2B_{12}H_{12}$ and $Na_2B_{12}H_{12}$. The phase transition from cubic *Pa*-3 to cubic *Fm*-3*m* space group symmetry occurring at 215 °C is not affected by different gas atmospheres. The ΔH of phase transition is evaluated to be ~ 9 kJ/mol $LiNaB_{12}H_{12}$ which is a compromise of that of $Li_2B_{12}H_{12}$ and $Na_2B_{12}H_{12}$, while the activation energy E_a evaluated as 376.4 kJ/mol is much higher than that of $Na_2B_{12}H_{12}$. The ionic conductivity at 277 °C reaches 0.79 S/cm, which is approximately 8 times as high as that for $Na_2B_{12}H_{12}$. The revealed Li/Na compositional disorder and the related positional disorder on the metal site are likely responsible for the improved superionic conductivity of $LiNaB_{12}H_{12}$. These interesting results demonstrate the strategy to improve the ionic conductivity by designing bimetallic dodecaborates.

Chapter 7

Summary and Outlook

Metal borohydrides $M(BH_4)_n$ with hydrogen capacity of 10 mass%, have been widely regarded as potential candidates for onboard hydrogen storage. Most of $M(BH_4)_n$, however, suffer from the degraded rehydrogenation hampered by the formation of stable metal dodecaborates $M_{2/n}B_{12}H_{12}$ as a dehydrogenation intermediate. On the other hand, stable $M_{2/n}B_{12}H_{12}$ favors the potential application as solid electrolyte. Systematic investigation on the thermal decomposition of $M_{2/n}B_{12}H_{12}$, therefore, is in great need to investigate its role in the dehydrogenation and rehydrogenation of borohydrides, as well as to develop superionic conductor.

In this dissertation, I developed a new solvent-free synthesis process via heat treatment of $M(BH_4)_n$ with $B_{10}H_{14}$. By using this method, I have successfully synthesized anhydrous $M_{2/n}B_{12}H_{12}$ comprised of alkali metals and alkaline earth metals. Systematic investigation of decomposition of $M_{2/n}B_{12}H_{12}$ indicates the different behaviors with those of the in-situ formed $M_{2/n}B_{12}H_{12}$ during dehydrogenation of $M(BH_4)_n$. Thermal stabilities of $M_{2/n}B_{12}H_{12}$ can be adjusted by designing bimetallic dodecaborate, suggesting the possibility for the improvement of rehydrogenation. Furthermore, $LiNaB_{12}H_{12}$ was found to exhibit outstanding superionic conductivity which is expected to be utilized as solid Na/Li electrolyte. The main achievements are summarized as below:

(1) I have developed a facile solvent-free synthesis process via heat treatment of hydrides or metal borohydrides with $B_{10}H_{14}$ as a boron source, according to the following equations:

$$2MH + 1.2B_{10}H_{14} \rightarrow M_2B_{12}H_{12} + 3.4H_2 \ (M = Li, Na) \quad (7.1)$$

$$2MBH_4 + B_{10}H_{14} \rightarrow M_2B_{12}H_{12} + 5H_2 \ (M = Li, Na, K) \quad (7.2)$$

Comparison on the yields of $M_2B_{12}H_{12}$ yields between equations (7.1) and (7.2) indicates that equation (7.2) is feasible for the synthesis of anhydrous $M_2B_{12}H_{12}$.

The synthesized $M_2B_{12}H_{12}$ experience multistep decomposition reactions: 1) $M_2B_{12}H_{12}$ releases hydrogen to form H-deficiency $M_2B_{12}H_{12-x}$ keeping the icosahedral B_{12} skeletons, 2) $M_2B_{12}H_{12-x}$ tend to polymerize and give rise to the formation of $(M_2B_yH_z)_n$ polymers. Such complicated decomposition pathway is distinct from those

of the in-situ formed $M_2B_{12}H_{12}$ during the dehydrogenation of corresponding MBH_4.

(2) Anhydrous alkaline earth metal dodecaborates $MgB_{12}H_{12}$ and $CaB_{12}H_{12}$ have been successfully synthesized for the first time using the developed solvent-free process in this dissertation. Similar to those of alkali metal dodecaborates, both $MgB_{12}H_{12}$ and $CaB_{12}H_{12}$ experience multistep decomposition accompanied with the formation of H-deficiency $MB_{12}H_{12-x}$ followed by the polymerization of $MB_{12}H_{12-x}$ to produce $(MB_yH_z)_n$ polymers. The synthesized $MgB_{12}H_{12}$ decomposes into amorphous B at 800 °C, whereas $CaB_{12}H_{12}$ may require much higher temperature to complete the decomposition. The lower electronegativity of Ca than that of Mg is considered to be responsible for the higher stability of $CaB_{12}H_{12}$ than that of $MgB_{12}H_{12}$.[111] Though the decomposition temperature range varies largely with the kind of metal M, all the decomposition behaviors of metal dodecaborates comprised of alkali metal or alkaline earth metal are fairly different with the dehydrogenation of corresponding borohydrides.

(3) I have successfully synthesized bimetallic dodecaborates $LiNaB_{12}H_{12}$, $Li_6K_4(B_{12}H_{12})_5$ and $Na_8K_2(B_{12}H_{12})_5$ for the first time, through heat treatment of two kinds of monometallic borohydrides with $B_{10}H_{14}$. The synthesized bimetallic dodecaborates exhibit different stabilities with their corresponding single counterparts, which indicate the feasibility to stabilize or destabilize dodecaborates by designing bimetallic dodecaborates.

(4) $LiNaB_{12}H_{12}$ transforms from *Pa*-3 (at room temperature) to *Fm*-3*m* symmetry at 215 °C, which is lower than that of $Li_2B_{12}H_{12}$ and $Na_2B_{12}H_{12}$. The ionic conductivity of $LiNaB_{12}H_{12}$ at 277 °C reaches 0.79 S/cm, which is approximately 8 times higher as that of $Na_2B_{12}H_{12}$ at the same temperature, demonstrating the high potentiality as a sodium solid electrolyte. The Li/Na positional disorder in $LiNaB_{12}H_{12}$ is suggested to be responsible for the improved superionic conductivity compared to its monometallic counterparts.

Based on the abovementioned achievements in this dissertation, our systematic investigation of metal dodecaborates $M_{2/n}B_{12}H_{12}$ strongly indicate that $M_{2/n}B_{12}H_{12}$ does not act as a dead end for reversible hydrogen storage of metal borohydrides $M(BH_4)_n$ with hydrogen capacity of 10 mass%. Furthermore, the tunable thermal stabilities of $M_{2/n}B_{12}H_{12}$ indicates the possibility of the improvement of the

reversibility of $M(BH_4)_n$. Continuous efforts are required to put on the clarification of dehydrogenation/rehydrogenation mechanism, metal borohydrides $M(BH_4)_n$, therefore, are expected to be further developed in order to meet the requirement of FCV onboard hydrogen storage. The replacement of high pressure tanks by advanced hydrogen storage materials such as $M(BH_4)_n$, will not only significantly increase the hydrogen storage density, but also largely reduce the construction cost of high pressure hydrogen infrastructures, accelerating the spread of hydrogen mediated society. In addition, the developed $LiNaB_{12}H_{12}$ shows superior ionic conductivity, which is approximately 8 times of that of β-Al_2O_3 solid electrolyte used in NAS battery, suggesting the $M_{2/n}B_{12}H_{12}$ are potential solid state electrolytes. Continuous investigations on the clarification of the improvement mechanism by bimetallic dodecaborate will provide profound insights for developing hydride based solid state electrolyte with outstanding ionic conductivity, which is expected to largely contribute to improving the energy storage efficiency and safety of rechargeable batteries.

References

1.http://en.wikipedia.org/wiki/Henry_Cavendish.

2.Schlapbach, L., Hydrogen as a Fuel and Its Storage for Mobility and Transport. *MRS bulletin* **2002**, *27*, 675-679.

3.Carcassi, M.; Fineschi, F., Deflagrations of H_2–Air and CH_4–Air Lean Mixtures in a Vented Multi-Compartment Environment. *Energy* **2005**, *30*, 1439-1451.

4.Suss, H.; Nimmerfroh, N. In *Hydrogen Peroxide in Chemical Pulp Bleaching*, ABTCP meeting on pulp bleaching at Vitoria, Espirito Santo, Brazil, **1996**.

5.http://webbook.nist.gov/chemistry/.

6.http://en.wikipedia.org/wiki/Heat_of_combustion#cite_ref-NIST_3-0.

7.Marbán, G.; Valdés-Solís, T., Towards the Hydrogen Economy? *International Journal of Hydrogen Energy* **2007**, *32*, 1625-1637.

8.http://www.kyushu-u.ac.jp/pressrelease/2015/2015_03_18_3.pdf.

9.Mao, S. S.; Shen, S.; Guo, L., Nanomaterials for Renewable Hydrogen Production, Storage and Utilization. *Progress in Natural Science: Materials International* **2012**, *22*, 522-534.

10.Züttel, A.; Borgschulte, A.; Schlapbach, L., *Hydrogen as a Future Energy Carrier*; John Wiley & Sons, **2011**.

11.Brimblecombe, P., *Air Composition and Chemistry*; Cambridge University Press, **1996**.

12.Kothari, R.; Buddhi, D.; Sawhney, R., Comparison of Environmental and Economic Aspects of Various Hydrogen Production Methods. *Renewable and Sustainable Energy Reviews* **2008**, *12*, 553-563.

13.Fujishima, A.; Honda, K., Electrochemical Photolysis of Water at a Semiconductor Electrode. *Nature* **1972**, 37-8.

14.Maeda, K.; Domen, K., Photocatalytic Water Splitting: Recent Progress and Future Challenges. *The Journal of Physical Chemistry Letters* **2010**, *1*, 2655-2661.

15.Higashi, M.; Abe, R.; Teramura, K.; Takata, T.; Ohtani, B.; Domen, K., Two Step Water Splitting into H_2 and O_2 under Visible Light by $ATaO_2N$ (A= Ca, Sr, Ba) and WO_3 with IO_3^-/I^- Shuttle Redox Mediator. *Chemical Physics Letters* **2008**, *452*, 120-123.

16.Turner, J.; Sverdrup, G.; Mann, M. K.; Maness, P. C.; Kroposki, B.; Ghirardi, M.; Evans, R. J.; Blake, D., Renewable Hydrogen Production. *International Journal of*

Energy Research **2008**, *32*, 379-407.

17.http://en.wikipedia.org/wiki/Hydrogen.

18.Züttel, A.; Wenger, P.; Sudan, P.; Mauron, P.; Orimo, S.-i., Hydrogen Density in Nanostructured Carbon, Metals and Complex Materials. *Materials Science and Engineering: B* **2004**, *108*, 9-18.

19.Zhou, L., Progress and Problems in Hydrogen Storage Methods. *Renewable and Sustainable Energy Reviews* **2005**, *9*, 395-408.

20.Züttel, A., Hydrogen Storage Methods. *Naturwissenschaften* **2004**, *91*, 157-172.

21.Walker, G., *Solid-State Hydrogen Storage: Materials and Chemistry*; Elsevier, **2008**.

22.Züttel, A., Materials for Hydrogen Storage. *Materials Today* **2003**, *6*, 24-33.

23.Sandrock, G., A Panoramic Overview of Hydrogen Storage Alloys from a Gas Reaction Point of View. *Journal of Alloys and Compounds* **1999**, *293*, 877-888.

24.Soloveichik, G. L., Metal Borohydrides as Hydrogen Storage Materials. *Material Matters* **2007**, *2*, 11-15.

25.http://www1.eere.energy.gov/vehiclesandfuels/pdfs/program/hstt_roadmap_june2013.pdf.

26.Nijkamp, M.; Raaymakers, J.; Van Dillen, A.; De Jong, K., Hydrogen Storage Using Physisorption–Materials Demands. *Applied Physics A* **2001**, *72*, 619-623.

27.http://en.wikipedia.org/wiki/Fullerene.

28.Purewal, J. Hydrogen Adsorption by Alkali Metal Graphite Intercalation Compounds. California Institute of Technology, **2010**.

29.Noh, J.; Agarwal, R.; Schwarz, J., Hydrogen Storage Systems Using Activated Carbon. *International Journal of Hydrogen Energy* **1987**, *12*, 693-700.

30.Iijima, S., Helical Microtubules of Graphitic Carbon. *Nature* **1991**, *354*, 56-58.

31.Jones, A. D. K.; Bekkedahl, T., Storage of Hydrogen in Single-Walled Carbon Nanotubes. *Nature* **1997**, *386*, 377.

32.Hirscher, M.; Becher, M., Hydrogen Storage in Carbon Nanotubes. *Journal of Nanoscience and Nanotechnology* **2003**, *3*, 3-17.

33.Weitkamp, J.; Fritz, M.; Ernst, S., Zeolites as Media for Hydrogen Storage. *International Journal of Hydrogen Energy* **1995**, *20*, 967-970.

34.Rosi, N. L.; Eckert, J.; Eddaoudi, M.; Vodak, D. T.; Kim, J.; O'Keeffe, M.; Yaghi, O. M., Hydrogen Storage in Microporous Metal-Organic Frameworks. *Science* **2003**,

300, 1127-1129.

35.Struzhkin, V. V.; Militzer, B.; Mao, W. L.; Mao, H.-k.; Hemley, R. J., Hydrogen Storage in Molecular Clathrates. *Chemical Reviews* **2007**, *107*, 4133-4151.

36.Dyadin, Y. A.; Larionov, E. G.; Manakov, A. Y.; Zhurko, F. V.; Aladko, E. Y.; Mikina, T. V.; Komarov, V. Y., Clathrate Hydrates of Hydrogen and Neon. *Mendeleev Communications* **1999**, *9*, 209-210.

37.Mao, W. L.; Mao, H.-k.; Goncharov, A. F.; Struzhkin, V. V.; Guo, Q.; Hu, J.; Shu, J.; Hemley, R. J.; Somayazulu, M.; Zhao, Y., Hydrogen Clusters in Clathrate Hydrate. *Science* **2002**, *297*, 2247-2249.

38.Lee, H.; Lee, J.-w.; Park, J.; Seo, Y.-T.; Zeng, H.; Moudrakovski, I. L.; Ratcliffe, C. I.; Ripmeester, J. A., Tuning Clathrate Hydrates for Hydrogen Storage. *Nature* **2005**, *434*, 743-746.

39.Strobel, T. A.; Taylor, C. J.; Hester, K. C.; Dec, S. F.; Koh, C. A.; Miller, K. T.; Sloan, E., Molecular Hydrogen Storage in Binary THF-H_2 Clathrate Hydrates. *The Journal of Physical Chemistry B* **2006**, *110*, 17121-17125.

40.Reilly Jr, J. J.; Wiswall Jr, R. H., Reaction of Hydrogen with Alloys of Magnesium and Nickel and the Formation of Mg_2NiH_4. *Inorganic Chemistry* **1968**, *7*, 2254-2256.

41.Kuijpers, F.; Van Mal, H., Sorption Hysteresis in the $LaNi_5$-H and $SmCo_5$-H Systems. *Journal of the Less Common Metals* **1971**, *23*, 395-398.

42.Van Vucht J.H.N., K. F. A., Bruning H.C.A.M., *Philips Res. Rep.,* **1970**, *25*, 133-140.

43.N. Furukawa, T. U., Sanyo Nimh Batteries Outperform Li–Ion Nikkei Electronics Asia. **1996**, 80-83.

44.Ledovskikh, A.; Verbitskiy, E.; Ayeb, A.; Notten, P., Modelling of Rechargeable Nimh Batteries. *Journal of Alloys and Compounds* **2003**, *356*, 742-745.

45.Feng, F.; Geng, M.; Northwood, D., Electrochemical Behaviour of Intermetallic-Based Metal Hydrides Used in Ni/Metal Hydride (MH) Batteries: A Review. *International Journal of Hydrogen Energy* **2001**, *26*, 725-734.

46.Liu, Y.; Cao, Y.; Huang, L.; Gao, M.; Pan, H., Rare Earth–Mg–Ni-Based Hydrogen Storage Alloys as Negative Electrode Materials for Ni/MH Batteries. *Journal of Alloys and Compounds* **2011**, *509*, 675-686.

47.Sakintuna, B.; Lamari-Darkrim, F.; Hirscher, M., Metal Hydride Materials for Solid Hydrogen Storage: A Review. *International Journal of Hydrogen Energy* **2007**,

32, 1121-1140.

48.Buschow, K.; Van Mal, H., Phase Relations and Hydrogen Absorption in the Lanthanum-Nickel System. *Journal of the Less Common Metals* **1972**, *29*, 203-210.

49.Akiba, E.; Iba, H., Hydrogen Absorption by Laves Phase Related BCC Solid Solution. *Intermetallics* **1998**, *6*, 461-470.

50.Reilly, J.; Wiswall Jr, R., Formation and Properties of Iron Titanium Hydride. *Inorganic Chemistry* **1974**, *13*, 218-222.

51.Bogdanović, B.; Schwickardi, M., Ti-Doped Alkali Metal Aluminium Hydrides as Potential Novel Reversible Hydrogen Storage Materials. *Journal of Alloys and Compounds* **1997**, *253*, 1-9.

52.Orimo, S.-i.; Nakamori, Y.; Eliseo, J. R.; Züttel, A.; Jensen, C. M., Complex Hydrides for Hydrogen Storage. *Chemical Reviews* **2007**, *107*, 4111-4132.

53.Hauback, B.; Brinks, H.; Jensen, C.; Murphy, K.; Maeland, A., Neutron Diffraction Structure Determination of $NaAlD_4$. *Journal of Alloys and Compounds* **2003**, *358*, 142-145.

54.Hauback, B.; Brinks, H.; Fjellvåg, H., Accurate Structure of $LiAlD_4$ Studied by Combined Powder Neutron and X-Ray Diffraction. *Journal of Alloys and Compounds* **2002**, *346*, 184-189.

55.Hauback, B.; Brinks, H.; Heyn, R.; Blom, R.; Fjellvåg, H., The Crystal Structure of $KAlD_4$. *Journal of Alloys and Compounds* **2005**, *394*, 35-38.

56.Fossdal, A.; Brinks, H.; Fichtner, M.; Hauback, B., Determination of the Crystal Structure of $Mg(AlH_4)_2$ by Combined X-Ray and Neutron Diffraction. *Journal of Alloys and Compounds* **2005**, *387*, 47-51.

57.Brinks, H.; Hauback, B., The Structure of Li_3AlD_6. *Journal of Alloys and Compounds* **2003**, *354*, 143-147.

58.Brinks, H.; Hauback, B.; Jensen, C.; Zidan, R., Synthesis and Crystal Structure of Na_2LiAlD_6. *Journal of Alloys and Compounds* **2005**, *392*, 27-30.

59.Ashby, E.; Kobetz, P., The Direct Synthesis of Na_3AlH_6. *Inorganic Chemistry* **1966**, *5*, 1615-1617.

60.Jensen, C.; Gross, K., Development of Catalytically Enhanced Sodium Aluminum Hydride as a Hydrogen-Storage Material. *Applied Physics A* **2001**, *72*, 213-219.

61.Clasen, H., Alanat‐Synthese Aus Den Elementen Und Ihre Bedeutung. *Angewandte Chemie* **1961**, *73*, 322-331.

62.Titherley, A. W., *J. Chem. Soc.* **1894**, *65*, 504.

63.Chen, P.; Xiong, Z.; Luo, J.; Lin, J.; Tan, K. L., Interaction of Hydrogen with Metal Nitrides and Imides. *Nature* **2002**, *420*, 302-304.

64.Wang, J.; Li, H.-W.; Chen, P., Amides and Borohydrides for High-Capacity Solid-State Hydrogen Storage—Materials Design and Kinetic Improvements. *MRS Bulletin* **2013**, *38*, 480-487.

65.Wang, J.; Liu, T.; Wu, G.; Li, W.; Liu, Y.; Araújo, C. M.; Scheicher, R. H.; Blomqvist, A.; Ahuja, R.; Xiong, Z., Potassium‐Modified $Mg(NH_2)_2$/2LiH System for Hydrogen Storage. *Angewandte Chemie International Edition* **2009**, *48*, 5828-5832.

66.Luo, W.; Stewart, K., Characterization of NH_3 Formation in Desorption of Li–Mg–N–H Storage System. *Journal of Alloys and Aompounds* **2007**, *440*, 357-361.

67.Luo, W.; Wang, J.; Stewart, K.; Clift, M.; Gross, K., Li–Mg–N–H: Recent Investigations and Development. *Journal of Alloys and Compounds* **2007**, *446*, 336-341.

68.Züttel, A.; Rentsch, S.; Fischer, P.; Wenger, P.; Sudan, P.; Mauron, P.; Emmenegger, C., Hydrogen Storage Properties of $LiBH_4$. *Journal of Alloys and Compounds* **2003**, *356*, 515-520.

69.Schlapbach, L.; Züttel, A., Hydrogen-Storage Materials for Mobile Applications. *Nature* **2001**, *414*, 353-358.

70.Semelsberger, T. A.; Brooks, K. P., Chemical Hydrogen Storage Material Property Guidelines for Automotive Applications. *Journal of Power Sources* **2015**, *279*, 593-609.

71.Nakamori, Y.; Orimo, S., *Borohydrides as Hydrogen Storage Materials*; Woodhead Publishing Limited: Cambridge, UK, **2008**.

72.Li, H.-W.; Yan, Y.; Orimo, S.-i.; Züttel, A.; Jensen, C. M., Recent Progress in Metal Borohydrides for Hydrogen Storage. *Energies* **2011**, *4*, 185-214.

73.Burg, A. B.; Schlesinger, H., Metallo Borohydrides. II. Beryllium Borohydride. *Journal of the American Chemical Society* **1940**, *62*, 3425-3429.

74.Schlesinger, H.; Brown, H. C., Metallo Borohydrides. III. Lithium Borohydride. *Journal of the American Chemical Society* **1940**, *62*, 3429-3435.

75.Schlesinger, H.; Sanderson, R.; Burg, A., A Volatile Compound of Aluminum, Boron and Hydrogen. *Journal of the American Chemical Society* **1939**, *61*, 536-536.

76.Schlesinger, H.; Sanderson, R. T.; Burg, A., Metallo Borohydrides. I. Aluminum Borohydride. *Journal of the American Chemical Society* **1940**, *62*, 3421-3425.

77.Schlesinger, H.; Brown, H. C.; Hoekstra, H. R.; Rapp, L. R., Reactions of Diborane with Alkali Metal Hydrides and Their Addition Compounds. New Syntheses of Borohydrides. Sodium and Potassium Borohydrides1. *Journal of the American Chemical Society* **1953**, *75*, 199-204.

78.Goerrig, D., German Patent 1077644, **1958**. *F27373 IVa/12i*.

79.James, B.; Wallbridge, M., Metal Tetrahydroborates. *Prog. Inorg. Chem* **1970**, *11*, 99-231.

80.Schlesinger, H.; Brown, H. C.; Hyde, E. K., The Preparation of Other Borohydrides by Metathetical Reactions Utilizing the Alkali Metal Borohydrides1. *Journal of the American Chemical Society* **1953**, *75*, 209-213.

81.Jeon, E.; Cho, Y., Mechanochemical Synthesis and Thermal Decomposition of Zinc Borohydride. *Journal of Alloys and Compounds* **2006**, *422*, 273-275.

82.Rude, L. H.; Corno, M.; Ugliengo, P.; Baricco, M.; Lee, Y.-S.; Cho, Y. W.; Besenbacher, F.; Overgaard, J.; Jensen, T. R., Synthesis and Structural Investigation of $Zr(BH_4)_4$. *The Journal of Physical Chemistry C* **2012**, *116*, 20239-20245.

83.Nakamori, Y.; Li, H.; Miwa, K.; Towata, S.-i.; Orimo, S.-i., Syntheses and Hydrogen Desorption Properties of Metal-Borohydrides $M(BH_4)_N$ (M= Mg, Sc, Zr, Ti, and Zn; N= 2-4) as Advanced Hydrogen Storage Materials. *Materials transactions* **2006**, *47*, 1898-1901.

84.Černý, R.; Filinchuk, Y.; Hagemann, H.; Yvon, K., Magnesium Borohydride: Synthesis and Crystal Structure. *Angewandte Chemie* **2007**, *119*, 5867-5869.

85.Züttel, A.; Wenger, P.; Rentsch, S.; Sudan, P.; Mauron, P.; Emmenegger, C., $LiBH_4$ a New Hydrogen Storage Material. *Journal of Power Sources* **2003**, *118*, 1-7.

86.Züttel, A.; Borgschulte, A.; Orimo, S.-I., Tetrahydroborates as New Hydrogen Storage Materials. *Scripta Materialia* **2007**, *56*, 823-828.

87.Orimo, S.-I.; Nakamori, Y.; Ohba, N.; Miwa, K.; Aoki, M.; Towata, S.-i.; Zuttel, A., Experimental Studies on Intermediate Compound of $LiBH_4$. *Applied Physics Letters* **2006**, *89*, 021920-021920-3.

88.Ohba, N.; Miwa, K.; Aoki, M.; Noritake, T.; Towata, S.-i.; Nakamori, Y.; Orimo, S.-i.; Züttel, A., First-Principles Study on the Stability of Intermediate Compounds of $LiBH_4$. *Physical Review B* **2006**, *74*, 075110.

89.Ozolins, V.; Majzoub, E.; Wolverton, C., First-Principles Prediction of Thermodynamically Reversible Hydrogen Storage Reactions in the Li-Mg-Ca-B-H System. *Journal of the American Chemical Society* **2009**, *131*, 230-237.

90.Johnson, D. A., Open University (12 August 2002). Metals and Chemical Change. *Royal Society of Chemistry* **2002**, 167.

91.Mauron, P.; Buchter, F.; Friedrichs, O.; Remhof, A.; Bielmann, M.; Zwicky, C. N.; Züttel, A., Stability and Reversibility of $LiBH_4$. *The Journal of Physical Chemistry B* **2008**, *112*, 906-910.

92.Soloveichik, G. L.; Gao, Y.; Rijssenbeek, J.; Andrus, M.; Kniajanski, S.; Bowman, R. C.; Hwang, S.-J.; Zhao, J.-C., Magnesium Borohydride as a Hydrogen Storage Material: Properties and Dehydrogenation Pathway of Unsolvated $Mg(BH_4)_2$. *International Journal of Hydrogen Energy* **2009**, *34*, 916-928.

93.Li, H.-W.; Kikuchi, K.; Nakamori, Y.; Miwa, K.; Towata, S.; Orimo, S., Effects of Ball Milling and Additives on Dehydriding Behaviors of Well-Crystallized $Mg(BH_4)_2$. *Scripta Materialia* **2007**, *57*, 679-682.

94.Li, H.-W.; Kikuchi, K.; Nakamori, Y.; Ohba, N.; Miwa, K.; Towata, S.; Orimo, S., Dehydriding and Rehydriding Processes of Well-Crystallized $Mg(BH_4)_2$ Accompanying with Formation of Intermediate Compounds. *Acta Materialia* **2008**, *56*, 1342-1347.

95.Hanada, N.; Chłopek, K.; Frommen, C.; Lohstroh, W.; Fichtner, M., Thermal Decomposition of $Mg(BH_4)_2$ under He Flow and H_2 Pressure. *Journal of Materials Chemistry* **2008**, *18*, 2611-2614.

96.Hwang, S.-J.; Bowman, R. C.; Reiter, J. W.; Rijssenbeek, J.; Soloveichik, G. L.; Zhao, J.-C.; Kabbour, H.; Ahn, C. C., NMR Confirmation for Formation of $[B_{12}H_{12}]^{2-}$ Complexes During Hydrogen Desorption from Metal Borohydrides. *The Journal of Physical Chemistry C* **2008**, *112*, 3164-3169.

97.Ozolins, V.; Majzoub, E.; Wolverton, C., First-Principles Prediction of a Ground State Crystal Structure of Magnesium Borohydride. *Physical Review Letters* **2008**, *100*, 135501.

98.Li, S.; Willis, M.; Jena, P., Reaction Intermediates During the Dehydrogenation of Metal Borohydrides: A Cluster Perspective. *The Journal of Physical Chemistry C* **2010**, *114*, 16849-16854.

99.Matsunaga, T.; Buchter, F.; Mauron, P.; Bielman, M.; Nakamori, Y.; Orimo, S.;

Ohba, N.; Miwa, K.; Towata, S.; Züttel, A., Hydrogen Storage Properties of $Mg[BH_4]_2$. *Journal of Alloys and Compounds* **2008**, *459*, 583-588.

100.Li, H.; Miwa, K.; Ohba, N.; Fujita, T.; Sato, T.; Yan, Y.; Towata, S.; Chen, M.; Orimo, S., Formation of an Intermediate Compound with a $B_{12}H_{12}$ Cluster: Experimental and Theoretical Studies on Magnesium Borohydride $Mg(BH_4)_2$. *Nanotechnology* **2009**, *20*, 204013.

101.Newhouse, R. J.; Stavila, V.; Hwang, S.-J.; Klebanoff, L. E.; Zhang, J. Z., Reversibility and Improved Hydrogen Release of Magnesium Borohydride. *The Journal of Physical Chemistry C* **2010**, *114*, 5224-5232.

102.Severa, G.; Rönnebro, E.; Jensen, C. M., Direct Hydrogenation of Magnesium Boride to Magnesium Borohydride: Demonstration of >11 Weight Percent Reversible Hydrogen Storage. *Chemical Communications* **2010**, *46*, 421-423.

103.Garroni, S.; Milanese, C.; Pottmaier, D.; Mulas, G.; Nolis, P.; Girella, A.; Caputo, R.; Olid, D.; Teixdor, F.; Baricco, M., Experimental Evidence of $Na_2[B_{12}H_{12}]$ and Na Formation in the Desorption Pathway of the $2NaBH_4$+ MgH_2 System. *The Journal of Physical Chemistry C* **2011**, *115*, 16664-16671.

104.Wang, L.-L.; Graham, D. D.; Robertson, I. M.; Johnson, D. D., On the Reversibility of Hydrogen-Storage Reactions in $Ca(BH_4)_2$: Characterization Via Experiment and Theory. *The Journal of Physical Chemistry C* **2009**, *113*, 20088-20096.

105.Yan, Y.; Li, H.-W.; Sato, T.; Umeda, N.; Miwa, K.; Towata, S.-i.; Orimo, S.-i., Dehydriding and Rehydriding Properties of Yttrium Borohydride $Y(BH_4)_3$ Prepared by Liquid-Phase Synthesis. *International Journal of Hydrogen Energy* **2009**, *34*, 5732-5736.

106.Gennari, F.; Esquivel, M., Synthesis and Dehydriding Process of Crystalline $Ce(BH_4)_3$. *Journal of Alloys and Compounds* **2009**, *485*, L47-L51.

107.Gennari, F.; Albanesi, L. F.; Rios, I., Synthesis and Thermal Stability of $Zr(BH_4)_4$ and $Zr(BD_4)_4$ Produced by Mechanochemical Processing. *Inorganica Chimica Acta* **2009**, *362*, 3731-3737.

108.Srinivasan, S.; Escobar, D.; Jurczyk, M.; Goswami, Y.; Stefanakos, E., Nanocatalyst Doping of $Zn(BH_4)_2$ for on-Board Hydrogen Storage. *Journal of Alloys and Compounds* **2008**, *462*, 294-302.

109.Fang, Z.; Ma, L.; Kang, X.; Wang, P.; Wang, P.; Cheng, H., In Situ Formation and

Rapid Decomposition of $Ti(BH_4)_3$ by Mechanical Milling $LiBH_4$ with TiF_3. *Applied Physics Letters* **2009**, *94*, 044104-044104-3.

110.Friedrichs, O.; Remhof, A.; Borgschulte, A.; Buchter, F.; Orimo, S.; Züttel, A., Breaking the Passivation—the Road to a Solvent Free Borohydride Synthesis. *Physical Chemistry Chemical Physics* **2010**, *12*, 10919-10922.

111.Nakamori, Y.; Miwa, K.; Ninomiya, A.; Li, H.; Ohba, N.; Towata, S.-i.; Züttel, A.; Orimo, S.-i., Correlation between Thermodynamical Stabilities of Metal Borohydrides and Cation Electronegativites: First-Principles Calculations and Experiments. *Physical Review B* **2006**, *74*, 045126.

112.Li, H.-W.; Orimo, S.-i.; Nakamori, Y.; Miwa, K.; Ohba, N.; Towata, S.; Züttel, A., Materials Designing of Metal Borohydrides: Viewpoints from Thermodynamical Stabilities. *Journal of Alloys and Compounds* **2007**, *446*, 315-318.

113.Nickels, E. A.; Jones, M. O.; David, W. I.; Johnson, S. R.; Lowton, R. L.; Sommariva, M.; Edwards, P. P., Tuning the Decomposition Temperature in Complex Hydrides: Synthesis of a Mixed Alkali Metal Borohydride. *Angewandte Chemie International Edition* **2008**, *47*, 2817-2819.

114.Ravnsbæk, D.; Filinchuk, Y.; Cerenius, Y.; Jakobsen, H. J.; Besenbacher, F.; Skibsted, J.; Jensen, T. R., A Series of Mixed ‐ Metal Borohydrides. *Angewandte Chemie* **2009**, *121*, 6787-6791.

115.Severa, G.; Hagemann, H.; Longhini, M. s.; Kaminski, J. W.; Wesolowski, T. A.; Jensen, C. M., Thermal Desorption, Vibrational Spectroscopic, and DFT Computational Studies of the Complex Manganese Borohydrides $Mn(BH_4)_2$ and $[Mn(BH_4)_4]^{2-}$. *The Journal of Physical Chemistry C* **2010**, *114*, 15516-15521.

116.Cerny, R.; Ravnsbæk, D. B.; Severa, G.; Filinchuk, Y.; D'Anna, V.; Hagemann, H.; Haase, D. r.; Skibsted, J.; Jensen, C. M.; Jensen, T. R., Structure and Characterization of $KSc(BH_4)_4$. *The Journal of Physical Chemistry C* **2010**, *114*, 19540-19549.

117.Hagemann, H.; Longhini, M.; Kaminski, J. W.; Wesolowski, T. A.; Cerny, R.; Penin, N.; Sørby, M. H.; Hauback, B. C.; Severa, G.; Jensen, C. M., $LiSc(BH_4)_4$: A Novel Salt of Li^+ and Discrete $Sc(BH_4)_4^-$ Complex Anions. *The Journal of Physical Chemistry A* **2008**, *112*, 7551-7555.

118.Vajo, J. J.; Skeith, S. L.; Mertens, F., Reversible Storage of Hydrogen in Destabilized $LiBH_4$. *The Journal of Physical Chemistry B* **2005**, *109*, 3719-3722.

119.Pinkerton, F.; Meyer, M., Reversible Hydrogen Storage in the Lithium Borohydride—Calcium Hydride Coupled System. *Journal of Alloys and Compounds* **2008**, *464*, L1-L4.

120.Shim, J.-H.; Lim, J.-H.; Rather, S.-u.; Lee, Y.-S.; Reed, D.; Kim, Y.; Book, D.; Cho, Y. W., Effect of Hydrogen Back Pressure on Dehydrogenation Behavior of $LiBH_4$-Based Reactive Hydride Composites. *The Journal of Physical Chemistry Letters* **2009**, *1*, 59-63.

121.Aoki, M.; Miwa, K.; Noritake, T.; Kitahara, G.; Nakamori, Y.; Orimo, S.; Towata, S., Destabilization of $LiBH_4$ by Mixing with $LiNH_2$. *Applied Physics A* **2005**, *80*, 1409-1412.

122.Yu, X.; Guo, Y.; Sun, D.; Yang, Z.; Ranjbar, A.; Guo, Z.; Liu, H.; Dou, S., A Combined Hydrogen Storage System of $Mg(BH_4)_2$−$LiNH_2$ with Favorable Dehydrogenation. *The Journal of Physical Chemistry C* **2010**, *114*, 4733-4737.

123.Yu, X.; Wu, Z.; Chen, Q.; Li, Z.; Weng, B.; Huang, T., Improved Hydrogen Storage Properties of $LiBH_4$ Destabilized by Carbon. *Applied Physics Letters* **2007**, *90*, 034106-034106-3.

124.Yin, L.; Wang, P.; Fang, Z.; Cheng, H., Thermodynamically Tuning $LiBH_4$ by Fluorine Anion Doping for Hydrogen Storage: A Density Functional Study. *Chemical Physics Letters* **2008**, *450*, 318-321.

125.Varin, R.; Chiu, C.; Wronski, Z. S.; Calka, A., The Effects of Oxidized and Oxide-Free Boron on the Mg-BH Nanohydrides Transformation in the Nearly Nanosized Powders. *Solid State Phenomena* **2007**, *128*, 47-52.

126.Li, H.-W.; Yan, Y.; Akiba, E.; Orimo, S.-i., Improved Dehydrogenation and Rehydrogenation Properties of $LiBH_4$ by Nanosized Ni Addition. *Materials Transactions* **2014**, *55*, 1134-1137.

127.Au, M.; Jurgensen, A.; Zeigler, K., Modified Lithium Borohydrides for Reversible Hydrogen Storage (2). *The Journal of Physical Chemistry B* **2006**, *110*, 26482-26487.

128.Bösenberg, U.; Kim, J. W.; Gosslar, D.; Eigen, N.; Jensen, T. R.; Von Colbe, J. B.; Zhou, Y.; Dahms, M.; Kim, D.; Günther, R., Role of Additives in $LiBH_4$–MgH_2 Reactive Hydride Composites for Sorption Kinetics. *Acta Materialia* **2010**, *58*, 3381-3389.

129.Gutowska, A.; Li, L.; Shin, Y.; Wang, C. M.; Li, X. S.; Linehan, J. C.; Smith, R.

S.; Kay, B. D.; Schmid, B.; Shaw, W., Nanoscaffold Mediates Hydrogen Release and the Reactivity of Ammonia Borane. *Angewandte Chemie International Edition* **2005**, *44*, 3578-3582.

130.Gross, A. F.; Vajo, J. J.; Van Atta, S. L.; Olson, G. L., Enhanced Hydrogen Storage Kinetics of $LiBH_4$ in Nanoporous Carbon Scaffolds. *The Journal of Physical Chemistry C* **2008**, *112*, 5651-5657.

131.Ngene, P.; van Zwienen, M. R.; de Jongh, P. E., Reversibility of the Hydrogen Desorption from $LiBH_4$: A Synergetic Effect of Nanoconfinement and Ni Addition. *Chemical Communications* **2010**, *46*, 8201-8203.

132.Liu, X.; Peaslee, D.; Jost, C. Z.; Baumann, T. F.; Majzoub, E. H., Systematic Pore-Size Effects of Nanoconfinement of $LiBH_4$: Elimination of Diborane Release and Tunable Behavior for Hydrogen Storage Applications. *Chemistry of Materials* **2011**, *23*, 1331-1336.

133.Bonatto Minella, C.; Garroni, S.; Olid, D.; Teixidor, F.; Pistidda, C.; Lindemann, I.; Gutfleisch, O.; Baró, M. D.; Bormann, R. d.; Klassen, T., Experimental Evidence of $Ca[B_{12}H_{12}]$ Formation During Decomposition of a $Ca(BH_4)_2$+MgH_2 Based Reactive Hydride Composite. *The Journal of Physical Chemistry C* **2011**, *115*, 18010-18014.

134.Yan, Y.; Li, H.-W.; Maekawa, H.; Miwa, K.; Towata, S.-i.; Orimo, S.-i., Formation of Intermediate Compound $Li_2B_{12}H_{12}$ During the Dehydrogenation Process of the $LiBH_4$–MgH_2 System. *The Journal of Physical Chemistry C* **2011**, *115*, 19419-19423.

135.Yan, Y.; Remhof, A.; Rentsch, D.; Lee, Y.-S.; Cho, Y. W.; Züttel, A., Is $Y(B_{12}H_{12})_3$ the Main Intermediate in the Decomposition Process of $Y(BH_4)_3$? *Chemical Communications* **2013**, *49*, 5234-5236.

136.Bösenberg, U.; Doppiu, S.; Mosegaard, L.; Barkhordarian, G.; Eigen, N.; Borgschulte, A.; Jensen, T. R.; Cerenius, Y.; Gutfleisch, O.; Klassen, T., Hydrogen Sorption Properties of MgH_2–$LiBH_4$ Composites. *Acta Materialia* **2007**, *55*, 3951-3958.

137.Kim, Y.; Hwang, S.-J.; Shim, J.-H.; Lee, Y.-S.; Han, H. N.; Cho, Y. W., Investigation of the Dehydrogenation Reaction Pathway of $Ca(BH_4)_2$ and Reversibility of Intermediate Phases. *The Journal of Physical Chemistry C* **2012**, *116*, 4330-4334.

138.Li, H.-W.; Akiba, E.; Orimo, S.-i., Comparative Study on the Reversibility of Pure Metal Borohydrides. *Journal of Alloys and Compounds* **2013**, *580*, S292-S295.

139.Minella, C. B.; Pistidda, C.; Garroni, S.; Nolis, P.; Baró, M. D.; Gutfleisch, O.; Klassen, T.; Bormann, R. d.; Dornheim, M., $Ca(BH_4)_2$+MgH_2: Desorption Reaction and Role of Mg on Its Reversibility. *The Journal of Physical Chemistry C* **2013**, *117*, 3846-3852.

140.Skripov, A. V.; Babanova, O. A.; Soloninin, A. V.; Stavila, V.; Verdal, N.; Udovic, T. J.; Rush, J. J., Nuclear Magnetic Resonance Study of Atomic Motion in $A_2B_{12}H_{12}$ (A= Na, K, Rb, Cs): Anion Reorientations and Na^+ Mobility. *The Journal of Physical Chemistry C* **2013**, *117*, 25961-25968.

141.Jemmis, E. D.; Balakrishnarajan, M. M., Ab Initio Predictions on Novel Stuffed Polyhedral Boranes. *Journal of the American Chemical Society* **2000**, *122*, 7392-7393.

142.Longuet-Higgins, H.; Roberts, M. d. V. In The Electronic Structure of an Icosahedron of Boron Atoms, Proceedings of the Royal Society of London A: Mathematical, Physical and Engineering Sciences, *The Royal Society*: **1955**; pp 110-119.

143.Sivaev, I. B.; Bregadze, V. I.; Sjöberg, S., Chemistry of Closo-Dodecaborate Anion $[B_{12}H_{12}]^{2-}$: A Review. *Collection of Czechoslovak Chemical Communications* **2002**, *67*, 679-727.

144.E. L. Muetterties, J. H. B., Y. T. Chia, W. H. Knoth, H. C. Miller, Chemistry of Boranes. Viii. Salts and Acids of $B_{10}H_{10}^{2-}$ and $B_{12}H_{12}^{2-}$. *Inorganic Chemistry* **1964**, *3*, 444–451.

145.Pitochelli, A. R.; Hawthorne, F. M., The Isolation of the Icosahedral $B_{12}H_{12}^{2-}$ Ion. *Journal of the American Chemical Society* **1960**, *82*, 3228-3229.

146.Miller, H.; Miller, N.; Muetterties, E., Synthesis of Polyhedral Boranes. *Journal of the American Chemical Society* **1963**, *85*, 3885-3886.

147.Miller, H.; Muetterties, E.; Boone, J.; Garrett, P.; Hawthorne, M., Borane Anions. *Inorganic Syntheses, Volume 10* **1967**, 81-91.

148.Johnson, J. W.; Brody, J. F., Lithium Closoborane Electrolytes III. Preparation and Characterization. *Journal of The Electrochemical Society* **1982**, *129*, 2213-2219.

149.Pitt, M. P.; Paskevicius, M.; Brown, D. H.; Sheppard, D. A.; Buckley, C. E., Thermal Stability of $Li_2B_{12}H_{12}$ and Its Role in the Decomposition of $LiBH_4$. *Journal*

of the American Chemical Society **2013**, *135*, 6930-6941.

150.Her, J.-H.; Zhou, W.; Stavila, V.; Brown, C. M.; Udovic, T. J., Role of Cation Size on the Structural Behavior of the Alkali-Metal Dodecahydro-Closo-Dodecaborates. *The Journal of Physical Chemistry C* **2009**, *113*, 11187-11189.

151.Chen, X.; Lingam, H. K.; Huang, Z.; Yisgedu, T.; Zhao, J.-C.; Shore, S. G., Thermal Decomposition Behavior of Hydrated Magnesium Dodecahydrododecaborates. *The Journal of Physical Chemistry Letters* **2009**, *1*, 201-204.

152.Verdal, N.; Wu, H.; Udovic, T. J.; Stavila, V.; Zhou, W.; Rush, J. J., Evidence of a Transition to Reorientational Disorder in the Cubic Alkali-Metal Dodecahydro-Closo-Dodecaborates. *Journal of Solid State Chemistry* **2011**, *184*, 3110-3116.

153.Paskevicius, M.; Pitt, M. P.; Brown, D. H.; Sheppard, D. A.; Chumphongphan, S.; Buckley, C. E., First-Order Phase Transition in the $Li_2B_{12}H_{12}$ System. *Physical Chemistry Chemical Physics* **2013**, *15*, 15825-15828.

154.Verdal, N.; Her, J.-H.; Stavila, V.; Soloninin, A. V.; Babanova, O. A.; Skripov, A. V.; Udovic, T. J.; Rush, J. J., Complex High-Temperature Phase Transitions in $Li_2B_{12}H_{12}$ and $Na_2B_{12}H_{12}$. *Journal of Solid State Chemistry* **2014**, *212*, 81-91.

155.Udovic, T. J.; Matsuo, M.; Unemoto, A.; Verdal, N.; Stavila, V.; Skripov, A. V.; Rush, J. J.; Takamura, H.; Orimo, S.-i., Sodium Superionic Conduction in $Na_2B_{12}H_{12}$. *Chem. Commun.* **2014**, *50*, 3750-3752.

156.Jena, P., Superhalogens: A Bridge between Complex Metal Hydrides and Li Ion Batteries. *The Journal of Physical Chemistry Letters* **2015**, *6*, 1119-1125.

157.He, L.; Li, H.-W.; Hwang, S.-J.; Akiba, E., Facile Solvent-Free Synthesis of Anhydrous Alkali Metal Dodecaborate $M_2B_{12}B_{12}$ (M= Li, Na, K). *The Journal of Physical Chemistry C* **2014**, *118*, 6084-6089.

158.David, W.; Callear, S.; Jones, M.; Aeberhard, P.; Culligan, S.; Pohl, A.; Johnson, S.; Ryan, K.; Parker, J.; Edwards, P., The Structure, Thermal Properties and Phase Transformations of the Cubic Polymorph of Magnesium Tetrahydroborate. *Physical Chemistry Chemical Physics* **2012**, *14*, 11800-11807.

159.Comănescu, C.; Capurso, G.; Maddalena, A., Nanoconfinement in Activated Mesoporous Carbon of Calcium Borohydride for Improved Reversible Hydrogen Storage. *Nanotechnology* **2012**, *23*, 385401.

160.http:// en.wikipedia.org/wiki/X-Ray_Crystallography.

161.http://www.icdd.com/.

162.Polenova, T., Protein NMR Spectroscopy: Spinning into Focus. *Nature Chemistry* **2011**, *3*, 759-760.

163.http://en.wikipedia.org/wiki/Mass_Spectrometry.

164.Jensen, T. R.; Nielsen, T. K.; Filinchuk, Y.; Jørgensen, J.-E.; Cerenius, Y.; Gray, E. M.; Webb, C. J., Versatile in Situ Powder X-Ray Diffraction Cells for Solid–Gas Investigations. *Journal of Applied Crystallography* **2010**, *43*, 1456-1463.

165.Hammersley, A.; Svensson, S.; Hanfland, M.; Fitch, A.; Hausermann, D., Two-Dimensional Detector Software: From Real Detector to Idealised Image or Two-Theta Scan. *International Journal of High Pressure Research* **1996**, *14*, 235-248.

166.Dyadkin, V., Snbl Tool Box. **2013**.

167.Vogel, S.; Ehm, L.; Knorr, K.; Braun, G., Automated Processing of 2D Powder Diffraction Data. *Adv X-ray Anal* **2002**, *45*, 31-33.

168.Rodríguez-Carvajal, J., Recent Advances in Magnetic Structure Determination by Neutron Powder Diffraction. *Physica B: Condensed Matter* **1993**, *192*, 55-69.

169.Barsoukov, E.; Macdonald, J. R., *Impedance Spectroscopy: Theory, Experiment, and Applications*; John Wiley & Sons, **2005**.

170.Evans, J.; Vincent, C. A.; Bruce, P. G., Electrochemical Measurement of Transference Numbers in Polymer Electrolytes. *Polymer* **1987**, *28*, 2324-2328.

171.Watanabe, M.; Nagano, S.; Sanui, K.; Ogata, N., Estimation of Li^+ Transport Number in Polymer Electrolytes by the Combination of Complex Impedance and Potentiostatic Polarization Measurements. *Solid State Ionics* **1988**, *28*, 911-917.

172.Chong, M.; Karkamkar, A.; Autrey, T.; Orimo, S.-i.; Jalisatgi, S.; Jensen, C. M., Reversible Dehydrogenation of Magnesium Borohydride to Magnesium Triborane in the Solid State under Moderate Conditions. *Chemical Communications* **2011**, *47*, 1330-1332.

173.Yan, Y.; Li, H.-W.; Maekawa, H.; Aoki, M.; Noritake, T.; Matsumoto, M.; Miwa, K.; Towata, S.-i.; Orimo, S.-i., Formation Process of $[B_{12}H_{12}]^{2-}$ from$[BH_4]^-$ During the Dehydrogenation Reaction of $Mg(BH_4)_2$. *Materials Transactions* **2011**, *52*, 1443-1446.

174.Purewal, J.; Hwang, S.-J.; Bowman, J., Robert C; Rönnebro, E.; Fultz, B.; Ahn, C., Hydrogen Sorption Behavior of the ScH_2−$LiBH_4$ System: Experimental Assesment of Chemical Destabilization Effects. *The Journal of Physical Chemistry C*

2008, *112*, 8481-8485.

175.Kim, C.; Hwang, S.-J.; Bowman Jr, R. C.; Reiter, J. W.; Zan, J. A.; Kulleck, J. G.; Kabbour, H.; Majzoub, E.; Ozolins, V., $LiSc(BH_4)_4$ as a Hydrogen Storage Material: Multinuclear High-Resolution Solid-State NMR and First-Principles Density Functional Theory Studies. *The Journal of Physical Chemistry C* **2009**, *113*, 9956-9968.

176.Stavila, V.; Her, J.-H.; Zhou, W.; Hwang, S.-J.; Kim, C.; Ottley, L. A. M.; Udovic, T. J., Probing the Structure, Stability and Hydrogen Storage Properties of Calcium Dodecahydro-Dodecaborate. *Journal of Solid State Chemistry* **2010**, *183*, 1133-1140.

177.Takahashi, T.; Kashiwakura, S.; Kanehashi, K.; Hayashi, S.; Nagasaka, T., Analysis of Atomic Scale Chemical Environments of Boron in Coal by ^{11}B Solid State NMR. *Environmental Science & Technology* **2010**, *45*, 890-895.

178.Friedrichs, O.; Remhof, A.; Hwang, S.-J.; Zuttel, A., Role of $Li_2B_{12}H_{12}$ for the Formation and Decomposition of $LiBH_4$. *Chemistry of Materials* **2010**, *22*, 3265-3268.

179.Her, J.-H.; Yousufuddin, M.; Zhou, W.; Jalisatgi, S. S.; Kulleck, J. G.; Zan, J. A.; Hwang, S.-J.; Bowman Jr, R. C.; Udovic, T. J., Crystal Structure of $Li_2B_{12}H_{12}$: A Possible Intermediate Species in the Decomposition of $LiBH_4$. *Inorganic Chemistry* **2008**, *47*, 9757-9759.

180.Tiritiris, I.; Schleid, T., Die Dodekahydro‐Closo‐Dodekaborate $M_2[B_{12}H_{12}]$ Der Schweren Alkalimetalle (M^+= K^+, Rb^+, NH_4^+, Cs^+) Und Ihre Formalen Iodid‐Addukte $M_3I[B_{12}H_{12}](\equiv MI\cdot M_2[B_{12}H_{12}])$. *Z. Anorg. Allg. Chem.* **2003**, *629*, 1390-1402.

181.Muetterties, E.; Merrifield, R.; Miller, H.; Knoth, W.; Downing, J., Chemistry of Boranes. III. 1 the Infrared and Raman Spectra of $B_{12}H_{12}^{2-}$ and Related Anions. *Journal of the American Chemical Society* **1962**, *84*, 2506-2508.

182.Nogi, N.; Tanaka, S., Ab-Initio Calculations of Raman, Ir-Active Vibrational Modes in Isotopically Modified B_{12} Icosahedral Clusters. *Journal of Solid State Chemistry* **2006**, *179*, 2927-2933.

183.Caputo, R.; Garroni, S.; Olid, D.; Teixidor, F.; Suriñach, S.; Baró, M. D., Can $Na_2[B_{12}H_{12}]$ Be a Decomposition Product of $NaBH_4$? *Physical Chemistry Chemical Physics* **2010**, *12*, 15093-15100.

184.Tiritiris, I.; Schleid, T.; Müller, K., Solid-State NMR Studies on Ionic Closo-Dodecaborates. *Applied Magnetic Resonance* **2007**, *32*, 459-481.

185.Lee, T. B., Computational Investigation of Condensed Phase Properties of Ionic Systems. **2012**.

186.Heřmánek, S., B NMR Spectra of Boranes, Main-Group Heteroboranes, and Substituted Derivatives. Factors Influencing Chemical Shifts of Skeletal Atoms. *Chem Rev* **1992**, *92*, 325-362.

187.Hwang, S.-J.; Bowman Jr, R. C.; Kim, C.; Zan, J. A.; Reiter, J. W., Solid State NMR Characterization of Complex Metal Hydrides Systems for Hydrogen Storage Applications. *Journal of Analytical Science & Technology* **2011**, *2*, A159-A162.

188.Yan, Y.; Remhof, A.; Hwang, S.-J.; Li, H.-W.; Mauron, P.; Orimo, S.-i.; Züttel, A., Pressure and Temperature Dependence of the Decomposition Pathway of $LiBH_4$. *Physical Chemistry Chemical Physics* **2012**, *14*, 6514-6519.

189.Remhof, A.; Yan, Y.; Rentsch, D.; Borgschulte, A.; Jensen, C. M.; Züttel, A., Solvent-Free Synthesis and Stability of $MgB_{12}H_{12}$. *Journal of Materials Chemistry A* **2014**, *2*, 7244-7249.

190.Martelli, P.; Caputo, R.; Remhof, A.; Mauron, P.; Borgschulte, A.; Züttel, A., Stability and Decomposition of $NaBH_4$. *The Journal of Physical Chemistry C* **2010**, *114*, 7173-7177.

191.Guo, Y.; Jia, J.; Wang, X.-H.; Ren, Y.; Wu, H., Prediction of Thermodynamically Reversible Hydrogen Storage Reactions in the KBH_4/M(M= Li, Na, Ca)$(BH_4)_N$ (N= 1, 2) System from First-Principles Calculation. *Chemical Physics* **2013**, *418*, 22-27.

192.He, L.; Li, H.-W.; Tumanov, N.; Filinchuk, Y.; Akiba, E., Facile Synthesis of Anhydrous Alkaline Earth Metal Dodecaborate $MB_{12}H_{12}$ (M = Mg, Ca) from $M(BH_4)_2$. *Submitted* **2015**.

193.Li, H.-W.; Matsunaga, T.; Yan, Y.; Maekawa, H.; Ishikiriyama, M.; Orimo, S.-i., Nanostructure-Induced Hydrogenation of Layered Compound MgB_2. *Journal of Alloys and Compounds* **2010**, *505*, 654-656.

194.Kulkarni, A. D.; Wang, L.-L.; Johnson, D. D.; Sholl, D. S.; Johnson, J. K., First-Principles Characterization of Amorphous Phases of $MB_{12}H_{12}$, M= Mg, Ca. *The Journal of Physical Chemistry C* **2010**, *114*, 14601-14605.

195.Tiritiris, I.; Schleid, T., Dodecahydro-Closo-Dodecaborates of the Heavy Alkaline-Earth Metals from Aqueous Solution: $Ca(H_2O)_7[B_{12}H_{12}]\bullet H_2O$, $Sr(H_2O)_8[B_{12}H_{12}]$, and $Ba(H_2O)_6[B_{12}H_{12}]$. *Z. Anorg. Allg. Chem.* **2001**, *627*, 1836-1845.

196.Li, H.-W.; Kikuchi, K.; Sato, T.; Nakamori, Y.; Ohba, N.; Aoki, M.; Miwa, K.; Towata, S.-i.; Orimo, S.-i., Synthesis and Hydrogen Storage Properties of a Single-Phase Magnesium Borohydride $Mg(BH_4)_2$. *Materials Transactions* **2008**, *49*, 2224-2228.

197.Jena, P., Superhalogens–a Bridge between Complex Metal Hydrides and Li-Ion Batteries. *The Journal of Physical Chemistry Letters* **2015**.

198.Li, H.-W.; Kikuchi, K.; Nakamori, Y.; Ohba, N.; Miwa, K.; Towata, S.; Orimo, S., Dehydriding and Rehydriding Processes of Well-Crystallized $Mg(BH_4)_2$ Accompanying with Formation of Intermediate Compounds. *Acta Materialia* **2008**, *56*, 1342-1347.

199.Ozolins, V.; Majzoub, E.; Wolverton, C., First-Principles Prediction of Thermodynamically Reversible Hydrogen Storage Reactions in the Li-Mg-Ca-B-H System. *Journal of the American Chemical Society* **2008**, *131*, 230-237.

200.Filinchuk, Y.; Richter, B.; Jensen, T. R.; Dmitriev, V.; Chernyshov, D.; Hagemann, H., Porous and Dense Magnesium Borohydride Frameworks: Synthesis, Stability, and Reversible Absorption of Guest Species. *Angewandte Chemie International Edition* **2011**, *50*, 11162-11166.

201.Schouwink, P.; Ley, M. B.; Tissot, A.; Hagemann, H.; Jensen, T. R.; Smrčok, Ľ.; Černý, R., Structure and Properties of Complex Hydride Perovskite Materials. *Nature Communications* **2014**, *5*.

202.Hueso, K. B.; Armand, M.; Rojo, T., High Temperature Sodium Batteries: Status, Challenges and Future Trends. *Energy & Environmental Science* **2013**, *6*, 734-749.

203.Ley, M. B.; Ravnsbæk, D. B.; Filinchuk, Y.; Lee, Y.-S.; Janot, R. l.; Cho, Y. W.; Skibsted, J.; Jensen, T. R., $LiCe(BH_4)_3Cl$, a New Lithium-Ion Conductor and Hydrogen Storage Material with Isolated Tetranuclear Anionic Clusters. *Chemistry of Materials* **2012**, *24*, 1654-1663.

204.Frisch, M.; Trucks, G.; Schlegel, H.; Scuseria, G.; Robb, M.; Cheeseman, J.; Scalmani, G.; Barone, V.; Mennucci, B.; Petersson, G., Gaussian 09 Package. Gaussian. *Inc.: Wallingford, CT, USA* **2009**.

205.Allis, D. G.; Hudson, B. S., Inelastic Neutron Scattering Spectrum of $Cs_2[B_{12}H_{12}]$: Reproduction of Its Solid-State Vibrational Spectrum by Periodic DFT. *The Journal of Physical Chemistry A* **2006**, *110*, 3744-3749.

206.Silva, R.; Teixeira, S.; Souza, A.; Santos, D.; Romero, M.; Rincón, J. M.,

Nucleation Kinetics of Crystalline Phases from a Kaolinitic Body Used in the Processing of Red Ceramics. *Applied Clay Science* **2011**, *52*, 165-170.
207.https://www.gamry.com/application-notes/EIS/basics-of-electrochemical-impedance-spectroscopy/.